Investigation into the molecular interaction between forkhead box P3 (FOXP3) and vitamin D receptor (VDR).

by

Jessica Sarah Hurwitz

(2232089)

a Dissertation

Submitted in fulfilment of the requirements for the degree

Master of Science

in

Molecular and Cell Biology

in the Faculty of Science, University of the Witwatersrand, Johannesburg, South Africa

Supervisor: Dr Sylvia Fanucchi

Co-supervisor: Dr Vanessa Meyer

June 2025

Declaration

I, Jessica Sarah Hurwitz, 2232089, am a student registered for the degree of Masters of Science (MSc) by dissertation at the University of the Witwatersrand, in the academic year 2025.

I hereby declare the following:

- I am aware that plagiarism is wrong.
- I confirm that the work submitted for assessment for the above degree is my own unaided work except where explicitly indicated otherwise.
- I have not submitted this work before for any other degree or examination at this or any other university.
- The information used in the Dissertation has not been obtained by me while employed by, or working under the aegis of, any person or organisation other than the University.
- I have followed the required conventions in referencing the work of others.
- I understand that the University of the Witwatersrand may take disciplinary action against me if there is evidence that this is not my own unaided work or that I have failed to acknowledge the source of the ideas or words in my writing.

Jessica Sarah Hurwitz 07/06/2025

Abstract

Forkhead box P3 (FOXP3) is a transcription factor that is essential in the differentiation of T cells into regulatory T cells (Tregs), which play a critical role in regulating the adaptive immune system. FOXP3 expression is in turn regulated by the vitamin D receptor (VDR) and its ligand, 1,25-dihydroxyvitamin D_3 (1,25(OH)D_3). VDR is a transcription factor with a diverse range of functions, including immune regulation. However, whether these two proteins cooperatively regulate the immune system through direct interaction following FOXP3 expression is yet unknown. This study aimed to determine whether the VDR ligand binding domain (LBD) and the DNA-binding forkhead domain (FHD) of FOXP3 interact in the presence and absence of 1,25(OH)D_3. Computational and experimental interaction studies were performed for cross-verification. An *in silico* study was done using LZerd and HDock to predict if the LBD of VDR interacted with the FHD of FOXP3 in the presence and absence of 1,25(OH)D_3. For the experimental studies, these domains were thus overexpressed in *E. coli* cells, purified using immobilised metal affinity chromatography, and were then structurally and functionally characterised. After successful overexpression and purification, the interaction was further studied *in vitro* using fluorescence anisotropy. VDR LBD was found to interact at helix 3 (the DNA binding helix) of FOXP3 FHD *in silico* when both in the presence and absence of 1,25(OH)D_3. Additionally, VDR LBD and FOXP3 FHD were found to interact *in vitro* only in the presence of 1,25(OH)D_3 with a K_d of 0.2 µM. No interaction occurred in the absence of 1,25(OH)D_3 *in vitro*. Thus, a medium affinity protein-protein interaction between the two immune regulatory proteins, VDR LBD and FOXP3 FHD, was discovered for the first time in this study, and 1,25(OH)D_3 was identified as being a key player in this interaction, furthering our understanding of their important role in the coregulation of the immune system.

Acknowledgments

I would like to extend my gratitude to my supervisors, Dr Sylvia Fanucchi and Dr Vanessa Meyer. Thank you for your support, encouragement and belief in me throughout this whole journey. Your knowledge and generosity to share your wisdom knows no bounds. Thank you for giving me the freedom to pursue my ideas, to make mistakes, and to learn from them.

To my graduate advisor, Professor Yasien Sayed, thank you for having an open-door policy and always encouraging the expansion of knowledge. I am grateful for all our conversations in the hallway and all the mini lectures from you in journal club on Fridays. Thank you to Professor Ikechukwu Achilonu for your insight throughout my project, especially with my protein expression.

Thank you so much to all the members of the PSFRU past and present, each one of you helped along the way with my project. A special thanks to Keiran McInnes, Alicia Joshua, Jessica Brothwell, Raymond Hartman, Dr Olamide Jeje, Tebogo Mokoto, and Dr Olalekan Onisuru.

I am grateful to the students of Dr Meyer's lab for imparting your knowledge on cell culture, it was not wasted. Thank you to Janet Wasinda, Prumohdya Dana Reddy, Kiara Naidoo, Caitlyn Chetty, and Nikita Nightingale.

Thank you to the University of Witwatersrand for providing me with the opportunity and the means to pursue my MSc degree.

Finally, a very special thank you to my Mom, Dad and Thomas for supporting me throughout this degree, through the good times and the hard times.

Table of Contents

List of Tables

List of Figures

List of Equations

Abbreviations

1,25(OH)D_3	1,25-dihydroxyvitamin D_3
AF1	Activation function 1
AF2	Activation function 2
B_{max}	Maximum observed binding
CD	Circular dichroism
DFIRE	Distance-scaled, finite ideal-gas reference
DNA	Deoxyribonucleic acid
DTT	Dithiothreitol
EDTA	Ethylenediaminetetraacetic acid
EMSA	Electrophoretic mobility shift assay
FHD	Forkhead domain
FOX	Forkhead box
FOXP	Forkhead box P
FOXP3	Forkhead box P3
GOAP	Generalised orientation-dependent, all-atom statistical potential
H	Helix
IEC	Ion exchange chromatography
IMAC	Immobilised metal affinity chromatography
IPEX	Immune dysregulation, polyendocrinopathy, enteropathy, and X-linked syndrome
IPTG	Isopropyl β-d-1-thiogalactopyranoside
K_d	Dissociation constant
LB	Lysogeny broth
LBD	Ligand binding domain
MRE	Mean residue ellipticity
NFAT	Nuclear factor of activated T cells
Ni^{2+}	Nickel
NR	Nuclear receptor
OD_{600}	Optical density at 600 nm
PBS	Phosphate buffered saline
PDB	Protein data bank

pET11a	Bacterial recombinant protein vector 11a
pMB1	Plasmid replicon
PMSF	Phenylmethylsulfonyl
RMSD	Root mean square deviation
RNA	Ribonucleic acid
rpm	Revolutions per minute
RXR	Retinoic acid receptor
SDS-PAGE	Sodium dodecyl sulphate polyacrylamide gel electrophoresis
SEC	Size exclusion chromatography
SOC	Super optimal broth with catabolite repression
TAE	Tris-acetate, Ethylenediaminetetraacetic acid
TB	Terrific broth
TCEP	Tris(2-carboxyethyl)phosphine
TEMED	Tetramethylethylenediamine
Tregs	Regulatory T cells
UV	Ultra-violet
V_0	Void volume
VDR	Vitamin D receptor
V_e	Elution volume
YT	Yeast extract tryptone

Chapter 1: Background and rationale

1.1 Immune system

The immune system consists of cells, tissues, and their soluble products, which all work together to recognise and fight off foreign pathogens that pose a threat to the individual's health (Delves and Roitt., 2000). Immunity is a complex process in which components of the immune system coordinate to prevent infections, eradicate existing infections, and then shut down once the threat has passed (Delves and Roitt., 2000). The immune system is made up of two parts, innate and adaptive , and they respond in a continuum to provide a strong defence for the body against foreign pathogens (Parkin and Cohen, 2001).

Cells of the immune system develop from a common progenitor, haematopoietic stem cells, through the process of haematopoiesis in the bone marrow (Figure 1.1) (Andrews, 1998; Balistreri et al., 2019). By cytokine stimulus, haematopoietic cells initially form haematopoietic and lymphocyte progenitors which then mature into leukocytes and lymphocytes through contact signals triggering the expression of certain cell surface antigens. Haematopoietic progenitors differentiate into innate immune system cells such as granulocytes, macrophages and dendritic cells, while natural killer, B and T cells differentiate from lymphocyte progenitors. Both T and B cells develop in the bone marrow, with T cells requiring extra influence from the thymus, completing their maturation there (Hardy and Hayakawa, 2001; Kumar et al., 2018). The bone marrow and thymus form the central lymphoid system (Tompkins and Howard, 2010). Lymphocytes need to encounter an antigen to trigger their differentiation into their antigen-specific lymphocyte and induce proliferation, which takes place in the peripheral lymphoid system such as the spleen and mucosal associated lymphoid tissue (Hardy and Hayakawa, 2001; Kumar et al., 2018).

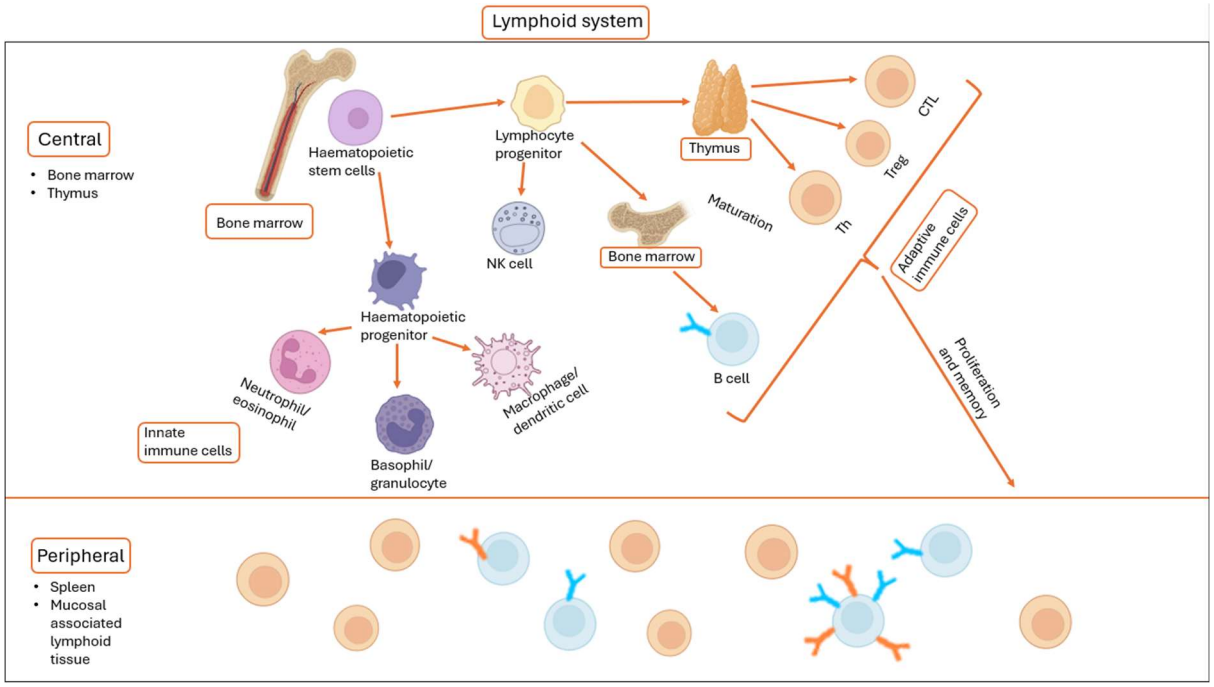

Figure 1.1. The development of immune cells through haematopoiesis in the lymphoid system. Haematopoiesis begins in the bone marrow of the central lymphoid system from haematopoietic stem cells. These differentiate into haematopoietic and lymphocyte progenitors. Within the bone marrow, haematopoietic progenitors differentiate into cells of the innate immune system, such as neutrophils, basophils, eosinophils, granulocytes, macrophages and dendritic cells. Another type of innate immune system cell, natural killer (NK) cells are also generated in the bone marrow through lymphocyte progenitors. Adaptive immune cells differentiate from lymphocyte progenitors. B cells differentiate in the bone marrow, while different T cells differentiate within the thymus. They differentiate into T helper cells (Th), Treg, and cytotoxic T lymphocytes (CTL). Once specific antigens are encountered, cells of the adaptive immune response, such as T and B cells, proliferate in tissues of the peripheral lymphoid system, such as the spleen or mucosal associated lymphoid tissue, and memory T and B cells are also formed in the peripheral lymphoid system. Created using Biorender.com.

Innate immunity mediates a rapid, non-specific response to infection, as the first line of defence (Turvey and Broide, 2010). It acts within the first few hours to days after infection, before adaptive immunity. The mechanisms of innate immunity are in place before infection occurs, allowing for immediate response to invading pathogens. It consists of barrier defence, compliment activation, pattern recognition by pattern recognition receptors, inflammation, phagocytosis, and target cell lysis (Figure 1.2). These responses are specific for structures that are common to groups of related pathogens; however, unlike adaptive immunity, fine differences between pathogens cannot be identified. As a result of non-specificity, no induction is required (Parkin and Cohen, 2001).

The barrier defences of the innate immune system consist of anatomical and physiological barriers. Anatomical barriers include intact skin, mucous membranes, or conjunctiva of the eyes. While the physiological barriers include the low pH in the stomach, hydrolytic enzymes present in body secretions, commensal organisms, and the flushing of the urinary tract (Figure 1.2). If the barrier defence is insufficient, the other innate defences activate (Hazlett and Wu, 2011).

The complement is a system of grouped enzymes that circulate in the blood innately in an inactive state. They get activated through signals from both the innate and adaptive immune system and contribute to fighting infections. Only when all these barriers are breached, do cells of the innate immune system (leukocytes) activate (Parkin and Cohen, 2001).

Innate immune cells have cell surface receptors called pattern recognition receptors that recognise pathogen- and damage- associated molecular patterns. The former are general antigens that come from pathogens, while the latter are antigens that come from damaged host cells that are either tumorigenic or infected with pathogens (Beutler, 2004). Antigens are specific peptides that are recognised by cells and products of the immune system and to which the immune system responds (Sam-Yellowe, 2021). When these patterns are recognised, inflammation, phagocytosis, or target cell lysis are triggered (Stossel, 1974; Tosi, 2005; Turvey and Broide, 2010).

Inflammation is caused by an accumulation of leukocytes at an extravascular site of a wound or infection. When pattern recognition receptors recognise pathogens, an intracellular signal transduction cascade is induced, allowing for the synthesis of pro-inflammatory cytokines, causing the pro-inflammatory process (Turvey and Broide, 2010). Cytokines are signals emitted by cells of the immune system to trigger response from other members of the immune system, causing inflammation (Figure 1.2) (Dinarello, 2000). During inflammation, cytokines will call on innate immune cells such as granulocytes and, if necessary, adaptive immune cells, to the site of injury or infection (Turvey and Broide, 2010). Granulocytes are short-lived cells of the innate immune system produced only during an immune response and migrate to the site of infection or injury (Dinarello, 2000). If the immune system fails to resolve the infection, chronic inflammation may occur which is pathological and could lead to tissue damage and immune system impairment (Lawrence and Gilroy, 2007).

Phagocytosis is carried out by leukocytes of the innate immune system such as neutrophils, macrophages, and dendritic cells. Neutrophils engulf only pathogens, while macrophages and dendritic cells engulf pathogens, dead host cells, as well as cellular debris and host macromolecules. Through phagocytosis, these leukocytes break down the cellular material or pathogens engulfed, and present unique antigens from the material on the major histocompatibility complex on their cell surface. These antigens that are presented can be recognised by cells of both the innate (natural killer cells) and adaptive immune system (Figure 1.2). Recognition of the specific antigens on the major histocompatibility complex is necessary for lymphocytes of the adaptive immune response to become activated and mediate antigen-specific attack (Stossel, 1974).

Target cell lysis is carried out by neutrophils, macrophages, and natural killer cells (Figure 1.2). Cells of the individual that pose a threat to the health of an individual, such as cancer cells or cells infected

with intracellular pathogens, express certain damage- and pattern-associated molecular patterns on their major histocompatibility complex on their cell surface. These molecules get recognised by the pattern recognition receptors of innate leukocytes, causing them to lyse the cancer or infected cell, in order to prevent further spread to the rest of the body (Tosi, 2005).

Adaptive immunity takes longer to become activated, but is more potent, self-tolerant, specific, and includes memory, having a more rapid response when the same pathogen is encountered the following time (Bonilla and Oettgen, 2010). When the innate immune system fails to irradicate infection on its own, it signals to the adaptive immune system (Figure 1.2). Cells of the adaptive immune system are lymphocytes, specifically T and B cells and their products, antibodies. Lymphocytes reside in tissues and specialised organs, as well as move around the body through the blood circulation and the lymphatic system. Lymphocytes express highly diverse receptors on their cell surface that recognise many different antigens (Honju and Habu, 1985; Hardy and Hayakawa, 2001; Bonilla and Oettgen, 2010; Kumar et al., 2018).

Humoral immunity is mediated by B lymphocytes and includes antibodies produced by B cells (Hardy and Hayakawa, 2001). Antibodies neutralise infections and target pathogens for elimination by phagocytes and the complement system. They recognise extracellular pathogens (Figure 1.2). Cell-mediated immunity on the other hand, is mediated by T lymphocytes and these cells only recognise pathogen antigens that are bound to host major histocompatibility complex. This is known as antigen presentation and recognition (Figure 1.2) (Bonilla and Oettgen, 2010). T lymphocytes include helper T cells, cytotoxic T lymphocytes and regulatory T cells (Tregs). Helper T cells secrete cytokines to alert other members of the immune system of infection and to recruit them to fight the infection. Cytotoxic T lymphocytes produce molecules that cause lysis of infected cells. Tregs inhibit the immune response through suppressing other lymphocytes, thus providing a means of regulation (Andersen et al., 2006; Luckheeram et al., 2012; Mijnheer et al., 2021).

Adaptive immunity is highly specific, and this is determined by the antigen recognition receptors present on the cell surface of T and B lymphocytes, T cell receptors and B cell receptors, respectively (Bonilla and Oettgen, 2010). When these receptors interact with the specific antigen, the lymphocyte is triggered to become activated. Clonal expansion occurs when an antigen is presented to antigen-specific lymphocytes, causing proliferation of the lymphocyte (Figure 1.2). Lymphocytes have huge diversity in the genetic code for T cell receptors and B cell receptors, giving them the ability to recognise large numbers of antigens (Hardy and Hayakawa, 2001; Kumar et al., 2018).

Adaptive immunity has memory, where an enhanced response to an antigen can be generated through previous exposure to the same antigen. This is known as secondary immune response and

triggers a faster, more effective immune response than the primary response, which is when the antigen is encountered for the first time. Memory develops through the generation of memory cells specific for antigens after each exposure to that antigen (Bonilla and Oettgen, 2010).

Adaptive immunity has self-tolerance, where cells of the immune system can recognise, respond to, and eliminate foreign antigens also known as non-self-antigens, presented on the major histocompatibility complex of innate immune cells, yet not react to the individual's own antigens, known as self-antigens, presented on the major histocompatibility complex of cells of the individual (Schwartz, 1989). The mechanism of self-tolerance is regulated in two ways. Central tolerance, through the elimination of lymphocytes with receptors that recognise self-antigens during early lymphocyte development. And peripheral tolerance, where lymphocytes that recognise self-antigens but were not eliminated during development, get suppressed by Tregs (Sakaguchi, 2004). When discrimination between self and non-self is dysregulated, autoimmune disorders, such as rheumatoid arthritis, multiple sclerosis, and type I diabetes arise (Sinha et al., 1990; Amrein et al., 2020).

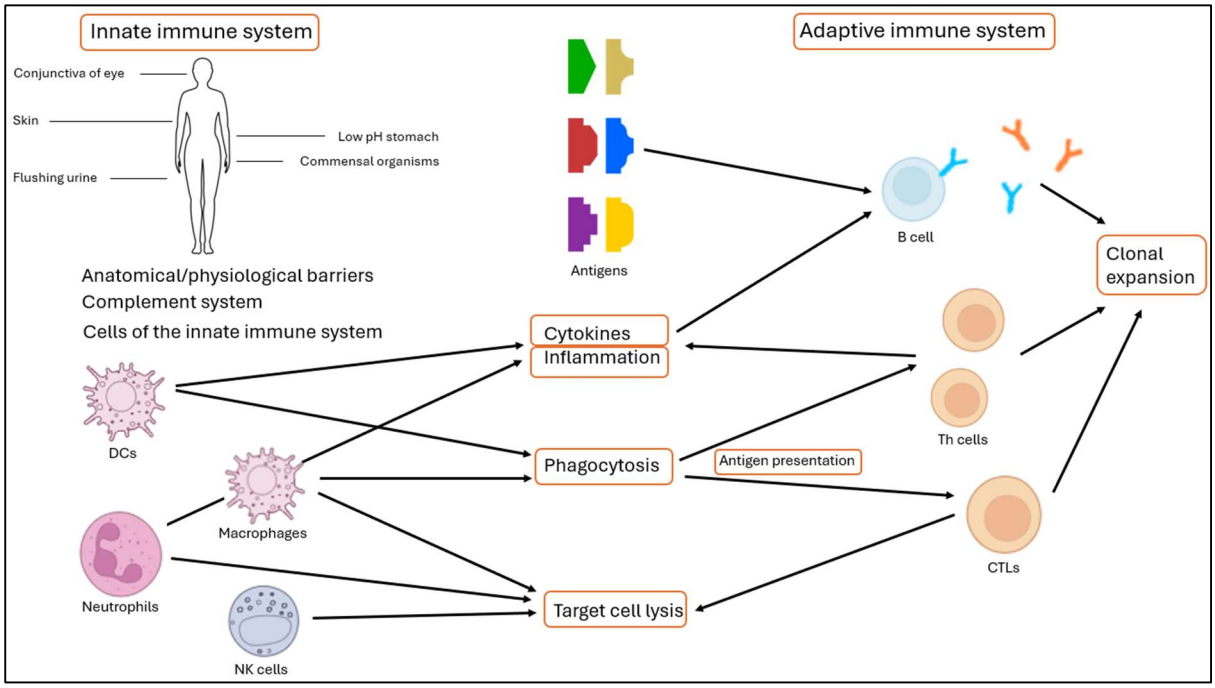

Figure 1.2. Schematic showing how the innate and adaptive immune system are interconnected. The innate immune system consists of anatomical/physiological barriers, such as conjunctiva of the eye, low pH of the stomach, the skin, flushing of urine, and commensal organisms, as well as the complement system and cells. Cells of the innate immune system such as dendritic cells and macrophages engulf pathogens in the process of phagocytosis, and then present pathogen-antigens on their cell surface. T helper (Th) cells and cytotoxic T lymphocytes recognise these antigens which triggers clonal expansion, full maturation, and memory of these cells. Dendritic cells and neutrophils of the innate immune system, as well as T cells from the adaptive immune system, release cytokines and play a role in inflammation. B cells and other cells of the adaptive immune system respond to these cytokines, as well as to extracellular antigens, and undergo clonal expansion. Cells of the innate immune system, such as neutrophils, macrophages, and natural killer (NK) cells, as well as cytotoxic T lymphocytes (CTLs) of the adaptive immune system, function in target cell lysis. Created using Biorender.com.

1.2 Regulatory T cells

All cells in the body, except red blood cells, express major histocompatibility complex molecules, presenting either self-antigens, or antigens generated via proteasomal degradation by cells of the innate immune system on their surface. T cells recognise antigen peptides on class I (cluster of differentiation 8^+ T cells) and class II (cluster of differentiation 4^+ T cells) major histocompatibility complex, presented by antigen presenting cells of the innate immune system. As mentioned, the recognition of self-antigens, known as self-tolerance, is an important aspect of the immune system, and is regulated by Tregs. The absence of self-tolerance can lead to the attack of the immune system on the body's own cells, leading to autoimmune disorders (Mijnheer et al., 2021). Treg development begins in the thymus with naive Tregs that are not fully suppressive themselves. Rather, they add to the pool of activated Tregs in the periphery, which are fully suppressive (Figure 1.3) (Kim, 2010).

Activated Tregs are Tregs that have already encountered antigens. Depending on which antigens they have encountered, their suppressive capabilities, as well as the tissue in which they reside, they have different cell surface receptors, known as memory markers. Central memory Tregs that are found in lymphoid tissues and are responsible for controlling central tolerance, express cluster of differentiation 45, C-C chemokine receptor type 7, cluster of differentiation 62L, and forkhead box P3 (FOXP3). Effector memory Tregs are found in peripheral tissues, generally where infection or inflammation is present, and are responsible for controlling peripheral tolerance. They also express cluster of differentiation 45, C-C chemokine receptor type 7, and cluster of differentiation 62L, with additional expression of cytotoxic T-lymphocyte-associated protein 4, cluster of differentiation 39, and cluster of differentiation 73. All Tregs are known to express cluster of differentiation 4 and cluster of differentiation 25 (Walker et al., 2005). Both naïve, and memory Tregs, are required to maintain self-tolerance and, in that manner, prevent autoimmune diseases (Kim, 2010). During the final stages of lymphocyte maturation, immature T cells that convey strong antigen recognition will undergo negative selection and cell death by Tregs. Tregs suppress T cells with strong antigen recognition through the release of cytokines such as interleukin 10 and transforming growth factor beta. Cell death of these strong antigen recognition T cells is necessary because they will have higher likelihood of not distinguishing between self and non-self and will attack cells that present self-antigens. Immature T cells with weak antigen recognition will survive in the process of positive selection, and will become mature T cells (Wilson, 1991). If this process of positive and negative selection is dysregulated, autoimmunity occurs (Mijnheer et al., 2021). This suppressive function of Tregs has therapeutic potential for autoimmune disorders.

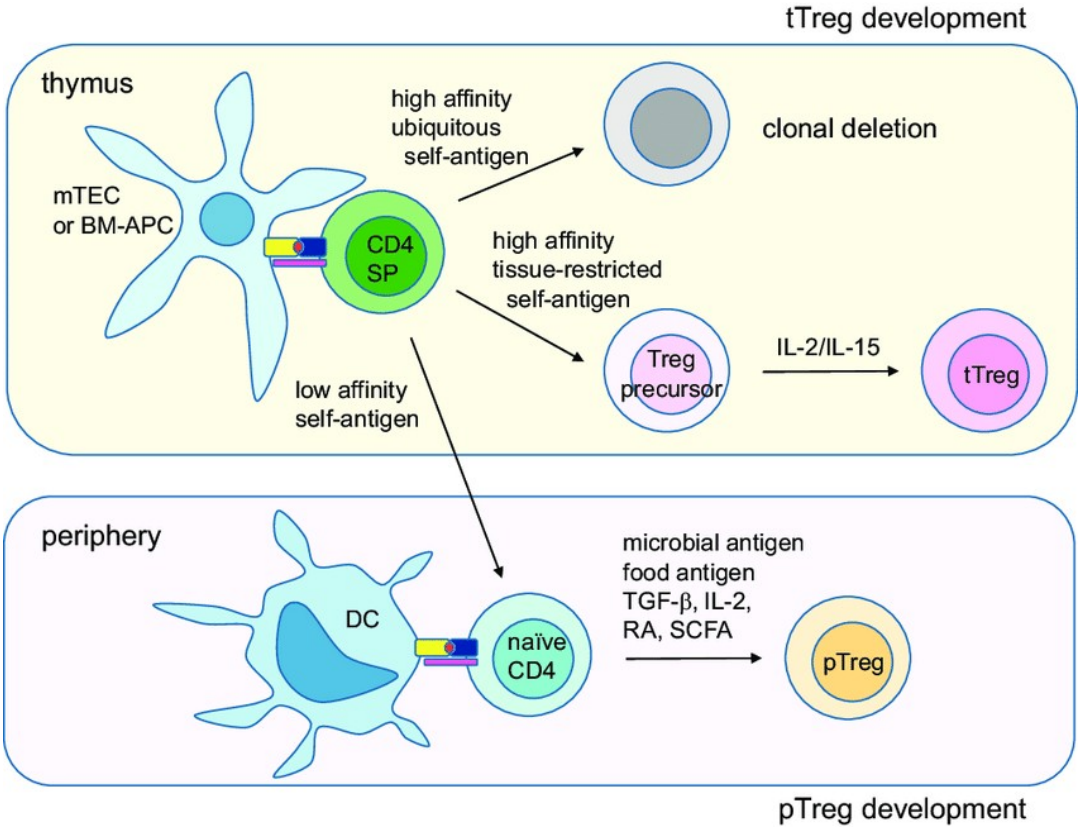

Figure 1.3. Development and differentiation of Treg cells. Treg cells can develop in the thymus (top image) or the periphery (bottom image). tTregs originate and mature in the thymus. When a CD4+ T cell interacts with medullary thymic epithelial cells or bone marrow-derived antigen presenting cells, showing suppressive activity, it will become a Treg precursor. With the expression of IL-2 and IL-15, the Treg precursor matures into a fully suppressive tTreg. In the periphery, naïve Tregs that are formed in the thymus encounter dendritic cells, with the addition of TGF-β, IL-2, RA, and SCFA, the naive Treg matures into a fully suppressive pTreg with memory markers (Diagram from Lee and Lee, 2018).

FOXP3 is the main driver of Treg differentiation from normal T helper cells and is expressed in both naïve and memory Tregs (Fontenot et al., 2003; Hori et al., 2003; Khattri et al., 2003). FOXP3 interacts with multiple transcription factors and adaptor proteins to regulate Treg differentiation, and its own expression is controlled by retinoic acid and transforming growth factor I, as well as by the vitamin D receptor (VDR) and its ligand, 1,25-dihydroxyvitamin D_3 (1,25(OH)D_3) (Bettelli et al., 2006; Kim, 2010; Bandukwala et al., 2011; Kang et al., 2012). FOXP3 and the proteins and molecules that regulate its expression are therefore essential in immune regulation.

1.2.1 FOXP3 function in Tregs

The development and function of Tregs is regulated by FOXP3 (Song et al., 2012). It does this by either repressing or activating expression of certain proteins involved in the functioning of Treg cells (Song et al., 2012). For example, FOXP3 is known to suppress the expression of nuclear factor of activated T cells (NFAT) and nuclear factor kappa-light-chain-enhancer of activated B cells, interleukin 2 in T cells and effector T cell cytokines (Song et al., 2012). Nuclear factor kappa-light-chain-enhancer of activated

B cells participates in the immune response in terms of apoptosis, preventing carcinogenesis, and increasing inflammatory response to infection. When it is suppressed, these immune responses are stopped (Dąbek et al., 2010). Examples of FOXP3 activated target genes include cluster of differentiation 25, glucocorticoid-induced tumour necrosis factor receptor related protein, cytotoxic T lymphocyte-associated antigen, and folate receptor 4 (Song et al., 2012). Glucocorticoid-induced tumour necrosis factor receptor related protein enhances the regulatory function of Tregs by inducing cytokines that control the activation of Tregs at the site of infection (Azuma, 2010). High levels of cluster of differentiation 25 induced by FOXP3 are involved in the capture of interleukin 2, making it unavailable to T cells. This, in combination with FOXP3 suppression of interleukin 2 in T cells, helps to suppress the immune response (MacKey-Cushman et al., 2011).

Mutations in FOXP3 have been noted to cause immune dysregulation polyendocrinopathy enteropathy X-linked syndrome (IPEX) in humans, a fatal autoimmune disorder characterised by an increased immune response (Bennett et al., 2001; Barzaghi et al., 2012). Children with IPEX disorder have a predisposition to developing diseases such as sepsis, pneumonia, and meningitis, generally leading to fatality in less than two years (Godfrey et al., 1991; Barzaghi et al., 2012). Because FOXP3 expression is regulated by VDR and 1,25(OH)D_3, VDR is notably involved in Treg differentiation (Kang et al., 2012).

1.2.2 VDR and 1,25(OH)D_3 function in Tregs

VDR is a transcription factor that has been noted to affect the activity of Tregs (Yang et al., 2013). It is expressed in most cells, including immune cells, such as monocytes, neutrophiles, dendritic cells and, of interest here, Tregs, as well as non-immune cells, such as fibroblasts, keratinocytes, and some cardiovascular cells (Okamoto and Koeffler, 2011; Pike et al., 2017). VDR specifically plays a regulatory role in immunity (Yuan et al., 2007; Kang et al., 2012). Lu et al., 2017, suggested that VDR regulates the differentiation of T cells to Treg cells through its association with FOXP3. The expression of VDR prevents naïve T cells from differentiating into T helper cells, and instead causes them to differentiate into Treg cells, thereby inhibiting the proliferation of effector T cells (Lu et al., 2017). In addition to VDR expression affecting T cells, 1,25(OH)D_3, has also been found to have an inhibitory effect on T cells, resulting in inhibition of the proinflammatory process (Veldman et al., 2000). It is suggested that this inhibitory effect is caused by 1,25(OH)D_3 binding to VDR and increasing the activity of Treg cells (Veldman et al., 2000). This is because when VDR is bound to 1,25(OH)D_3, the expression of FOXP3 is upregulated in Tregs (Kang et al., 2012). There is a vitamin D response element in the promoter element of the gene that codes for FOXP3 (*foxp3* gene) and therefore VDR can bind *foxp3* and regulate its expression (Hsieh et al., 1995; Kang et al., 2012). Indeed, multiple autoimmune disorders have been linked to 1,25(OH)D_3 deficiency, including systemic lupus erythematosus and rheumatoid arthritis

(Yang et al., 2013). Individuals with hereditary 1,25(OH)D_3 resistant rickets have been found to have mutations in VDR (Issa et al., 1998).

1.3 Transcription factors

Every cell in the body contains the same set of genes, but the genes are not all expressed in the same way (Latchman, 1997). For cells to acquire unique features and differentiate to form tissues with unique functions, transcription needs to be regulated in a cell-type specific manner. This regulation is brought about by a specific group of proteins known as transcription factors (Latchman, 1997).

To carry out their function, transcription factors are suited with multiple domains, generally facilitating both protein-deoxyribonucleic acid (DNA) and protein-protein interactions (Lefebvre et al., 2007). Protein-DNA interaction allows transcription factors to bind the enhancer or silencer regions on the DNA, thereby allowing regulation of the expression of the specific genes (Jolma et al., 2013). The ability of transcription factors to interact with DNA is shared between all transcription factors (Inukai et al., 2017). Hydrogen bonds form between the side chains of the transcription factor amino acids, and the bases of either the DNA major or minor groove with which the transcription factor is interacting (Jolma et al., 2013). The geometry and the number of hydrogen bonds that occur at this interface determines the specificity of the protein-DNA interaction (Coulocheri et al., 2007; Jolma et al., 2013). Protein-protein interactions enable crosstalk between the enhancer or silencer and the promoter, which modulates the ribonucleic acid (RNA) polymerase II binding, and therefore gene expression (Wan et al., 2019). Protein-protein interactions can be facilitated by either covalent or non-covalent bonds with non-covalent interactions being weaker and therefore transient, allowing dissociation and reassociation of complexes, necessary for regulation (Westermarck et al., 2013).

Transcription factors can be transcription activators or repressors (Latchman, 1997). Transcription activators bind enhancer regions, increasing the level of gene expression, and transcription repressors bind silencer regions, decreasing, or switching off, gene expression (Latchman, 1997). Transcriptional repressors carry out their function either by binding to specific regulatory sequences in the DNA, binding competitively to the DNA binding site of the transcriptional activator for that gene, binding directly to the transcription activator in its activation domain, or by interacting with components in the pre-initiation complex (Olins and Olins, 2003). Transcriptional activators function by either interacting with the pre-initiation complex or co-activators (Olins and Olins, 2003). Certain transcription factors can be both activators and repressors, such as FOXP3 and VDR (Song et al., 2012; Yang et al., 2013). The mechanism of action of a transcription factor may differ depending on the consensus sequence it interacts with, and the cell type in which the transcription factor is expressed

(Cowell, 1994). Two very important transcription factors in Tregs, and therefore immune regulation, are FOXP3 and VDR (Song et al., 2012; Yang et al., 2013).

1.4 FOXP3

1.4.1 FOX family

FOXP3 is part of the forkhead box (FOX) proteins. FOX proteins are a family of transcription factors that regulate a diverse range of processes related to development and immunity and can act as transcriptional repressors or activators (Lehmann et al., 2003). They are involved in early development of tissues from all three germ layers, as well as in the establishment of the body axis (Lehmann et al., 2003). Therefore, they are important for the formation of a variety of organs (Lehmann et al., 2003). FOX proteins are found in multiple species ranging from yeasts to humans (Alvarez et al., 2001). As well as being regulators of development, FOX proteins have also been found to be involved in tumorigenesis and cell cycle control (Hillion et al., 1997; Alvarez et al., 2001) .

All FOX proteins share similar structural features, falling under the winged helix class of transcription factors, containing a DNA binding domain of approximately 100 residues in length (Clark et al., 1993). This DNA binding domain is called the forkhead domain (FHD), which gives the FOX proteins their name (Clark et al., 1993). It consists of three alpha helices flanked by beta strands that are connected by an arrangement of loops (Roy and Kundu, 2021). Helix 3 in the FOX protein FHD is the helix that binds with the major groove of DNA during transcriptional activity of all FOX proteins (Friedman and Kaestner, 2006). In the family of FOX proteins there are 17 subclasses or clades, ranging from A to Q, with forkhead box P (FOXP) being involved in tissue development, and specifically FOXP3, in immune regulation (Kaestner et al., 2000). In all these subclasses, the sequence of amino acids in the FHD is conserved across species (Kaestner et al., 2000).

1.4.2 FOXP subfamily

FOXPs have multiple domains, a leucine zipper region, an FHD, a zinc finger domain, and an N-terminal repressor domain. The leucine zipper and zinc finger domains facilitate dimerisation and oligomerisation of FOXPs either with themselves or other proteins (Figure 1.4A). The FHD is involved in DNA binding (Clark et al., 1993). Most FOXPs contain a glutamine-rich region, while FOXP3 has a proline-rich region (Clark et al., 1993). These glutamine/proline-rich regions facilitate protein-protein interactions, enabling FOXPs to act as transcriptional repressors or activators. To perform transcriptional activity, the FHD naturally undergoes domain swapping, leading to the formation of a domain swapped, or head-to-head, dimer (Stroud et al., 2006; Chen et al., 2015). In forming this structure, monomers exchange and subsequently intertwine their structural elements (Bandukwala et al., 2011). While both FHD monomers contribute structural elements, the dimer functions as a

single unit (Yang et al., 2004). There are four members of the FOXP subfamily, namely FOXP1-4. FOXP1 is involved in brain and lung development, tumour suppression, and B cell development (Banham et al., 2001; Ferland et al., 2003; Hu et al., 2006; Shu et al., 2007). FOXP2 is involved in early embryonic development and is seen to be expressed in neural, cardiovascular, and intestinal tissues (Shu et al., 2007). FOXP4 has been implicated in kidney and prostate cancer (Teufel et al., 2003; Long et al., 2012), while FOXP3 is specifically involved in immune regulation, being a marker of Treg cell differentiation (Bennett et al., 2001; Brunkow et al., 2001).

1.4.3 FOXP3 structure

Being part of the FOXP subfamily, the structure of FOXP3 is made up of multiple domains, including the leucine zipper domain and the FHD (Yang et al., 2004). Both domains are essential for dimerisation of FOXP3 which is necessary for its transcriptional activity (Chae et al., 2006; Bandukwala et al., 2011; Perumal et al., 2024) . Contrary to other members of the FOXP subfamily, the FHD of FOXP3 exists solely as a dimer, due to its domain swapping being stabilised not only by the proline, alanine substitution at residue 372, but also by a substitution of tyrosine with phenylalanine at residue 373 (Bandukwala et al., 2011; Perumal et al., 2015). Additionally, domain swapping is what allows FOXP3 FHD to bind to two separate DNA sites by allowing the chromatin to loop, bringing distant regions of the genome physically closer in proximity and activating or repressing transcription of the gene of interest (Figure 1.4B) (Bandukwala et al., 2011; Chen et al., 2015). *In vivo*, mutations in the leucine zipper domain have been noted to associate with autoimmune diseases by disrupting FOXP3 dimerisation, which reduces the ability of FOXP3 to bind to promoter regions of genes to regulate their expression (Chae et al., 2006).

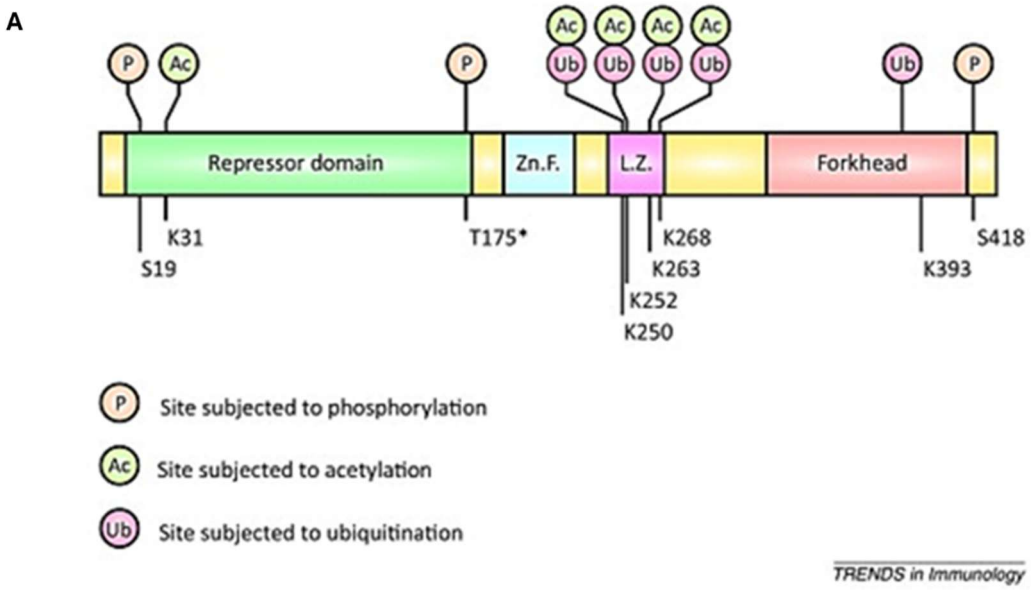

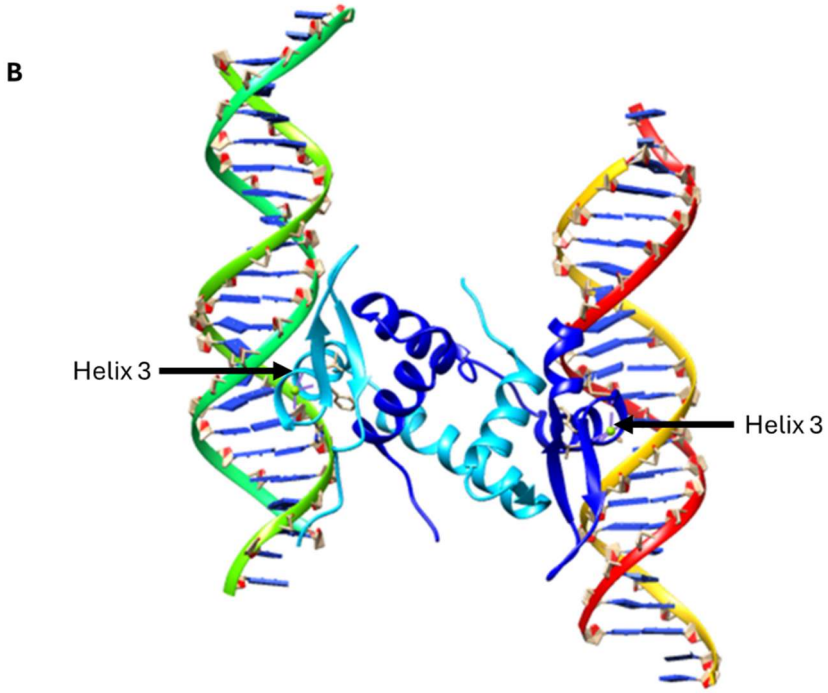

Figure 1.4. The structure of FOXP3 FHD. A: Domain structure diagram for FOXP3. The green represents the repressor domain, the red the DNA binding forkhead domain, the purple represents the dimerisation domain characterised by leucine zipper, and the blue represents the zinc finger domain. S19, T175, and S418 are sites of phosphorylation. K31 is a site of acetylation. K393 is a site of ubiquitination. And K250, K252, K263, and K268 are sites of ubiqitination and acetylation. Diagram from van Loosdregt and Coffer, 2014. *B: The PDB structure of FOXP3 forkhead domain bound to DNA. The forkhead domain forms a head-to-head homodimer, where the monomers are indicated by light and dark blue. This allows it to bind to two strands of DNA, indicated by the green, red and yellow DNA strands. Structure from PDB, 3qrf. Figure modified from Bandukwala et al., 2011 using Chimera 1.16.*

1.5 VDR and 1,25(OH)D_3

1.5.1 Nuclear receptor family

The vitamin D receptor is a nuclear receptor from the steroid/retinoid/thyroid hormone receptor superfamily (Hsieh et al., 1995). Proteins of this family are regulated not only by specific steroids, retinoids, and thyroid hormones, but also by corepressors and coactivators, as well as other regulatory proteins (Mangelsdorf et al., 1995; Oñate et al., 1995; Plevin et al., 2005). Contrary to other intercellular messengers, which act via binding to cell surface receptors, ligands for nuclear receptors can enter the cell and directly interact with their receptors (Mangelsdorf et al., 1995). Nuclear receptors recognise sequences in the genome known as hormone response elements (Echeverria and Picard Didier, 2010). The human genome codes for 48 nuclear receptors where the physiological relevance is very diverse, from involvement in cell proliferation to metabolism and reproduction. Additionally, their implications in pathological processes includes neurological syndromes, cancers, and autoimmune disorders (Evans, 1988; Mangelsdorf et al., 1995; Wu et al., 2011; Mazaira et al., 2018).

The general structure of nuclear receptors includes five domains, A-E, with some members having a sixth F domain (Figure 1.5) (Mangelsdorf et al., 1995). The A/B domain is at the N-terminal end and is highly variable containing distinct transactivation regions and is therefore also known as the activation function 1 (AF1) domain. The C domain contains two zinc fingers and functions as a conserved DNA binding domain. The zinc finger region of nuclear receptors mediates homodimerisation, as well as heterodimerisation with retinoid X receptor (RXR) (Yang et al., 2013). All nuclear receptors are known to form monomers, homodimers or RXR-heterodimers. The arrangement of the heterodimer closely resembles the homodimer arrangement, except that the homodimer interface has nearly perfect symmetric organisation, while that of the heterodimer is asymmetric (Germain et al., 2006). The D domain is a short region allowing localisation of the receptors in the nucleus. The E domain is a C-terminal conserved region for ligand binding, also known as the ligand binding domain (LBD) (Figure 1.6) (Rochel et al., 2000). It is the LBD that facilitates interactions of nuclear receptors to form heterodimers (Mangelsdorf et al., 1995). The activation function 2 (AF2) short helix in the LBD lies in an open conformation in the absence of ligand binding, allowing corepressors to bind (Glass and Rosenfeld, 2000). In the presence of allosterically binding ligands, its conformation changes, affecting the receptor's interaction with coactivators and corepressors (Glass and Rosenfeld, 2000). Based on the structural evolution of the DNA binding domains and ligand binding domains, there are 7 subfamilies of nuclear receptors (NR0-NR6). NR0 nuclear receptors contain only one of the conserved domains, either the DNA binding domain, or the ligand binding domain. Within subfamilies, nuclear receptors share a correlation between DNA binding and dimerisation ability but differ in their ligand-binding ability. VDR belongs to the NR1 subfamily, also known as steroid receptors (Rochel et al., 2000).

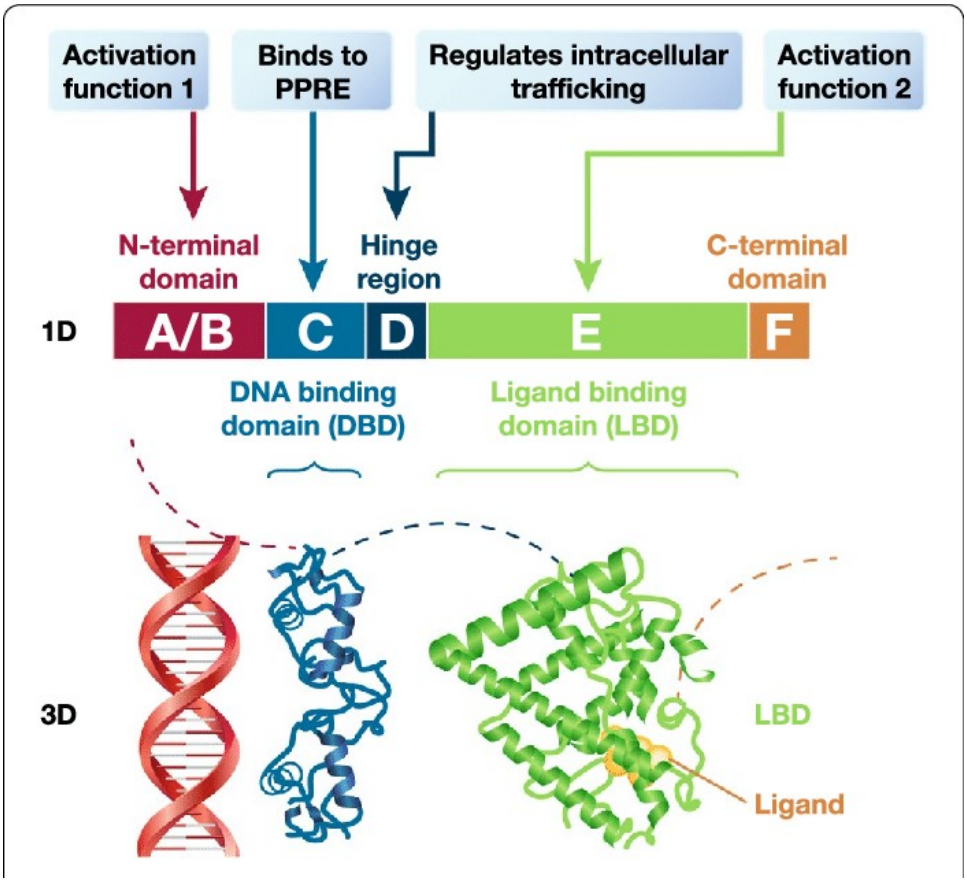

Figure 1.5. Domain structure diagram of nuclear receptors. The activation function 1 domain is represented as the A/B red domain, the DNA binding domain, C, is represented by blue and binds to PPRE, domain D is the hinge region and regulates the intracellular trafficking, the E domain is the ligand binding domain and binds the ligand, it is also known an activation function 2, some nuclear receptors have a fifth F domain shown in orange. Diagram from Fruchart et al., 2019.

1.5.2 Steroid receptors

VDR is a steroid receptor (Rochel et al., 2000). Steroid receptors reside in the nucleus. They act to repress genes in the absence of ligand through binding hormone response elements and forming a complex with corepressors (Glass and Rosenfeld, 2000). In the presence of ligand, the corepressor complexes are then dissociated and replaced with coactivator complexes, allowing for the chromatin of the hormone response elements to open, facilitating activation of genes of interest (Chen and Evans, 1995; Hörlein et al., 1995; Glass and Rosenfeld, 2000). Through interaction with other transcription factors, steroid receptors in the presence of their ligand can regulate the gene expression of composite response elements (Claessens and Gewirth, 2004).

1.5.3 VDR structure

VDR consists of a conserved DNA binding domain as part of the steroid receptors, and a ligand binding domain specific to itself. The DNA binding domain of VDR, which is characterised by terminal zinc fingers, binds vitamin D response elements that are present in genes that are regulated by VDR (Kang et al., 2012). The ligand of VDR, 1,25(OH)D_3, interacts with all residues in the β strands (Rochel et al.,

2000). Trp-286 in the β1 strand is specific to VDR and assists in the positioning the ligand (Figure 1.6) (Rochel et al., 2000). VDR in the absence of 1,25(OH)D_3, but in the presence of vitamin D response elements, forms a homodimer. As the concentration of 1,25(OH)D_3 increases in the nucleus, it causes VDR to dissociate from itself and form a monomer. The binding of 1,25(OH)D_3 to monomeric VDR allows VDR to heterodimerise with RXR and bind to vitamin D response elements (Cheskis and Freedman, 1994; Yang et al., 2013). The VDR, 1,25(OH)D_3, RXR, vitamin D response elements complex then recruits coactivators or corepressors to the gene to regulate gene expression (Yang et al., 2013). As part of nuclear receptors, VDR heterodimerisation with RXR is necessary for transcriptional activity. VDR forms homodimers with itself or heterodimers with RXR via its zinc finger domain. A highly conserved domain of VDR is found at residues 244-263, while the region responsible for RXR heterodimerisation is found at residues 325-332 and 382-402 (Yang et al., 2013). The transactivation of VDR is mediated by phosphorylation in both the LBD and the DNA binding domain at serine 208 and serine 51, respectively (Margolis and Christakos, 2010; Yang et al., 2013). VDR-mediated transcription involves transcription factor IID, TATA binding protein-associated factors, and p160 coactivators, having histone acetylase activity. Through recruitment of c-adenosine monophosphate-response element binding protein and histone methyltransferases by the p160 coactivators, a multi-subunit complex is formed. VDR-interacting protein then recruits RNA-polymerase to mediate VDR-mediated transcription. (Margolis and Christakos, 2010).

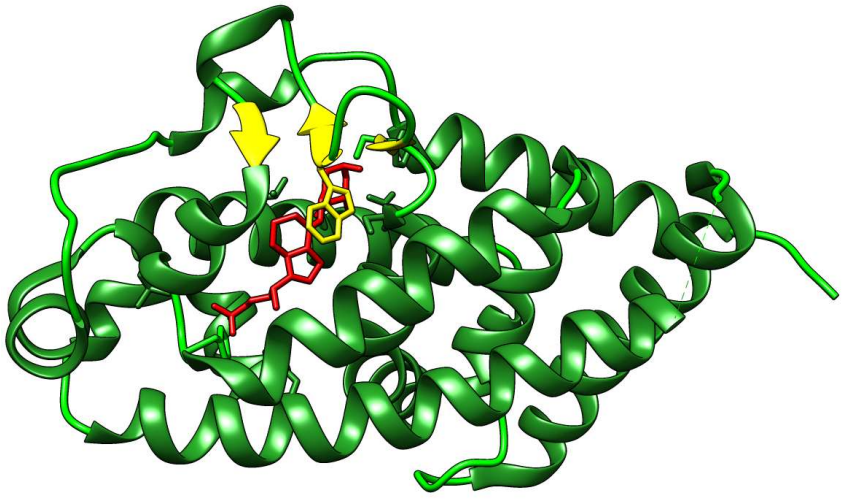

Figure 1.6. Crystal structure of the ligand binding domain of VDR. Helices are shown in dark green, beta sheets in yellow, coils in light green, and the 1,25(OH)D_3 ligand in red. Structure from PDB, 1db1 (Rochel et al., 2000), modelled using Chimera 1.16.

1.6 Association between VDR, 1,25(OH)D_3, and FOXP3

Until now, the regulation of FOXP3 expression at a gene level by VDR and 1,25(OH)D_3 has been studied and discussed. However, the possibility is there that FOXP3 and VDR, whether in the presence or

absence of 1,25(OH)D_3, also interact at a protein level. The association between VDR and FOXP3 is supported by data obtained from STRING (https://string-db.org/ version 11.5; Figure 1.13) (Szklarczyk et al., 2015). VDR and FOXP3 are therefore both functionally linked, through their combined roles in Tregs, and molecularly linked, through VDR being a transcription factor driving FOXP3 expression.

The string search results are shown in Figure 1.7. Text-mining, and experimentally determined links were found between FOXP3 and VDR with scores of 0.402 (medium confidence) and 0.062 (below low confidence), respectively. The text-mining data for associations between FOXP3 and VDR revealed associations through examining the correlation between FOXP3 levels in Tregs and Treg activity, with 1,25(OH)D_3 levels. Autoimmune encephalomyelitis mice supplemented with the VDR ligand, 1,25(OH)D_3, expressed lower levels of *Foxp3* mRNA in Tregs (de Oliveira et al., 2020). 1,25(OH)D_3 induces Tregs in the spleen, spinal cord, and lymph nodes of experimental autoimmune encephalomyelitis mice, and there is a correlation between the suppressive activity of Tregs and 1,25(OH)D_3 levels in the serum of multiple sclerosis patients (Dankers et al., 2017).

Experimentally determined interactions were only found between related proteins, forkhead box O, and nuclear receptors Ultraspiracle, and small heterodimer partner in other organisms such as *Drosophila melanogaster* and *Mus musculus* through co-localisation studies and co-immunoprecipitation pulldown assays (Wei et al., 2011; Koyama et al., 2014). No experimental interactions were noted between FOXP3 and VDR in these organisms or in *Homo sapiens*.

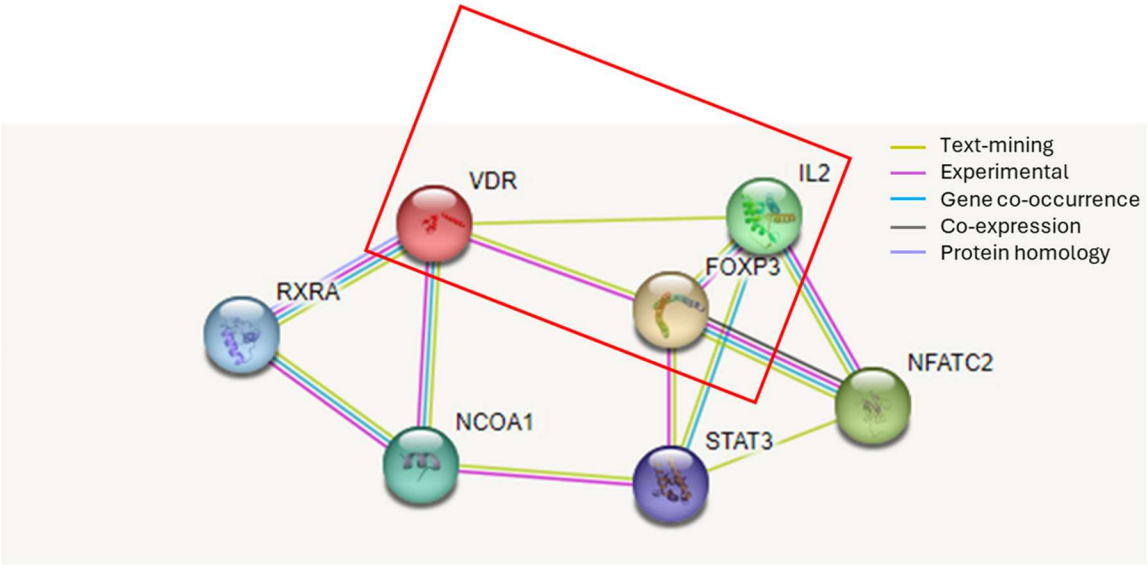

Figure 1.7. String results showing FOXP3 and VDR association. Text mining is shown in yellow and experimentally determined shown in pink. Both FOXP3 and VDR also have an association with IL2. Gene co-occurrence is represented by the blue lines. Black indicates co-expression of the proteins. STRING-DB https://string-db.org.

1.7 Rationale

Mutations in both *VDR* and *foxp3*, as well as 1,25(OH)D_3 deficiency, have been associated with various autoimmune diseases (Cantorna and Mahon, 2005; Arnson et al., 2011; Hajas et al., 2011; Holick, 2011). As seen in previous studies, there is an association between FOXP3 and VDR (Kang et al., 2012; Dankers et al., 2017; de Oliveira et al., 2020). However, this association has been proven between VDR and 1,25(OH)D_3 with the *foxp3* gene, or between FOXP3 levels in Tregs with 1,25(OH)D_3. It is not known whether FOXP3 and VDR directly interact with each other, and the impact that 1,25(OH)D_3 would have on this potential interaction. This would be a necessary key mechanism in determining the pathophysiology of autoimmune diseases.

A reductionist research approach is taken in this study by only using the two domains of the two proteins outside of a cellular environment. Within the network of immune regulation, there are so many interactions. To study only 1 interaction, the proteins needed to be isolated, and not even the whole proteins, but just the domains that are suspected to interact with each other. The specific domains, FHD of FOXP3 and LBD of VDR were chosen as a starting point in this research. Reductionist research works on the idea that by breaking studies down into their individual components, and then studying those individual parts, a better understanding of larger, more complicated networks and systems can be gained (Sarkar, 1992; Nagel, 2007). The FHD of FOXP3 is an important domain where DNA binding, and therefore transcriptional activation occurs (Bandukwala et al., 2011). The LBD of VDR is where 1,25(OH)D_3 binding occurs, and it also facilitates interactions with corepressors and coactivators (Rochel et al., 2000). To experimentally determine if the two proteins interacted with each other, they needed to be overexpressed and purified. Therefore, using domains where these protocols had already been optimised, allowed for the research to focus on the interaction between the proteins. The FHD of FOXP3 and the LBD of VDR have both been overexpressed and purified before (Rochel et al., 2000). The protocol for FOXP3 FHD has been well documented in our research Unit and therefore it could be used without optimisation, the protocol for which was kindly provided by Alicia Joshua. VDR LBD had not been overexpressed in our Unit before and therefore optimisation was required; however, it has been overexpressed successfully by others (Rochel et al., 2000) for crystallisation.

It is hypothesised that the association between VDR and FOXP3 goes beyond the gene expression level to a protein-protein level, where the LBD of VDR can further interact with the FHD of FOXP3. It is yet unknown whether 1,25(OH)D_3 binding to VDR LBD influences the interaction between the two proteins and discovering this will aid in the understanding of 1,25(OH)D_3 deficiency in autoimmune diseases. Binding of 1,25(OH)D_3 to VDR facilitates its heterodimerisation with other proteins, such as

RXR (Cheskis and Freedman, 1994). Therefore, it is hypothesised that the interaction between VDR LBD and FOXP3 FHD will only occur in the presence of 1,25(OH)D_3.

It has been proven that a decrease in FOXP3 levels is associated with a decrease in immune regulation, therefore leading to autoimmunity, as there are no cells to switch off nonself-tolerant cells or immune cells after infection (Godfrey et al., 1991; Barzaghi et al., 2012) . Because FOXP3 expression is regulated by multiple factors, including VDR and 1,25(OH)D_3, we want to find out whether VDR LBD physically interacts with the FOXP3 FHD in order to understand the role that VDR, 1,25(OH)D_3, and FOXP3 play in immune regulation (Song et al., 2012). Physical interactions between transcription factors with and without ligands can change the activity of these proteins. Both FOXP3 and VDR can act as transcriptional repressors or activators, depending on the ligands, corepressors, or coactivators interacting with them (Cheskis and Freedman, 1994; Lehmann et al., 2003). This protein-protein interaction will be tested using interaction studies such as molecular docking, and fluorescence anisotropy.

Whether these two proteins cooperatively regulate the immune system through direct protein-protein or protein-protein-ligand interaction following FOXP3 expression is yet unknown. Discovering this will aid in the understanding of these two proteins and their roles in various autoimmune disorders, which could improve the current understanding of the pathophysiology of autoimmune disorders.

1.8 Aim and objectives

To determine if the VDR ligand binding domain interacts with the FOXP3 forkhead domain in the presence or absence of 1,25(OH)D_3.

1.8.1 Objectives

1. Determine if VDR LBD is predicted to interact with FOXP3 FHD using molecular docking (*in silico*).
2. Overexpress and purify both VDR LBD and FOXP3 FHD in BL21(DE3) and T7 *Escherichia coli* cells, respectively.
3. Structurally characterise the secondary structure using far-UV circular dichroism (CD), the tertiary structure using intrinsic tryptophan fluorescence, and the quaternary structure using size exclusion chromatography (SEC) of the overexpressed and purified FOXP3 FHD and VDR LBD. Since they were expressed in *E. coli* cells, the structural integrity of these mammalian proteins needed to be confirmed.
4. Functionally characterise VDR LBD and FOXP3 FHD using thermal shift assay and electrophoretic mobility shift assay (EMSA), respectively to determine that they were in their functionally folded states after overexpression and purification.
5. Determine whether FOXP3 FHD and VDR LBD interact *in vitro* in the presence and absence of 1,25(OH)D_3 using fluorescence anisotropy.

Chapter 2: Methods

2.1 Molecular docking

To confirm if VDR LBD and FOXP3 FHD interact with each other *in silico,* molecular docking was performed. Molecular docking is used as a computational prediction tool for protein-protein interaction. Using rigid body docking, the interface of the protein-protein complex could be determined based on the structures of each of the proteins individually (Vakser, 2014). The crystal structure 1DB1 (Rochel et al., 2000) of VDR LBD bound with 1,25(OH)D_3 was taken from the protein data bank (PDB). It was then docked using HDock (Yan et al., 2020a) rigid body docking with chains F and G of the crystal structure 3QRF (Bandukwala et al., 2011) of FOXP3 FHD to predict the interface between the two protein domains. Hdock was chosen as a hybrid approach can be used, increasing the reliability of the results, and it is user-friendly (Yan et al., 2020a). HDock provided the top 10 binding models based on the docking score, where the more negative the score, the more spontaneous the interaction was predicted to be, and a confidence score of above 0.7 indicates that the interaction is likely to occur based on a shape-based pairwise scoring function based on rotations and translations (Yan et al., 2017). The 1,25(OH)D_3 was removed from 1DB1 and docking was again performed using LZerd (Christoffer et al., 2021) and HDock (Yan et al., 2020a). HDock generated the same result as with the ligand bound and therefore LZerd was used to cross-verify the results. LZerd was used for cross-verification as it takes the entire 3-dimensional shape of the proteins into consideration, which is important for protein-protein docking (Christoffer et al., 2021). The LZerd server provided the top 10 binding models based on i) Ranksum, which gives the model's overall rank based on the ranks of three knowledge-based potentials, ii) generalised orientation-dependent, all-atom statistical potential (GOAP) score, which considers distances and orientations between pairwise atom distances, iii) distance-scaled, finite ideal-gas reference (DFIRE) and iv) ITScore scores, which both consider pairwise atom distances (Christoffer et al., 2021). The top models from each server were chosen and then viewed and modelled using Chimera 1.16 (Pettersen et al., 2004). The interactions between VDR LBD and FOXP3 FHD were indicated using Tools > Structure Analysis > Find Clashes/Contacts, then designating all the atoms in chain A of 1DB1 and checking the designated atoms against all other atoms (Pettersen et al., 2004). To observe whether the presence of 1,25(OH)D_3 in the VDR LBD structure changes its conformation, and therefore whether it would affect interaction with FOXP3 FHD, as well as to observe if the predicted interaction position of FOXP3 FHD to VDR LBD would interfere with the rest of the VDR structure, the full-length VDR structure was obtained from AlphaFold 3 (Abramson et al., 2024). The full-length apo-VDR structure was superimposed with the crystal structure of VDR LBD in the presence of 1,25(OH)D_3 (1DB1) using Chimera 1.16, Tools > Structure Comparison > Matchmaker and selecting chain A of the crystal structure with which to

superimpose the full-length structure. The predicted full-length VDR structure was then docked with FOXP3 FHD (3QRF) using HDock. The docked model was validated by considering the docking score, confidence score, and ligand RMSD, and the contacts were viewed using Chimera 1.16 (Pettersen et al., 2004) as above.

2.2 Recombinant protein expression

2.2.1 Vector acquisition

Bacterial recombinant protein vector 11a (pET11a) (Figure 2.1A) was obtained from GenScript (https://www.genscript.com) for each protein. One vector contained the gene for FOXP3 FHD (Figure 2.1B) and the other for VDR LBD (Figure 2.1C) that were inserted directionally in the 5' *Nde*I and 3' *Bam*HI restriction sites. The pET11a plasmid contained a plasmid replicon (pMB1) origin which coded for 15-60 copies per cell (Dubendorfft and Studier, 1991).

A

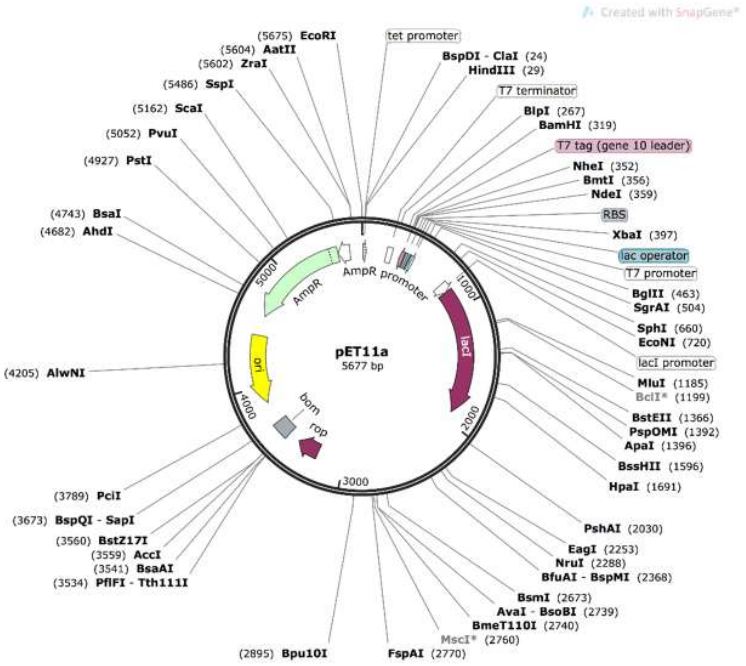

B

FOXP3 FHD

CATATGGCTAGCATGACTGGTGGACAGCAAATGGGTATGCACCATCATCATCATCATTCTTCTGGTCTGGTGCCAC
GCGGTTCTATGCGACCCCCTTTCACCTACGCCACGCTCATCCGCTGGGCCATCCTGGAGGCTCCAGAGAAGCAG
CGGACACTCAATGAGATCTACCACTGGTTCACACGCATGTTTGCCTTCTTCAGAAACCATCCTGCCACCTGGAAG
AACGCCATCCGCCACAACCTGAGTCTGCACAAGTGCTTTGTGCGGGTGGAGAGCGAGAAGGGGGCTGTGTGG
ACCGTGGATGAGCTGGAGTTCCGCAAGAAACGG

C

VDR LBD

ATGGCTTCAATGACAGGGGGACAGCAAATGGGCATGCACCACCACCACCACCACTCCAGCGGTTAGTTCCGC
GTGGTTCCGACAGCCTGCGTCCGAAATTGTCTGAGGAGCAGCAACGTATTATCGCGATCCTGTTAGATGCACATC
ACAAAACGTACGACCCGACCTACAGCGACTTTTGTCAGTTTCGTCCTCCGGTTCGTGTGAACGATGGTGGTGGC
AGCGTTACCCTGGAGCTCTCTCAGCTGTCTATGCTTCCCCACCTGGCTGACTTGGTTTCCTATAGCATTCAAAAGG
TGATTGGTTTTGCGAAGATGATCCCGGGCTTCCGCGATCTGACCAGTGAAGATCAGATTGTGCTGCTGAAGAGC
TCGGCGATTGAGGTAATCATGCTGCGTAGCAATGAGTCGTTCACCATGGATGACATGAGCTGGACGTGCGGTAA
TCAGGACTATAAATACCGCGTCAGCGACGTGACAAAAGCCGGCCATTCTTTGGAGCTGATCGAACCGCTGATCA
AATTCCAGGTTGGTCTCAAGAAGCTGAACCTGCATGAAGAAGAGCATGTTCTGCTAATGGCGATCTGCATTGTG
TCCCCGGATCGTCCGGGGGTGCAAGACGCGGCTCTGATTGAGGCCATCCAAGACAGACTTTCCAACACCCTGC
AAACCTACATTCGCTGCCGTCATCCACCGCCGGGCTCACATCTGTTATATGCAAAGATGATCCAAAAGTTGGCGG
ATTTGCGCAGCTTGAATGAAGAACACAGCAAACAGTATCGCTGCCTGTCCTTTCAGCCGGAATGTAGCATGAAA
CTGACTCCGCTGGTCCTGGAAGTGTTCGGCAACGAGATCAGC

Figure 2.1. pET11a vector construction for FOXP3 FHD and VDR LBD. A: Map of the pET11a plasmid containing ori site in yellow, AmpR site in light green, restriction enzyme site in grey, lacI region in purple with a promoter upstream. Diagram from https://www.addgene.org/vector-database/2625/. B: Codon-optimised DNA sequence of FOXP3 FHD created for recombinant vector construction. The protein sequence for the FHD of FOXP3 (residues 336-417) obtained from 3QRF from PDB, with a His-tag (purple) and a cleavage site (yellow) was reverse-translated and then the DNA sequence was codon-optimised for expression in a bacterial host. C: DNA sequence of VDR LBD created for recombinant vector construction. The protein sequence for the LBD of VDR (residues 118-427) obtained from 1DB1 from PDB, with a His-tag (purple) and a cleavage site (yellow) was reverse-translated and then the DNA sequence was codon-optimised for expression in a bacterial host.

2.2.2 Transformation

Transformation is a necessary step in cloning where the bacteria take up, and therefore are transformed with, the recombinant vector (Rosano and Ceccarelli, 2014). The pET11a vector (GenScript, USA) containing the gene coding for FOXP3 FHD was added to chemically competent T7 *E. coli* cells (New England Biolabs, USA) at a concentration of 20 ng/µL. Chemically competent BL21(DE3), BL21(DE3) plysS, and T7 *E. coli* cells (New England Biolabs, USA) were transformed with the pET11a vector containing the gene coding for the VDR LBD for expression trials in different cell lines at the same DNA concentrations. After expression trials, it was decided that for subsequent VDR LBD overexpression, the BL21(DE3) *E. coli* cells were to be used.

The heat shock method of transformation was used for all cell lines and vectors (Mandel and Higa, 1970). A control and transformed tube of cells were incubated at 0 °C for 30 minutes, then incubated at 42 °C for 45 seconds, followed by a 0 °C incubation for 5 minutes. To help the cells recover, 950 µL of super optimal broth with catabolite repression (SOC) media (0.5% yeast (Sigma-Aldrich, USA), 2% tryptone (Sigma-Aldrich, USA), 10 mM NaCl (Sigma-Aldrich, USA), 2.5 mM KCl (Lasec, Cape Town, South Africa), 10 mM $MgCl_2$ (Sigma-Aldrich, USA), 20 mM glucose (Sigma-Aldrich, USA)) was added to both control and treated cells, and they were incubated at 37 °C for 1 hour, with shaking at 220 revolutions per minute (rpm). Agar plates with 2x yeast extract tryptone (YT) media (1% yeast extract, 1.6% tryptone, and 0.5% NaCl, with 1.5% agar (Sigma-Aldrich, USA), and 0.1 mg/mL ampicillin) were streaked with T7 *E. coli* cells transformed with FOXP3 FHD. Agar plates with lysogeny broth (LB) media (0.5% yeast extract, 1% tryptone, and 1% NaCl, with 1.5% agar, and 0.01% ampicillin) were streaked with VDR LBD transformed BL21(DE3) *E. coli* cells. Glycerol stocks for each protein were prepared for subsequent overexpression with 1:1 ratio of cells to 70% glycerol (ACE chemicals, South Africa).

After transformation, the GeneJET plasmid miniprep kit (ThermoFisher Scientific, USA) was used to extract plasmid DNA. Cell suspension to a total volume of 15 mL was centrifuged for 2 minutes at 12 000 x *g* and the supernatant discarded. After which, the pelleted cells were resuspended in 250 µL of resuspension solution with RNase A (ThermoFisher, USA). Next, 250 µL of lysis solution (ThermoFisher, USA) was added to the resuspended cells and mixed thoroughly until the solution became viscous and clear. The solution was incubated for 5 minutes at room temperature, after which 350 µL of neutralisation solution (ThermoFisher, USA) was added. The solution was mixed by inversion until the lysate looked cloudy. The lysate was centrifuged for 5 minutes at 12 000 x *g* to pellet chromosomal DNA and cell debris. The supernatant was then transferred to a GeneJET spin column (ThermoFisher, USA) and centrifuged for 1 minute at 12 000 x *g*. The flow-through was discarded. Following this, 500 µL of wash solution containing ethanol was added to the column and centrifuged for 1 minute at 12 000 x *g.* After the flow-through was discarded, the wash step was then repeated. The flow-through

was discarded and the column centrifuged for 1 minute at 12 000 x g to remove any residual wash solution. The column was transferred to a fresh tube. Subsequently, 50 µL of elution buffer (ThermoFisher, USA) was added to the column and incubated for 2 minutes at room temperature. To elute plasmid DNA, the solution in the column was centrifuged for 2 minutes at 12 000 x *g*. The column was discarded and the plasmid DNA in the new tube was sent to Inqaba Biotechnology Industries, RSA for sequencing to confirm the identity of the sequence for each FOXP3 FHD and VDR LBD that the cells were transformed with.

2.2.3 Recombinant protein overexpression for FOXP3 FHD

FOXP3 FHD glycerol stock from transformation above, was added to 100 mL of 2x YT broth with ampicillin and grown for 16 hours at 37 °C with shaking at 220 rpm. The next day, 2 L of autoclaved 2x YT broth with ampicillin was inoculated with 1:30 of the cells grown overnight. The media containing the cells was grown at 37 °C with shaking at 170 rpm until the optical density at 600 nm (OD_{600}) reached 0.8 as measured on the Jasco V-730Bio UV-Vis Double Beam Spectrophotometer (Jasco, UK) (absorbance directly correlates to OD at a wavelength of 600 nm). The cells were then induced to express protein by adding 0.3 mM Isopropyl β-d-1-thiogalactopyranoside (IPTG) (Melford, UK) and incubated for 4 hours at 30 °C with 170 rpm shaking. IPTG has a dual induction mechanism. It acted as an allolactose mimic, suppressing the lac repressor both in the bacterial host genome, and in the pET11a vector downstream of the T7 promoter sequence, thereby the T7 polymerase could be expressed. This allows the process of transcription of recombinant plasmids, through T7 polymerase binding to the T7 promoter in the recombinant plasmid. The protein sequence then gets translated by the host cell machinery (Dubendorfft and Studier, 1991). After 4 hours, the cell suspension was centrifuged at 5 000 x *g* for 5 minutes at 4 °C to pellet the cells from the media, and the supernatant was discarded. The cell pellet was resuspended in equilibration buffer (20 mM Tris-HCl (Sigma-Aldrich, USA), 30 mM imidazole (Sigma-Aldrich, USA), 500 mM NaCl, pH 7.5) and stored at –20 °C until purification.

2.2.4 Recombinant protein overexpression for VDR LBD

VDR LBD had not been expressed in our Unit before, and therefore the overexpression protocol needed to be optimised. Through multiple expression trials, different conditions with varying cell lines, media, IPTG concentrations, time of induction, expression time and temperature, as well as the presence of chaperones and L-arabinose, were tested (Table 2.1).

For trials 1 and 2 (Table 2.1), BL21(DE3) *E. coli* cells were grown to an optical density at 600 nm (OD_{600}) of 0.7 at 37°C in LB media. Different IPTG concentrations for induction were tested for different expression times and temperatures. A range of IPTG concentrations between 0 and 1 mM needed to be tested. Therefore, to begin, 0, 0.2, 0.4, and 0.6 were tested based on a previous protocol in the

Unit for a different nuclear receptor (Lakhi and Fanucchi, 2024). For the third and fifth trial, a different cell line was tested: BL21(DE3) plysS *E. coli* cells in LB media (trial 3) and terrific broth (TB) media (trial 5). Different times of induction, times of expression, and IPTG concentrations were tested. The fourth trial tested another different cell line: T7 *E. coli* cells were grown to an OD_{600} of 0.7 in LB media with different IPTG concentrations and times of expression being tested. The sixth and seventh trials used chaperones to help the correct folding of VDR LBD during translation. BL21(DE3) *E. coli* cells co-transformed with pET11a vector containing the genetic code for VDR LBD, and pKJE7 vector (GenScript) containing the code for chaperones dnaJ, dnaK, and grpE, were grown in LB media containing ampicillin, 25 µg/mL chloramphenicol, and L-Arabinose to an OD_{600} 0.6. Differing IPTG and L-Arabinose concentrations, expression temperatures and times were tested. All trials had an uninduced control where no IPTG was added. Trial 8, which was used for VDR LBD overexpression and purification, was done with a 4 L culture of BL21(DE3) *E. coli* cells with the pET11a vector containing the genetic code for VDR LBD. The cells were grown to an OD_{600} 0.7 in LB media, after which, they were induced with 1 mM IPTG and expressed for 6 hours at 20°C.

Table 2.1. Expression trial conditions for VDR LBD.

Trial	Cell line (*E. coli*)	Media	[IPTG] (mM)	Time of Induction (OD_{600})	Temperature (°C)	Expression time (hours)	Chaperones	[L-arabinose] (mg/mL)
1	BL21(DE3)	LB	0, 0.2, 0.4, 0.6	0.7	20	16, 18, 20, 22, 24	No	0
2	BL21(DE3)	LB	0, 0.3, 0.5	0.7	30 20	0, 4, 6 0, 16, 20, 24	No	0
3	BL21(DE3) plysS	LB	0, 1	0.3, 0.7, 1	18	0, 16, 20, 24	No	0
4	T7	LB	0, 0.3, 1	0.7	18	0, 16, 20, 24	No	0
5	BL21(DE3) plysS	TB	0, 0.1, 0.2, 1	1	24	0, 20	No	0
6	BL21(DE3)	LB	0, 0.5	0.6	30	0, 4	Yes	0.5
7	BL21(DE3)	LB	0, 0.5	0.6	30 18	0, 4, 6 0, 16, 20, 24	Yes	0, 0.5, 4
8	BL21(DE3)	LB	1	0.7	20	6	No	0

Notes: IPTG: Isopropyl ß-d-1-thiogalactopyranoside, OD_{600}: optical density at 600 nm

The final trial which yielded the best results was used for full overexpression of VDR LBD for purification and subsequent experiments. A glycerol stock of BL21(DE3) *E. coli* cells containing the

plasmid coding for VDR LBD, was grown at 37°C for 16 hours in LB media with shaking at 220 rpm. The next day, 4 L of autoclaved LB broth with ampicillin was inoculated with the overnight cell growth at a 1:30 ratio of cell growth to media. The media containing the cells were grown at 37°C with shaking at 170 rpm until the OD_{600} reached 0.8. After which, the cells were induced with 1 mM IPTG and incubated for 6 hours at 20 °C with 170 rpm shaking. After expression, the cell suspension was centrifuged at 5000 xg for 5 minutes at 4 °C to separate the cells from the media, and the supernatant was discarded. The cell pellet was resuspended in equilibration buffer and stored at -20 °C until purification.

2.3 Purification of overexpressed FOXP3 FHD and VDR LBD

Frozen cell suspension from overexpression of each FOXP3 FHD and VDR LBD was thawed for 20 minutes, then 1 mM phenylmethylsulfonyl (PMSF) (Roche, Germany), 100 µM lysozyme (Sigma-Aldrich, USA), and 0.01 mg/mL DNase I (Merck, Germany) were added to the half-thawed lysate. PMSF was used to prevent protein degradation from bacterial cell proteases. DNase I was used to improve purification of the protein by reducing the viscosity of the lysate. With both proteins being transcription factors which bind DNA, the DNase I also ensured that the bacterial DNA was removed from the protein thereby improving its purity from contaminating DNA (James, 1978). The lysate was fully thawed for a further 20 minutes with inversion. The thawed lysate was sonicated for 10 repetitions of 3 seconds at 50% power, 5 times. Centrifugation at 18 000 x *g* for 25 minutes at 4 °C was done to pellet the cell debris, leaving the soluble overexpressed protein in the supernatant. The supernatant was filtered and then purified using immobilised metal affinity chromatography (IMAC) on the ÄKTA® start protein purification system (Sigma Aldrich, USA).

2.3.1 Immobilised metal affinity chromatography

Overexpressed FOXP3 FHD and VDR LBD were purified using a nickel (Ni^{2+}) IMAC HiTrap column (GE Healthcare, USA). IMAC is a purification technique that works by separating molecules based on their affinity to a resin containing metal ions, such as Ni^{2+}. Histidine in the poly His-tags present on the N-terminus of each of the proteins contains an imidazole ring which has high affinity to the Ni^{2+} on the IMAC column. Imidazole in histidine has a nitrogen atom which donates an electron pair to form a complex with the Ni^{2+} ion (Block et al., 2009). The column was equilibrated with 5 column volumes of equilibration buffer and then the supernatant was loaded onto the column and the flow-through was collected. The column was then subjected to a salt wash buffer (20 mM Tris-HCl, 30 mM imidazole, 1.5 M NaCl, pH 7.5) for 5 column volumes to remove any non-specific binding to the column and any DNA that might have been bound to the proteins, and fractions were collected. Equilibration buffer was again added to the column for 5 times the column volume. Elution buffer (20 mM Tris, 300 mM imidazole, 500 mM NaCl pH 7.5) was then added to the column for stepwise elution of the protein off

the column. This was done for 5 column volumes and fractions were collected at the rising of the peak, the peak, and the tail of the peak. As the soluble lysate was passed through the column, the protein tagged with the poly-His tag bound successfully to the resin, while the rest of the supernatant flowed through. The bound proteins were eluted by using a high imidazole concentration because imidazole competes for resin binding, allowing the protein to be recovered from the column (Sulkowski, 1985). Equilibration buffer was then added to the column for 5 column volumes, and then 20% ethanol for 10 column volumes in which to store the column.

2.3.2 Further purification of VDR LBD using ion exchange chromatography

IMAC purification was sufficient on its own to produce pure FOXP3 FHD; however, it was not sufficient on its own for purifying VDR LBD. To further purify VDR LBD, ion exchange chromatography (IEC) was performed. VDR LBD has a predicted pI of 6.3. Therefore, equilibration and elution buffers with a pH of 7.5 were used, giving the protein an overall negative charge. IEC is a chromatography technique used to separate proteins based on their pI, and therefore they will separate according to their charge at a specific pH. A HiTrap® Q High Performance column (Sigma-Aldrich, USA) was used, which is a strong anion exchanger, meaning that it is positively charged. The column was equilibrated with 5 column volumes of equilibration buffer (20 mM Tris-HCl, pH 7.5) and the flow-through was collected. At the pH of the buffers, 7.5, VDR LBD is negatively charged, therefore when loaded onto the column, it binds to the column. The protein was eluted by placing 5 column volumes of the elution buffer (20 mM Tris-HCl, 1M NaCl, pH 7.5) through the column using stepwise elution with 20%, 50%, 80% and 100% elution buffer for 15 mL each. Fractions were collected at each percentage. Purified VDR LBD was then immediately dialysed against Tris buffer (20 mM Tris, 150 mM NaCl, pH 7.5) to lower the salt concentration of the buffer.

2.4 Quality check

To confirm the purity and concentration of the purified FOXP3 FHD and VDR LBD, absorbance was measured for each protein at 280 nm using the Jasco V-730Bio UV-Vis Double Beam Spectrophotometer (Jasco, UK). Absorbance of three biological replicates was measured for 5 accumulations at 280 nm and 340 nm to determine the concentration of FOXP3 FHD and VDR LBD. FOXP3 FHD was dialysed against phosphate buffered saline (PBS) buffer (1.37 M NaCl, 0.027 M KCl, 0.1 M Na_2HPO_4, 0.018 M KH_2PO_4, pH 7.4) and diluted with dilution factors 1, 0.5, 0.25, 0.125, 0.0625. VDR LBD was dialysed against potassium phosphate buffer (10 mM KH_2PO_4, 10 mM K_2HPO_4, 50 mM K_2SO_4, pH 7.6) and diluted with dilution factors 0.4, 0.2, 0.1, 0.05, 0.025. To correct for protein aggregation to give a better estimate of protein concentration, the absorbance measured at 340 nm was subtracted from that measured at 280 nm as aggregated proteins absorb at 340 nm. A blank

containing only buffer was measured on the machine and it automatically blanked for the samples. Parameters used were photometric mode: Abs, response: 0.96 sec, 3 accumulations.

Aromatic residues, particularly tryptophan, found in proteins absorb light at a wavelength of 280 nm, while aggregated proteins absorb at 340 nm. From the corrected absorbance at 280 nm, the concentration was determined using Beer-Lambert's law (Equation 2.1).

$$A = \varepsilon c l$$

Equation 2.1. Beer-Lambert law relating absorbance to concentration. A is absorbance at 280 nm, ε is the extinction coefficient and l is the pathlength which is 1 cm.

Using spectra measurement on the Jasco V-730Bio UV-Vis Double Beam Spectrophotometer (Jasco, UK), an absorbance spectrum from 240-350 nm for both FOXP FHD and VDR LBD was determined, and the protein purity from DNA contamination was calculated based on the absorbance at 280 nm divided by the absorbance at 260 nm (Equation 2.2).

$$Purity\ ratio = \frac{A_{280}}{A_{260}}$$

Equation 2.2. Purity ratio. A_{280} is the absorbance at 280 nm (wavelength at which proteins absorb light), and A_{260} is the absorbance at 260 nm, which is the wavelength that nucleic acids absorb light).

2.4.1 SDS-PAGE

To view the purified proteins and determine their molecular weight, purity and solubility, tricine sodium dodecyl sulfate polyacrylamide gel electrophoresis (SDS-PAGE) was done. Using the Bio-Rad Mini Protean(R) kit (Bio-Rad Laboratories, USA) this technique was used to test how effective the purification was. SDS-PAGE is a non-native electrophoretic technique, meaning that the proteins get denatured by the SDS and acquire a uniform negative charge, enabling proteins to get separated in a gel based on their size using an electric field. A 15% separating gel was prepared using 33% of 3 M Tris-HCl buffer (3 M Tris-HCl, 0.3% SDS, pH 8.45), 33% acrylamide-bisacrylamide 3 (48% acrylamide, 1.5% bis-acrylamide (Sigma-Aldrich, USA)), distilled water, 10% of 80% glycerol, 22% distilled water, 0.5% of 10% ammonium persulfate (Sigma-Aldrich, USA), and 0.2% tetramethylethylenediamine (TEMED) (Sigma-Aldrich, USA). A 4% stacking gel was prepared using 25% of 3 M Tris-HCl buffer, 8% acrylamide-bisacrylamide 3, 66% distilled water, 0.8% of 10% ammonium persulfate, and 0.2% TEMED. The purpose of the stacking gel was for the proteins to line up and start migrating at the same location in the gel. The purpose of the separating gel was for the proteins to be separated based on size alone (Laemmli, 1970). The purified FOXP3 FHD and VDR LBD proteins denatured with sample buffer (12% SDS, 6% β-mercaptoethanol (Sigma-Aldrich, USA), 30% glycerol, 0.05% Coomassie G-250 (Sigma-Aldrich, USA), and 150 mM Tris-HCl, pH 7) were loaded into the wells of the gel as well as a 10-180

kDa PageRuler™ Prestained Protein Ladder (Thermofisher, USA). Cathode buffer (100 mM Tris-HCl, 100 mM Tricine, and 1% SDS, pH 8.25) was added to the centre of the cassette between the gels of the Bio-Rad Mini Protean(R) kit, and anode buffer (100 mM Tris-HCl, pH 8.9) was added to the surrounding of the cassette. SDS-PAGE was then performed for an hour and a half at 160 V (Schägger, 2006). β-mercaptoethanol was added to denature the cysteine bonds to fully linearise the proteins. The PageRuler™ Prestained Protein Ladder (Thermofisher, USA) contained proteins of known molecular weight. It is known that the molecular weight of the FOXP3 FHD monomer is 12 938.93 Da, while that of the VDR LBD monomer is 32 231.09 Da, with the His-tags as obtained from Protparam (https://web.expasy.org/protparam/). Therefore, bands were expected to appear for these proteins at those sizes relative to the PageRuler™ Prestained Protein Ladder. The gel was stained overnight for viewing using stain (50% methanol, 10% acetic acid, and 0.25% Coomassie G-250). The stain that had not bound protein bands were removed using destain (50% methanol, and 10% acetic acid) overnight. The stained protein bands could then be observed and further saved using the Molecular Imager® Gel Doc™ XR System (Bio-Rad).

2.5 Structural characterisation

To determine if the proteins were purified with their structural integrity, and to structurally characterise the proteins according to secondary, tertiary, and quaternary structure, far ultra-violet (UV) CD, intrinsic tryptophan fluorescence, and SEC were done, respectively.

2.5.1 Far-UV Circular dichroism for secondary structure characterisation

Far-UV CD was performed on both FOXP3 FHD and VDR LBD. It measures the difference in absorptions by the sample between left- and right-hand circularly polarised light (Kelly and Price, 2000). A light source was sent through a monochromator to get a single wavelength of light. It was then passed through a polariser, which made it linearly polarised. Then, by being passed through the phase plate, the light became circularly polarised. The circularly polarised light then hits the sample, which can absorb it, having a chiral peptide backbone, and then transmits the light differently based on the chirality of the molecule's polypeptide backbone. The differential emission of light from the sample is detected by the detector and a spectrum can be created. The spectrum therefore gives insight into the global peptide backbone structure of the protein, hence the protein's secondary structure (Kelly and Price, 2000).

FOXP3 FHD in elution buffer, purified using IMAC was dialysed against PBS buffer, while VDR LBD after IEC was dialysed against potassium phosphate buffer. Purified FOXP3 FHD was placed into snakeskin dialysis tubing, 3.5K MWCO; 22 mm (LTC Tech, Thermofisher, South Africa), and purified VDR LBD was

placed into snakeskin dialysis tubing, 10K MWCO; 22 mm. Both were submerged in 300 mL of PBS (FOXP3 FHD) or potassium phosphate buffer (VDR LBD) for 3 hours twice and then overnight at 4 °C, a 1:200 ratio of protein to buffer. This was to remove buffer components from elution buffer that are not compatible with the CD machine, such as imidazole and NaCl. Three biological replicates of FOXP3 FHD in PBS buffer were made up to 6 µM concentration, and 10 µM of VDR LBD was diluted in potassium phosphate buffer. Three biological replicates of denatured FOXP3 FHD were made up to 6 µM with an addition of 7 M urea (Sigma-Aldrich, USA), and 7 µM with an addition of 8 M urea for VDR LBD. Urea was used to denature the protein to compare the spectra of the native and denatured protein and confirm the predominate secondary structures in each of the proteins, thereby giving an indication of the proteins fold. To determine if the buffer component of 1,25(OH)D_3 (ethanol) or 1,25(OH)D_3 affected the secondary structures of FOXP3 FHD and VDR LBD, three biological replicates each of FOXP3 FHD and VDR LBD in the presence of the 12 µM and 20 µM ligand, 1,25(OH)D_3, respectively and the buffer component of the ligand, 0.5% ethanol were also made. 1,25(OH)D_3 (Glentham, UK) was solubilised in ethanol (ACE chemicals) at 1 mg/ml.

Far-UV CD was performed on all the above samples using the Jasco J-1500 spectropolarimeter (Jasco, USA) with the following conditions: Spectra were recorded from 180 to 260 nm with a data pitch of 0.5. A continuous scanning mode was used with a scanning speed of 100 nm/min and a response of 1 second. The bandwidth used was 2.5 nm. Five accumulations were performed on each of the three biological replicates for both native apo-, denatured-apo-, and native liganded FOXP3 FHD and VDR LBD. The mdeg was recorded for each wavelength between 180 and 260 nm and was then converted to mean residue ellipticity (MRE) (Equation 2.3), which considers the number of residues in the protein and the concentration of the protein.

$$MRE\ (\deg cm^2 dmol^{-1}) = \frac{mdeg}{(10 * c * n * l)}$$

Equation 2.3. Formula to calculate MRE from mdeg for far-UV CD. The components consist of c: Molar protein concentration, n: the number of residues in the protein, l: pathlength in cm.

A far-UV CD spectrum was created, which gives important information about the secondary structure of the protein in the sample, with different secondary structures having characteristic spectra (Figure 2.2) (Kelly and Price, 2000). The shape of the graph for FOXP3 FHD and VDR LBD was used to determine the secondary structure of the protein by comparing it to the characteristic curves in Figure 2.2. Both

proteins had been crystalised before and therefore the shape of the graph could be compared to the predominant secondary structures present in the crystal structures.

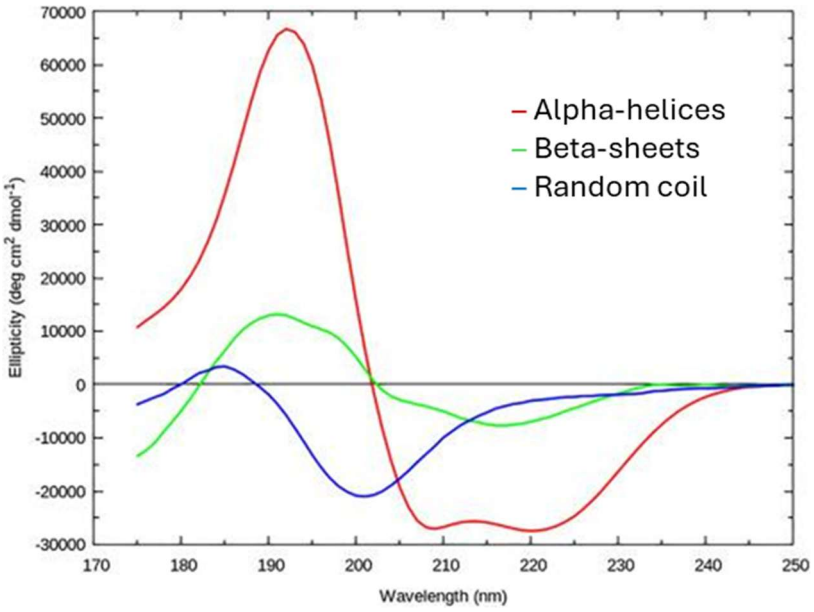

Figure 2.2. Characteristic far-UV CD spectra for different secondary structures of proteins. The red graph is the spectrum that indicates alpha helices with a peak at 190 nm, and two troughs at 210 and 220 nm, the green represents beta-sheets with a smaller peak at 190 nm and a single, smaller trough between 210 and 220 nm, and the blue is random coils with a peak at 180 nm, a trough at 200 nm, and then levelling out at around 220 nm. Graph adapted from Rogers et al., 2019.

2.5.2 Intrinsic tryptophan fluorescence for tertiary structure characterisation

Fluorescence is a category of luminescence, which is the emission of light from a substance (Lakowicz, 1985). It occurs when an electron returns to ground state (S_0) from an excited state (S_1) and releases a photon, following the principle illustrated by the Jablonski diagram (Lakowicz, 1985). Tryptophan is an aromatic amino acid that is sensitive to the polarity of an environment, emitting light at a higher wavelength than they absorb at, thereby emitting fluorescence (Ghisaidoobe and Chung, 2014). When tryptophan is excited at 295 nm, it emits light at a range of 330 nm in a non-polar environment, and up to 350 nm in a more polar environment.

A fluorescence spectrum was generated to give an indication of the fold of the protein. The wavelength at which tryptophan fluoresces, as well as the fluorescence intensity, differs based on the environment in which it is. Light gets absorbed by tryptophan present within proteins at 295 nm and fluoresces at 330 nm in a more non-polar environment, having a red shift to 350 nm in a more polar environment. This shift between native and denatured proteins gives an indication of the specific folding characteristic of the protein, therefore if it is in the native folded state based on its tertiary structure (Lakowicz, 1985).

Fluorescence spectra were recorded using the Jasco FP-6300 spectrofluorometer (Jasco, USA) for 6 µM FOXP3 FHD in the native state and in the denatured state, which was done in the presence of 7 M urea, and for 10 µM VDR LBD in the native state and in the denatured state, also in the presence of 8 M urea. Fluorescence spectra were also recorded for FOXP3 FHD and VDR LBD in the presence of 12µM and 50 µM 1,25(OH)D_3, respectively, and in the presence of 0.5% ethanol. The following parameters were used, the samples were excited at 295 nm with emission and excitation bandwidths at 5 nm. The fluorescence spectrum was measured from 295 to 450 nm with a scanning speed of 200 nm/min. The average of three accumulations of three biological replicates for each native and denatured sample was used to construct the spectrum. Observing a difference between the spectra of the native and denatured states gave an indication that the overexpressed proteins were structurally intact.

2.5.3 Quaternary structure characterisation

2.5.3.1 VDR LBD disulfide-linked dimer

To confirm if VDR LBD formed disulfide bond homodimers, SDS-PAGE was performed with VDR LBD in sample buffer with and without β-mercaptoethanol (reducing agent). VDR LBD exists in nature in a reducing environment in the nucleus (Tata, 2002). Therefore, to maintain all cysteine residues in the reduced state, VDR LBD was kept in buffer containing 5 mM reducing agent, dithiothreitol (DTT) for most experiments, except fluorescence anisotropy where Tris(2-carboxyethyl)phosphine (TCEP) was used.

2.5.3.2 Size exclusion chromatography

SEC is a comparative chromatographic technique that separates proteins based on their size (Barth, et al., 1994). When a sample is passed through the column, the pores trap smaller molecules, retarding their migration, while larger molecules do not get trapped and elute out first. By measuring the elution volume and protein standards, the relative molecular weight of globular proteins can be determined. The log of the molecular weight is inversely proportional to the elution volume (Barth, et al., 1994). The determined molecular weight of a protein can then be compared to that of a protein in monomer form, thereby determining the oligomeric state of a protein (Blumenfeld and Gardner, 1985).

SEC was performed using a HiLoad™ 16/60 Superdex™ 75 prep grade column (GE healthcare, USA) to confirm if FOXP3 FHD and VDR LBD were in their correct oligomeric states. FOXP3 FHD has a molecular weight of 12 938.93 Da and VDR LBD has a molecular weight of 32 231.09 Da, as determined by ProtParam (https://web.expasy.org/protparam/). FOXP3 FHD exists as a homodimer (Bandukwala et al., 2011), and VDR LBD is expected to be in monomeric form in the presence of reducing agent. The HiLoad™ 16/60 Superdex™ 75 prep grade column was equilibrated using filtered and degassed equilibration buffer, then each of the samples were loaded onto the column and equilibration buffer

was passed through the column. Fractions were collected and then an SDS-PAGE was performed to visualise the proteins collected in each fraction.

Standards used (GE healthcare low range gel filtration calibration kit) consisted of blue dextran (2000 kDa), ovalbumin (44 kDa), conalbumin (75 kDa), ribonuclease A (13.7 kDa), carbonic anhydrase (29 kDa), and aprotinin (6.5 kDa). These were separated according to the instructions given by the manufacturer's and a standard curve was plotted using the $\log_{Mw}$ of each protein standard with the ratio of the elution volumes (V_e) to the void volume (V_0). The equation of the linear regression of the curve was then used in order to calculate the sizes of FOXP3 FHD and VDR LBD based on their elution volumes. In this way, SEC was used to confirm both the size and the quaternary structure of the proteins.

2.6 Functional assays

To determine if the purified proteins were each functional, the DNA binding ability of FOXP3 FHD, and the ligand binding ability of VDR LBD were tested using EMSA, and thermal shift assay, respectively.

2.6.1 Electrophoretic mobility shift assay for FOXP3 FHD

EMSA is a native electrophoretic technique used to observe protein-DNA interactions. It uses the principle that protein bound to DNA forms a larger complex and therefore migrates through the gel slower than unbound DNA (Hellman and Fried, 2007). FOXP3 FHD is a transcription factor, therefore its primary function is to bind to its consensus DNA. EMSA was therefore performed to check the functionality of the purified FOXP3 FHD. FOXP3 FHD consensus sequence ATAAACA was used, with the specific sequence: AGATAAACAAGTGTAAACAAT obtained from Bandukwala et al., 2011. An 8% polyacrylamide gel was made using Tris-acetate, Ethylenediaminetetraacetic acid (EDTA) buffer (TAE) (400 mM Tris, 25 mM EDTA (Sigma-Aldrich, USA), pH 7.8), bisacrylamide monomer solution, and 20% triethylene glycol (Sigma-Aldrich, USA). DNA to protein complexes of 1:0, 1:1, 1:3, 1:5, 1:8, 1:10, 1:15, and 1:20 were prepared with EMSA binding buffer (10 mM HEPES (Sigma-Aldrich, USA), 1 mM EDTA, 100 mM KCl, 0.1 mg/mL bovine serum albumin (Sigma-Aldrich, USA), 1 mM $MgCl_2$, 10% glycerol, pH 7.8). The samples were incubated for 30 minutes at 4°C and then loaded in the wells of the gel. The EMSA was run using the Bio-Rad Mini PROTEAN™ Tetra Cell (Bio-Rad, USA) with TAE running buffer for 2 hours at 4 °C. To observe the bands, the DNA was stained afterwards using GelRed (Sigma-Aldrich, Germany) and observed using the Molecular Imager® Gel Doc™ XR System (Bio-Rad).

2.6.2 Thermal shift assay for VDR LBD

Thermal shift assay relies on monitoring the melting temperature of a protein throughout thermal denaturation (Huynh and Partch, 2015). By measuring a change in protein thermal stability, changes in protein structure can be determined. The stability of proteins bound to ligand differs to protein

unbound to ligand, where a shift in the melting temperature is expected to be observed upon ligand binding (Henderson et al., 2020).

For the thermal shift assay, 25 µM of purified VDR LBD in Tris buffer containing 5 mM DTT was incubated with SYPRO-Orange dye in a 96-well plate (Lasec, Cape Town, South Africa) with and without 50 µM 1,25(OH)D_3. Each measurement was performed in triplicate. The reaction was performed on a CFX-96 Thermal Cycler (Bio-Rad, Hercules, CA) with temperatures increasing from 10-90 °C. By gradually increasing the temperature, VDR LBD will denature and aggregate. At each temperature, the solubility content in percentage based on the fluorescence intensity of the SYPRO-Orange dye was measured. As the temperature increases, the theory is that the more aggregated protein, the lower the percent of soluble proteins. A melt or aggregation curve was plotted using temperature increase against relative fluorescent unit for both VDR LBD individually and VDR LBD in the presence of 1,25(OH)D_3. Each parameter was done in triplicate and then the averages were used for the graph construction. From this melt curve, the temperature at which the highest fluorescence intensity occurred, and therefore the peak of the melt curve, was determined as the melting temperature (Tm) of the protein with and without 1,25(OH)D_3 (Henderson et al., 2020). A change in the melting temperature for the protein in the absence and presence of ligand is suggestive of ligand binding (Henderson et al., 2020).

2.7 Interaction assay

With the main aim of this study being an investigation into the physical interaction between FOXP3 FHD and VDR LBD in the presence and absence of 1,25(OH)D_3, the potential interaction between these two proteins was investigated *in vitro* using fluorescence anisotropy.

2.7.1 Labelling of VDR LBD with a fluorophore for fluorescence anisotropy

VDR LBD in Tris buffer with 5 mM (TCEP) was labelled with AlexaFluor™ 555 C2-Maleimide (Thermofisher, USA). TCEP was used as a reducing agent instead of DTT, as DTT can quench the fluorescence of the fluorophore (Kumar et al., 2008). A 5:1 ratio of dye to protein was mixed and incubated for 1 hour at room temperature with inverting, and then overnight at 4°C. Excess dye was removed the following day using Pierce™ dye removal columns (Thermofisher, USA). The labelling efficiency was confirmed using the Nanodrop One spectrophotometer, only considering bound dye (ThermoFisher, USA). The percentage of fluorescent dye compared to protein in the mixture was calculated based on the concentrations obtained from the Nanodrop One spectrophotometer using Equation 2.4.

$$Labelling\ efficiency = \frac{[Alexa - 555]\ \mu M}{[Protein]\ \mu M} * 100$$

Equation 2.4. Labelling efficiency of protein labelled with AlexaFluor™ 555 C2-Maleimide. The concentration of label in µM is divided by the concentration of protein in µM and multiplied by 100 to get the percentage of protein labelled.

2.7.2 Fluorescence anisotropy

Fluorescence anisotropy was used to determine the potential interaction of FOXP3 FHD and VDR LBD through measuring rotational motion of molecules labelled with a dye that can fluoresce. When a molecule rotates, it emits horizontal and vertical polarised light. Anisotropy is the difference between horizontally and vertically polarised light of the fluorescence emitted from a fluorophore (Figure 2.5) (Knutson et al., 1986; Steiner, 2002). Fluorophore bound to a protein that is free to rotate in solution with a higher, non-restricted rotational motion loses most of the polarisation emitted, therefore has a lower anisotropy. When a fluorophore is bound to a protein-protein or protein-protein-ligand complex, a larger molecule with a lower, more restricted rotational motion, the light emitted by the fluorophore retains more polarisation, therefore having a higher anisotropy.

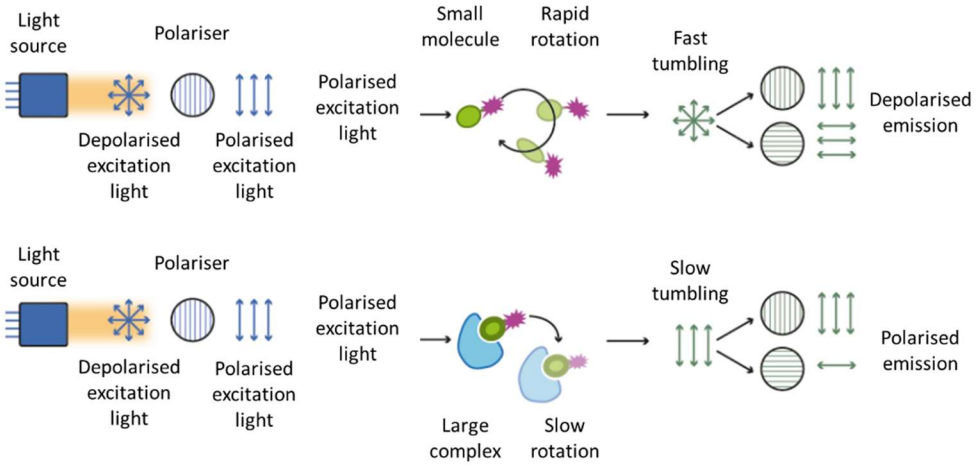

Figure 2.3. Diagram of the light emission for fluorescence anisotropy. A light source gets polarised and excites a molecule. The top diagram shows a small molecule exhibiting rapid rotation (unbound protein) being excited by polarised light. The difference between the polarised emission is small due to fast tumbling, thereby giving a low anisotropy. The bottom diagram shows a large complex (protein bound to protein) being excited by polarised light. The complex exhibits slow rotation, therefore slow tumbling resulting in a lower depolarisation rate and emitting a higher polarised light, thereby having higher anisotropy. Diagram from Fluorescence Polarisation Detection ("Fluorescence Polarization Detection | BMG LABTECH," n.d.).

The anisotropy of the protein complex was measured in the presence and absence of 1,25(OH)D_3 using a PerkinElmer LS-50 fluorescence spectrophotometer equipped with an anisotropy filter. The excitation wavelength of 556 nm and an emission wavelength of 572 nm of the AlexaFluor™ 555 C2-Maleimide was used. The average of 10 accumulations of 3 biological replicates was measured and plotted using SigmaPlot 15.0 and a single saturation ligand-binding non-linear regression curve was constructed. The dissociation constant (K_d) and maximum observed binding B_{max} of the interactions were determined using the equation of the regression curve in Equation 2.5. The G-factor was

calculated using the Equation 2.6. This was used to normalise for the potentially different sensitivity to vertical and horizontal polarised light by the detection system in the PerkinElmer LS-50 fluorescence spectrophotometer (Kitchner et al., 2022).

$$y = \frac{B_{max}(x)}{K_d + x}$$

Equation 2.5. Equation of the ligand-binding non-linear regression curve for fluorescence anisotropy. B_{max} is the maximum number of interaction sites, K_d is the affinity concentration, the concentration of titrant to reach half the B_{max}, y is the relative fluorescence anisotropy, and x is the concentration of titrant.

$$\mathrm{G} = \frac{I_{HV}}{I_{HH}}$$

Equation 2.6. Equation for the grating factor for fluorescence anisotropy. I_{HV} is the fluorescence intensity of horizontally polarised emission for vertically polarised excitation, and I_{HH} is the fluorescence intensity of horizontally polarised emission for horizontally polarised excitation.

Chapter 3. Results

To determine whether VDR LBD and FOXP3 FHD interact, *in silico* and *in vitro* experiments were performed for cross-verification. Molecular docking was performed to predict whether VDR LBD and FOXP3 FHD had the potential to interact with each other. Once an interaction was predicted, experimental methods were performed to confirm the computational prediction. Both proteins were overexpressed and purified for use. Expression needed to be optimised for VDR LBD as it had not been expressed in our Unit before. No expression trials were needed for FOXP3 FHD as a protocol was already established in the Unit. The two purified proteins needed to be structurally and functionally characterised in the presence and absence of ligand before interaction experiments could be performed. Once the two proteins were found to have their structural and functional integrity, fluorescence anisotropy was performed to determine the potential interaction between the two proteins with and without ligand.

3.1 Molecular docking

FOXP3 FHD interacts with VDR LBD *in silico* in the presence and absence of 1,25(OH)D_3 with high confidence of 0.9 (Figure 3.1A and B). Two docking programmes, HDock and LZerd, were used to increase our confidence in the predicted interaction between the proteins by cross verifying the results of each programme. Both programmes showed FOXP3 FHD interacting with parts of VDR LBD, albeit at different locations, while VDR LBD is predicted to interact at the same place on FOXP3 FHD, namely the DNA recognition helix, helix 3. The top models from each HDock (Figure 3.1A) and LZerd (Figure 3.1B) were viewed using Chimera 1.16 with the contacts between the two proteins visualised. Figure 3.1A shows the FOXP3 FHD and VDR LBD docked model generated by HDock with a docking score of -267.93, a confidence score of 0.9136 and a ligand root mean square deviation (RMSD) of 100.76 Å. Figure 3.1B shows the FOXP3 FHD and VDR LBD docked model generated by LZerd which has a GOAP score of -69674.38 with a GOAP rank of 108, a DFIRE score of -41915.36 with a DFIRE rank of 76 and an ITScore score of -22532.19 with an ITScore rank of 7, having a total rank of 191. These scores are knowledge-based potentials, and the more negative the score, the more likely the interaction is predicted to happen. They take into account the distances between pairwise atom distances and orientations at the interaction site (Christoffer et al., 2021).

The full length apo-VDR structure was predicted using AlphaFold 3 (Abramson et al., 2024) The predicted apo structure superimposes with the ligand crystal structure (1DB1) (Figure 3.2A). Docking with the predicted full length VDR structure from AlphaFold 3 and the FOXP3 FHD dimer (3QRF) using HDock showed interaction at a different position than with the isolated domains (Figure 3.1). Model 1 showed FOXP3 FHD interacting with the DNA binding domain of VDR. Model 2 was used as it was

the top-ranking model where FOXP3 FHD interacted with the LBD of VDR (Figure 3.2B). Interaction was predicted to occur with a docking score of -285.51, a confidence score of 0.9376 and a ligand RMSD of 128.44.

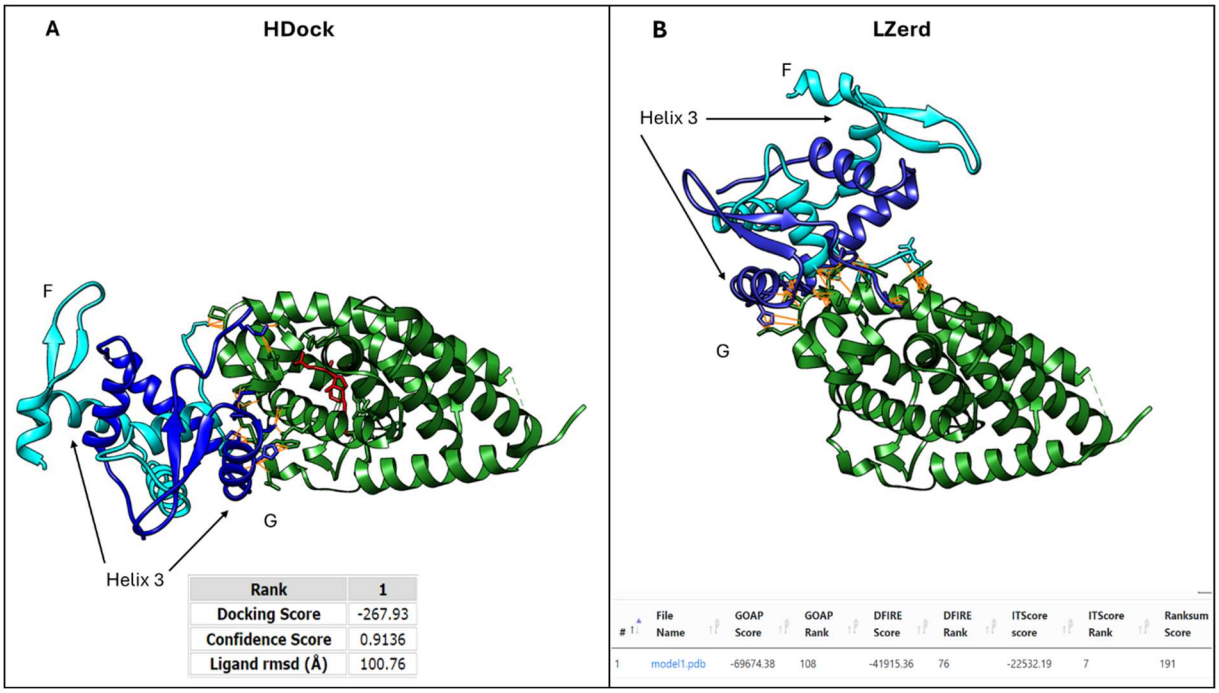

Figure 3.1. VDR LBD docks to FOXP3 FHD at helix 3. The ribbon models show that VDR LBD docks to FOXP3 FHD with and without 1,25(OH)D_3 as predicted by HDock (A) and LZerd (B). HDock shows VDR LBD with 1,25(OH)D_3 (PDB 1DB1) docked to FOXP3 FHD (PDB 3QRF). LZerd shows VDR LBD without 1,25(OH)D_3 (1DB1) docked to FOXP3 FHD (3QRF). The highest-ranking pose from both programmes was viewed using Chimera 1.16 (Pettersen et al., 2004) *and these are shown here. VDR LBD is in green, 1,25(OH)D_3 is in red, and FOXP3 FHD dimer is in blue. The interactive forces between the two proteins are shown in orange, no hydrogen bonds were predicted between the proteins. VDR is seen to interact with helix 3 of FOXP3 FHD as predicted by both HDock and LZerd, indicated by the arrows (HDock, LZerd, Chimera 1.16).*

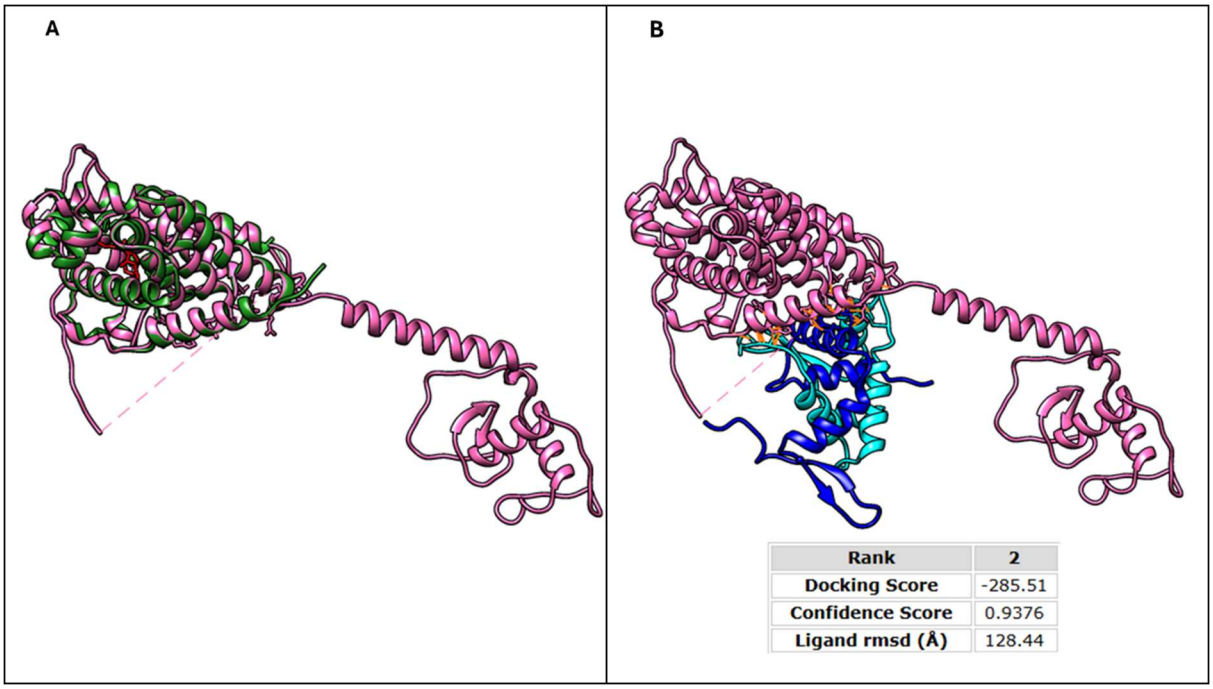

Figure 3.2. Full-length VDR superimposition and docking. Predicted full-length VDR is in pink, VDR LBD crystal structure is in green, 1,25(OH)D_3 is in red, FOXP3 FHD dimer is in blue. Contacts are shown in orange. A: Full-length VDR as predicted by AlphaFold 3 superimposes with VDR LBD crystal structure (1DB1). B: Full-length VDR docked with FOXP3 FHD dimer (3QRF) using HDock. Interaction occurs at a different place to the isolated domains (HDock, Chimera 1.16).

3.2 Expression and purification

The following results have been gained from experimental work to compliment and build on the *in silico* work in section 3.1. To observe the interaction between the two proteins, they needed to be expressed and purified.

3.2.1 Expression trials

The process of overexpressing the soluble form of VDR LBD needed to be optimised as it was being done for the first time in this laboratory. Overexpression in the supernatant is indicative of soluble protein, while overexpression found in the pellet is indicative of insoluble protein (Figure 3.3). Many different conditions were trialled, and SDS-PAGE was performed for each condition on both the pellet and the supernatant. A thick overexpression band being observed at 32 kDa in the supernatant sample (the expected size of VDR LBD) was used to determine whether the conditions were optimal.

For the first trial (Figure 3.3A), differing IPTG concentration and time of expression were tested based on a protocol used in the laboratory for another nuclear receptor, oestrogen receptor (Lakhi and Fanucchi, 2024). Transformed BL21(DE3) *E. coli* cells were used in LB media. Cells were induced with different IPTG concentrations: 0, 0.2, 0.4, and 0.6 mM at an OD_{600} of 0.7. Expression was done at 20 °C for a total of 24 hours, with samples taken at 16, 18, 20, 22, and 24 hours for time trials. For all the IPTG concentrations, except for 0 mM, a thick band was observed at around 32 kDa in the pellet samples. No bands were observed in the supernatant samples for these conditions, therefore more trials needed to be done.

In the second trial (Figure 3.3B), the cell line, media, temperature, and time of induction and expression was kept the same as the first trial, while different IPTG concentrations were tested. Another temperature and time of expression was also tested based on the overexpression of FOXP3 FHD, for which a protocol was already established in the laboratory and kindly provided for by Alicia Joshua. Transformed BL21(DE3) *E. coli* cells in LB media were used. At an OD_{600} of 0.7, the cells were induced with either 0, 0.3, or 0.5 mM IPTG. One set of cells was expressed at 30°C for a total of 6 hours, while the other set was expressed at 20°C for a total of 24 hours. At 30 °C, time trial samples were taken at 0, 4, and 6 hours, and at 20°C, time trial samples were taken at 0, 16, 20, and 24 hours to trial different times of expression. Again, a thick band was observed in the pellet samples for all time, IPTG, and temperature trials, except for 0 mM IPTG and 0 hours, where no expression would have occurred. No soluble protein was observed as there was no band in the supernatant sample for any of the conditions, therefore further trials needed to be done.

Because all the time, temperature and IPTG concentrations used had already yielded insoluble protein, it was suspected that changing the cell line might improve the soluble overexpression of VDR LBD.

BL21(DE3) plysS *E. coli* cells are specifically used to prevent basal leaky expression. In the previous trials, the protein was being overexpressed, however, it was insoluble. Basal expression could cause the protein to form inclusion bodies through too much expression of the protein too early on in the process (Kawe et al., 2009). In the third trial (Figure 3.3C), transformed BL21(DE3) plysS *E. coli* cells were used in LB media. Different times of expression and times of induction were tested in this trial. At an OD_{600} of 0.3, 0.7, and 1, the cells were induced with 0 and 1 mM IPTG and left to express for a total of 24 hours at 18 °C. The temperature was lowered to also prevent basal expression and the formation of inclusion bodies. Samples were taken at 0, 16, 20, and 24 hours of expression. A thick overexpression band was again noted in the pellet samples of all the conditions except for 0 hours and 0 mM IPTG. A very thin band was observed in the supernatant sample of 1 mM IPTG at OD_{600} 0.3 at 20 and 24 hours. However, the band was not thick enough for purification and further experiments, therefore more trials were performed.

The cell line was changed to T7 *E. coli* cells, again testing to see if a different cell line would improve soluble expression of VDR LBD. In the fourth trial (Figure 3.3D), transformed T7 *E. coli* cells were used in LB media and expression was again performed at 18 °C as this temperature had given the best result so far in the previous trial. Different IPTG concentrations and different expression times were again tested. At OD_{600} 0.7, the cells were induced with 0, 0.3, and 1 mM IPTG and samples were taken at 0, 16, 20, and 24 hours. This trial yielded worse results, with VDR LBD being overexpressed in the pellet only, even at 0 mM IPTG, indicating leaky expression of the protein, and no band was present at 32 kDa in the supernatant samples.

Going back to BL21(DE3) plysS *E. coli* cells, which had so far given the best results, the media was changed to TB media to give the cells more nutrients and to try improving soluble overexpression of the protein. For the fifth trial (Figure 3.3E), transformed BL21(DE3) plysS *E. coli* cells were used in TB media. This time, they were induced at an OD_{600} of 1, to try test a different induction time, with 0, 0.1, 0.2, and 1 mM IPTG being used. They were set to express for a total of 20 hours at a temperature of 24 °C (a shorter time was done for a higher temperature). Samples were taken at 0 and 20 hours for each IPTG concentration. Overexpression was observed in the pellet samples at 20 hours, even at 0 mM IPTG, indicating leaky expression again.

So far, none of the conditions yielded soluble overexpression of VDR LBD. Many factors influence protein folding and therefore solubility. Because VDR is a human protein and is normally expressed in eukaryotic cells, it was suspected that it needed assistance in protein folding in *E. coli* cells. Therefore, the sixth trial (Figure 3.3F) used BL21(DE3) *E. coli* cells that were co-transformed with pET11a vector containing VDR LBD genetic code, as well as pKJE7 vector encoding chaperones dnaK, dnaJ, and grpE.

With chaperones present, L-Arabinose needed to be added to the media to induce chaperone expression. This trial was performed in LB media and used the suggested conditions for chaperone expression, 0.5 mg/mL L-Arabinose, 0.5 mM IPTG at OD_{600} 0.6, and expressed for 4 hours at 30 °C. These conditions worked to yield a low concentration of soluble protein as seen by the thin bands present in the supernatant samples of 0 and 0.5 mM IPTG at 4 hours. Another trial was done using the chaperones and testing different L-Arabinose concentrations, as well as different temperatures and expression times to get a higher concentration of protein.

For the seventh trial (Figure 3.3G), the same co-transformed BL21(DE3) *E. coli* cells were used in LB broth with 0, 0.5, and 4 mg/mL. The cells were induced with 0.5 mM IPTG at OD_{600} of 0.6, after which expression was done at 30 °C for a total of 6 hours, with samples being taken at 0, 4, and 6 hours, and at 18 °C for a total of 24 hours, with samples being taken at 0, 16, 20, and 24 hours. This trial showed that the chaperones assist VDR LBD protein folding, because under 0 mg/mL L-Arabinose and 0.5 mM IPTG at both 30 °C and 18 °C, thick overexpression bands were observed at 32 kDa in the pellet and not in the supernatant. However, the conditions of 0.5 mg/mL L-Arabinose, 0.5 mM IPTG induction at OD_{600} 0.6 at 18 °C for 24 hours, yielded the highest soluble overexpression of VDR LBD. In both the sixth and seventh expression trials (Figure 3.3F and G), expression bands of the chaperones can be observed with dnaK being around 70 kDa, dnaJ around 40 kDa, and grpE around 15 kDa (The UniProt Consortium, 2024).

A 4 L overexpression was performed and the protein purified under the conditions with the chaperones that yielded the best results above, co-transformed BL21(DE3) *E. coli* cells in LB media with 0.5 mg/mL L-Arabinose, 0.5 mM IPTG induction at OD_{600} 0.6 at 18 °C for 24 hours. While this yielded soluble protein, it did not work for further purification because the chaperones could unfortunately not be purified from the sample. Therefore, a large volume, 4 L trial was done without chaperones using the following conditions: BL21(DE3) *E. coli* cells in LB media, with induction of 1 mM IPTG at OD_{600} of 0.7, followed by a 6-hour incubation at 20 °C (Figure 3.3H). Even though most of the protein was insoluble under these conditions, enough protein was soluble within the 4 L to purify and use for further experiments.

A

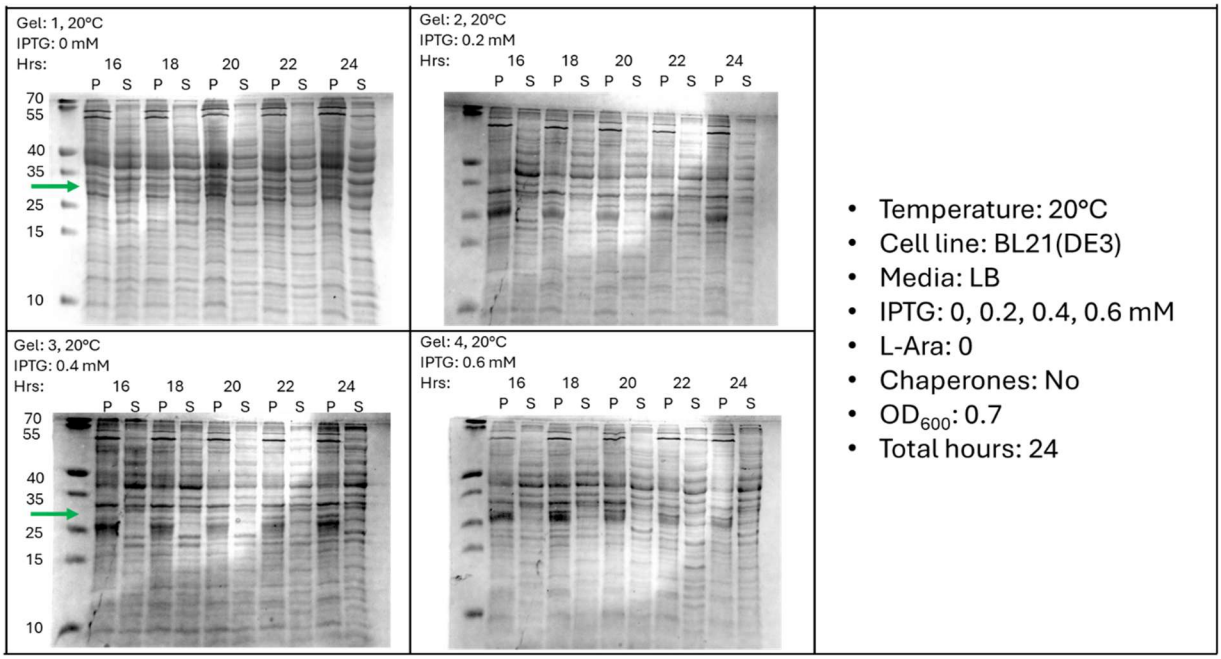

- Temperature: 20°C
- Cell line: BL21(DE3)
- Media: LB
- IPTG: 0, 0.2, 0.4, 0.6 mM
- L-Ara: 0
- Chaperones: No
- OD_{600}: 0.7
- Total hours: 24

B

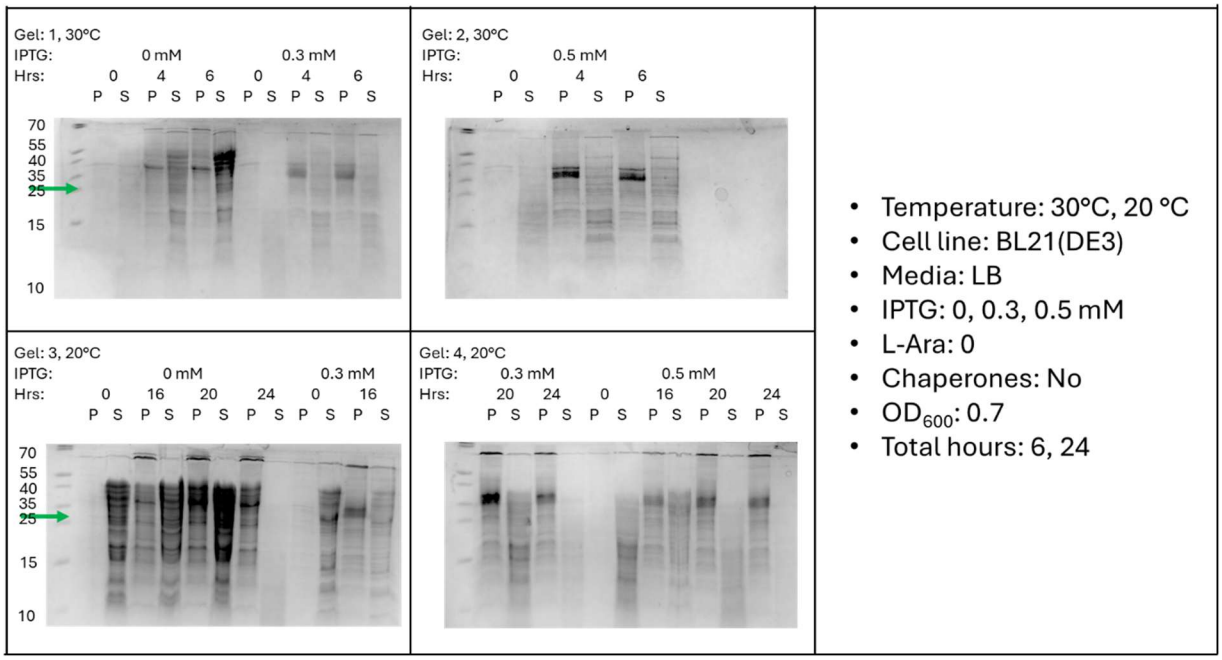

- Temperature: 30°C, 20 °C
- Cell line: BL21(DE3)
- Media: LB
- IPTG: 0, 0.3, 0.5 mM
- L-Ara: 0
- Chaperones: No
- OD_{600}: 0.7
- Total hours: 6, 24

C

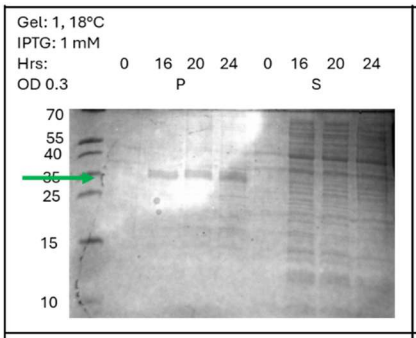

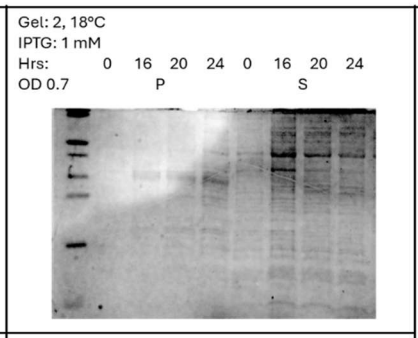

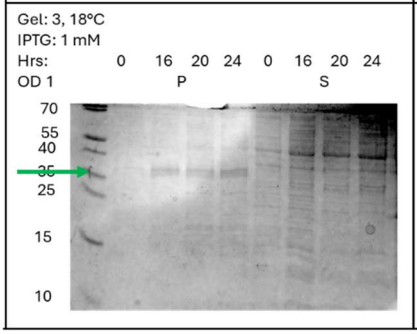

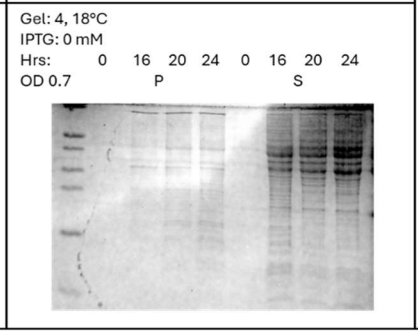

- Temperature: 18°C
- Cell line: BL21(DE3) plysS
- Media: LB
- IPTG: 1 mM
- L-Ara: 0
- Chaperones: No
- OD_{600}: 0.3, 0.7, 1
- Total hours: 24

D

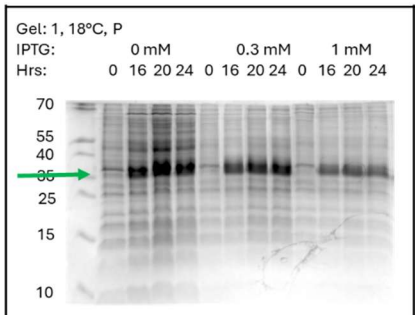

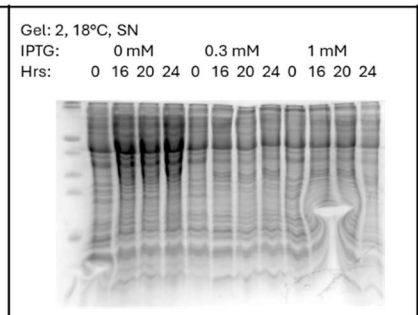

- Temperature: 18°C
- Cell line: T7
- Media: LB
- IPTG: 0, 0.3, 1 mM
- L-Ara: 0
- Chaperones: No
- OD_{600}: 0.7
- Total hours: 24

E

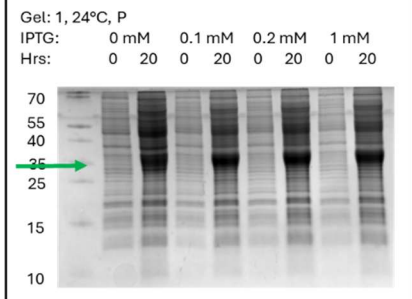

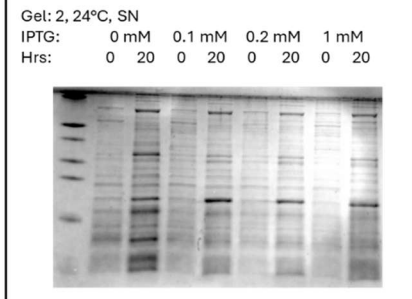

- Temperature: 24°C
- Cell line: BL21(DE3) plysS
- Media: TB
- IPTG: 0, 0.1, 0.2, 1 mM
- L-Ara: 0
- Chaperones: No
- OD_{600}: 1
- Total hours: 20

F

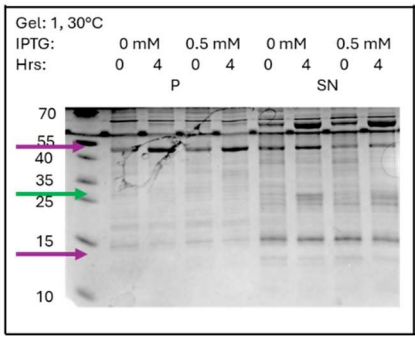

- Temperature: 30°C
- Cell line: BL21(DE3)
- Media: LB
- IPTG: 0, 0.5 mM
- L-Ara: 0.5 mg/mL
- Chaperones: Yes
- OD_{600}: 0.6
- Total hours: 4

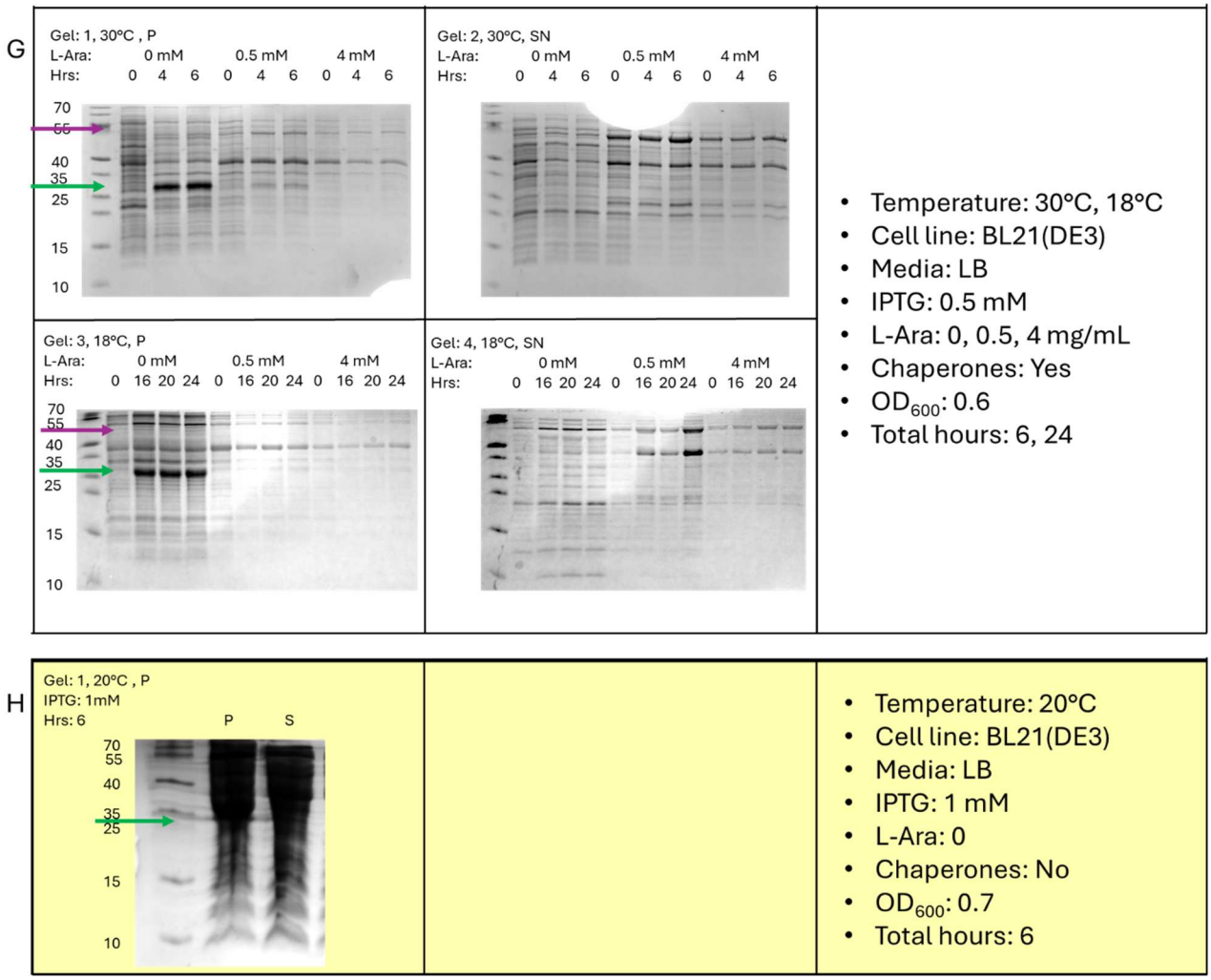

Figure 3.3. SDS-PAGE from expression trials for VDR LBD. The temperatures, IPTG concentration, L-Ara concentration, time of induction, time of expression, and pellet and supernatant are all represented above the lane of each gel for which the condition was tested. The green arrows indicate a thick overexpression band representative of VDR LBD at 32 kDa and the purple arrows indicate chaperone overexpression. Each trial has a control with no IPTG, indicated as 0 IPTG. A: BL21(DE3) E. coli cells in LB media. Overexpression of VDR LBD occurred in the pellet for all conditions except for 0 mM IPTG. B: Overexpression of VDR LBD in the pellet for all the conditions except for 0 mM IPTG and 0 hours. C: BL21(DE3) plysS E. coli cells in LB media. The same overexpression pattern was seen as in A and B. D: T7 E. coli *cells in LB media. Overexpression was seen in the pellet for all IPTG concentrations for all times except 0 hours. E: BL21(DE3) plysS* E. coli *cells in terrific broth (TB) media. Small expression band is observed in the supernatant. Overexpression bands are seen in the pellet for 20 hours at each IPTG concentration, except 0 mM IPTG. F: BL21(DE3)* E. coli *cells in LB media. Chaperones present with 0.5 mg/mL L-arabinose. Small expression bands are seen in the supernatant for IPTG concentrations at 4 hours. G: BL21(DE3) E. coli cells in LB media. Chaperones were present with 0, 0.5 and 4 mg/mL L-arabinose. H: BL21DE3 E. coli cells, OD_{600} 0.7, 1 mM IPTG, 20°C, 6 hours. Overexpression bands are seen in both pellet and supernatant, yielding the best results, with condition H being used for further overexpression of VDR LBD.*

3.2.2 Purification of FOXP3 FHD and VDR LBD

Expression trials for FOXP3 FHD were not done in this study as the conditions had already been optimised in the Unit previously and provided for by Alicia Joshua. Once the conditions for protein overexpression had been optimised for VDR LBD (section 3.2.1) and FOXP3 FHD, the proteins could be overexpressed and purified.

The BL21(DE3) *E. coli* cells were successfully transformed with a pET11a vector containing the genetic code for VDR LBD. Transformation of T7 *E. coli* cells with a recombinant pET11a vector containing the genetic code for FOXP3 FHD was also successful. The plasmid of each protein was extracted using the GeneJET plasmid miniprep kit and sent to Inqaba Biotech for sequencing. The extracted plasmid sequence was compared against the original VDR LBD and FOXP3 FHD sequences used using BLAST (Altschul et al., 1990) and was confirmed to be correct.

Growth of both transformed T7 *E. coli* cells and BL21(DE3) *E. coli* cells yielded single colonies, which were then grown in respective culture broth for 16 hours (2x YT media for FOXP3 FHD, and LB media for VDR LBD), yielding cell growth that was used for the overexpression of FOXP3 FHD and VDR LBD in T7 and BL21(DE3) *E. coli* cells, respectively.

VDR LBD was successfully overexpressed in BL21(DE3) *E. coli* cells in 4L of LB media at 20 °C for 4 hours with shaking at 180 rpm, after induction with 1 mM IPTG at an OD_{600} of 0.7 (Figure 3.3H). Most of the protein overexpression was insoluble, as seen by a thick band in the pellet (lane 2, Figure 3.4B). However, enough of the protein was soluble with a band present at 32 kDa in the supernatant (lane 3, Figure 3.4B).

FOXP3 FHD was successfully overexpressed in 2x YT media for 4 hours at 30 °C with shaking at 180 rpm after induction with 0.3 mM IPTG once the cells that were inoculated with the overnight growth and left to grow at 37 °C with shaking at 180 rpm had reached an OD_{600} of 0.8. FOXP3 FHD was overexpressed in both the supernatant and pellet, as seen in lane 2 and 3 of Figure 3.5B, respectively. These are representative purification results as both proteins were expressed and purified many times to complete all the experiments.

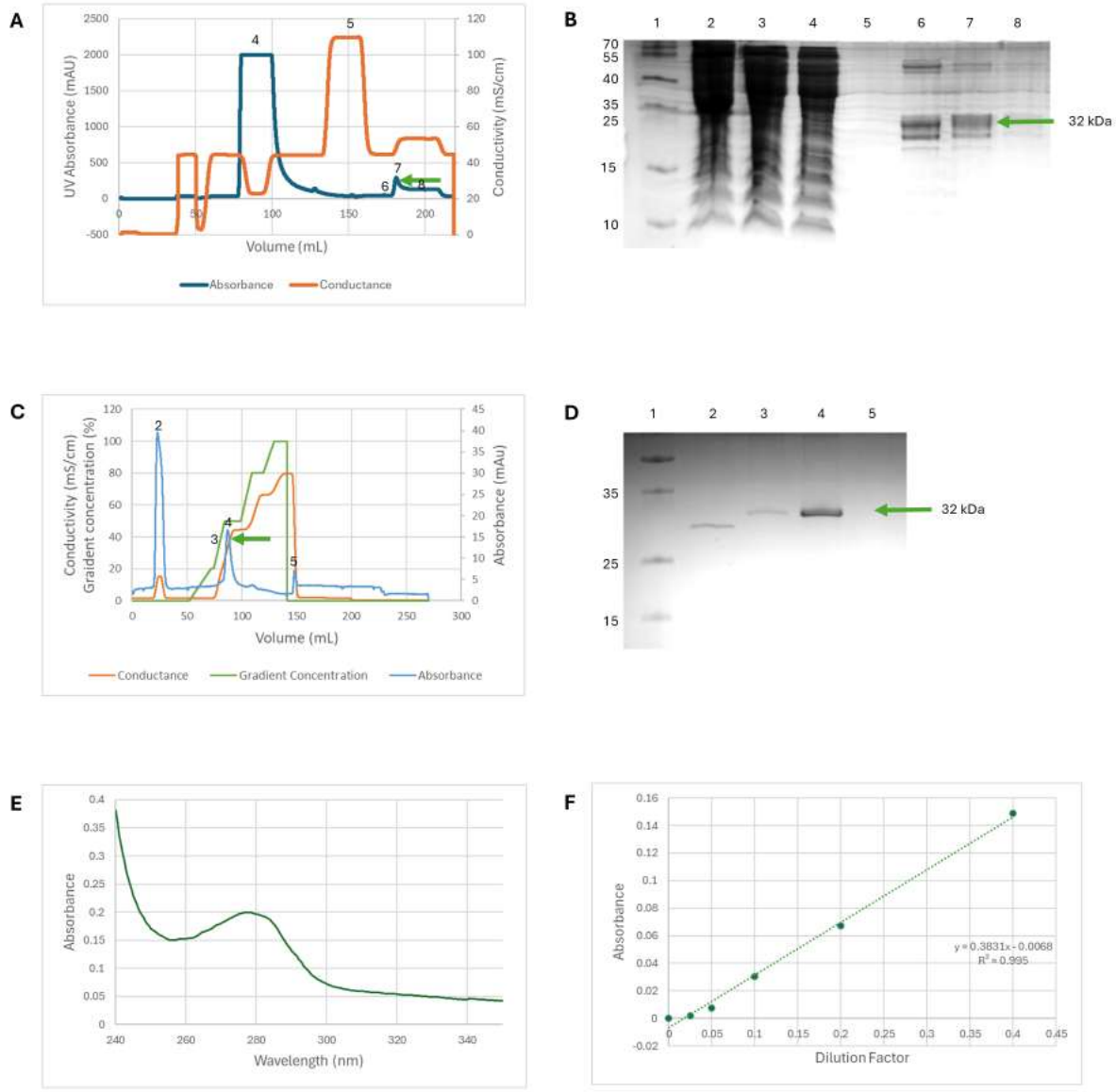

Figure 3.4. Purification of VDR LBD overexpressed in BL21(DE3) E. coli cells in LB media with 1 mM IPTG at OD_{600} 0.7 for 6 hours at 20°C. A: Elution profile of VDR LBD from IMAC purification (Blue: absorbance; orange: conductance; Peak 4: flow through, Peak 5: salt wash, Peak 6-8 = VDR LBD elution. B: SDS-PAGE gel of the purification of VDR LBD (left to right: 1 = molecular weight marker, 2 = pellet, 3 = supernatant, 4 = flow through, 5 = salt wash, 6-8 = VDR LBD elution. C: Chromatogram of VDR LBD purified using IEC with a positively charged HiTrap® Q High Performance column (Blue: absorbance; orange: conductivity, green: gradient concentration; Peak 2 = flow through; Peak 3, 4 = VDR LBD elution, Peak 5 = no protein). D: SDS-PAGE gel of the fractions collected from IEC of VDR LBD (from left to right, 1 = molecular weight marker; 2 = flow through, 3, 4 = elution peak, 5 = no protein. E: Absorbance spectrum to measure the quality of purified VDR. F: Straight line graph of absorbance at different dilutions of VDR LBD to determine protein concentration. VDR LBD was purified at a concentration of 8.8 µM.

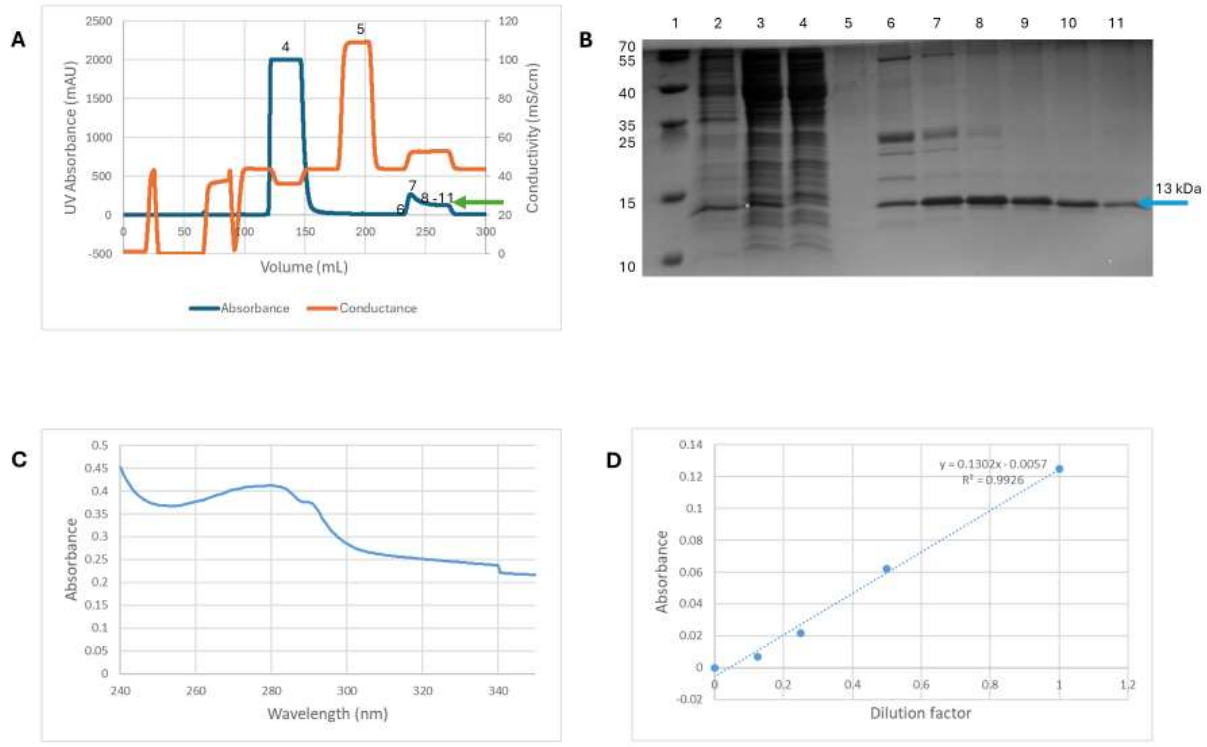

Figure 3.5. Purification of FOXP3 FHD. A: Purification curve of FOXP3 FHD (Absorbance: blue, conductance: orange; Peak 4: flow through; Peak 5: salt wash; Peaks 6-11: FOXP3 FHD elution). B: SDS-PAGE gel of the IMAC purification of FOXP3 FHD (from left to right: 1 = molecular weight marker; 2 = pellet; 3 = supernatant; 4 = flow through; 5 = salt wash; 6-11 = FOXP3 FHD elution). C: Absorbance spectrum of purified FOXP3 FHD. D: Graph of absorbance versus dilution factor of purified FOXP3 FHD. The concentration of FOXP3 FHD was calculated to be 5.21 µM. 16.86 mg protein per Litre culture.

The supernatant from the cell lysate for each protein was successfully purified using IMAC with a Nickel column (Figure 3.4 and 3.5). Figures 3.4A and 3.5A show the purification curve of the overexpressed VDR LBD and FOXP3 FHD respectively using IMAC purification. FOXP3 FHD was successfully purified using this method, but the VDR LBD sample was not fully pure and required an additional purification step. Therefore, ion exchange chromatography was performed on the eluted fractions (Figure 3.4C and D).

VDR LBD was successfully further purified using anion exchange IEC with gradient elution. Contaminants eluted out with the equilibration buffer containing no NaCl at around 20 mL, as seen by the peak labelled 2 and the corresponding band (lane 2) that is below the 32 kDa band observed for pure VDR LBD (lane 4) in the SDS-PAGE (Figure 3.4C and D). The pI of VDR LBD is 6.3 and therefore the protein is negatively charged at a pH of 7.5, allowing it to bind the positive HiTrap® Q High Performance column. Pure VDR LBD was eluted out with 50% elution buffer (0.5 M NaCl), indicated by peak 4 at around 80 mL. Another peak was observed after the buffer was changed back to 0% elution buffer and 100% equilibration buffer (peak 5, Figure 3.4C), but nothing was observed on the SDS-PAGE (Lane 5, Figure 3.4D). This was done to make sure the high salt concentration came out of

the column. Figure 3.4D confirms that the protein eluted is pure as observed by the single band at 32 kDa in lane 3 and 4 of the SDS-PAGE.

An absorbance spectrum from 240 nm to 350 nm was measured to assess the quality of purified VDR LBD (Figure 3.4E) and FOXP3 FHD (Figure 3.5C). The absorbance at 340 nm suggests a degree of protein aggregation. There should be zero absorbance at 340 nm, however both VDR LBD and FOXP3 FHD have a small amount of absorbance at 340 nm, indicating protein aggregation. However, the graph at 340 nm is flat for both proteins and the peak absorbance at 280 nm is higher, indicating that there is enough unaggregated protein to use in further experiments. Aggregates were removed by centrifugation and transferring the supernatant to a new tube before further experiments were conducted. Both spectra have a peak at 280 nm and a trough at 260 nm, with a 280/260 ratio of 1.3 for VDR LBD and 1.1 for FOXP3 FHD (Figure 3.4E and 3.5C). Protein absorbs at 280 nm, while DNA absorbs at 260 nm. Both purified proteins appear to have some DNA contamination, which was noted during further experiments as it could interfere with protein interactions. VDR LBD was purified at a concentration of 8.8 µM, 70.88 mg per litre of culture, as determined from the equation of the straight line y=0.3831x-0.0068 (Figure 3.4F). FOXP3 FHD was purified at a concentration of 5.21 µM, 16.86 mg per litre of culture (Figure 3.5D). These are low protein concentrations and for further studies the proteins were concentrated to the necessary concentrations.

Overall, both proteins, VDR LBD and FOXP3 FHD, were successfully purified in sufficient quantities that are sufficiently pure and in good enough quality for subsequent experiments.

3.3 Structural and functional characterisation of overexpressed and purified proteins

Both VDR LBD and FOXP3 FHD are mammalian proteins that were overexpressed in an *E. coli* host. Therefore, their structures and functions needed to be characterised to confirm that they were folded in the correct structure and were functional for further interaction experiments. 1,25(OH)D_3 solubilised in ethanol was used for subsequent functional and interaction experiments in the presence of both proteins. Therefore, to rule out that any changes in the interaction between the two proteins in the presence and absence of 1,25(OH)D_3 were due to structural changes or signal interference either by 1,25(OH)D_3 or ethanol, the effect of 1,25(OH)D_3 and ethanol on the folding of VDR LBD and FOXP3 FHD, as well as on the spectroscopic signals was tested. Before the structure of VDR LBD and FOXP3 FHD was characterised in the presence of 1,25(OH)D_3, it was tested whether 1,25(OH)D_3 absorbs light. It was also tested whether the wavelength of light that it absorbs would interfere with the spectroscopic signals of intrinsic tryptophan fluorescence (excitation at 295 nm) and, later, fluorescence anisotropy (excitation at 556 nm). Therefore, 1,25(OH)D_3 solubilised in 99% ethanol at 1 mg/mL, and diluted to 100 µM in Tris/HCl buffer, was found to have an absorbance with a peak at 280

nm, and no absorbance at 556 nm (Figure 3.6A). After dilution of 1,25(OH)D_3 into protein, the concentration of ethanol was 0.5% of the total sample, and the structural effects of this were tested using far-UV CD and intrinsic tryptophan fluorescence.

3.3.1 VDR LBD structural and functional characterisation

The secondary, tertiary and quaternary structures for VDR LBD were characterised. These were done using far-UV CD, intrinsic tryptophan fluorescence, and SEC, respectively. Both the native and urea denatured states of VDR LBD were used to confirm that the protein structural integrity was intact. The spectra for folded protein differ from the spectra for unfolded protein when using both far-UV CD and intrinsic tryptophan fluorescence, showing that the purified protein is folded. Reduced and non-reduced SDS-PAGE shows that VDR LBD forms disulfide bond dimers and needs to be kept in reducing agent. SEC shows that the protein in the presence of reducing agent is pure and the correct size for a monomer with no dimer peak present.

The shape of the far-UV CD spectrum for the native protein in Figure 3.6B is representative of the characteristic alpha helical curve indicated in Figure 2.3, with troughs around 208 and 222 nm, confirming the dominant alpha helical secondary structure as expected of the VDR LBD structure. The shape of the curve for the denatured protein in Figure 3.6B has no characteristic shape which indicates that the denatured protein has lost its secondary structure, thereby confirming that the secondary structure of the native VDR LBD has its integrity after overexpression and purification.

The fluorescence spectrum of the native protein in Figure 3.6C has a peak around 330 nm, while that of the denatured protein shows a red shift and has a small peak at around 350 nm. This indicates that tryptophan residues are being exposed to a more polar environment upon addition of urea and therefore suggests protein unfolding, further confirming the correct tertiary folded structure of the native VDR LBD that was overexpressed and purified. The decrease in fluorescence intensity when the protein is denatured could mean that tryptophan residues are more exposed to a molecule likely to quench its intrinsic fluorescence, for example a cysteine residue.

Far-UV CD was performed with VDR LBD in the presence of 1,25(OH)D_3 and 0.5% ethanol, compared with VDR LBD on its own, and 1,25(OH)D_3 on its own. As mentioned above, native VDR LBD exhibits alpha-helical secondary structure as depicted by the shape of the curve in Figure 3.6D. VDR LBD in the presence of 0.5% ethanol, and VDR LBD in the presence of 1,25(OH)D_3 exhibit the same alpha-helical secondary structure as apo-VDR LBD, as seen by the three spectra superimposing in Figure 3.6D. 1,25(OH)D_3 has no characteristic secondary structure.

The fluorescence spectrum of VDR LBD in the presence of 0.5% ethanol is the same shape as the fluorescence spectrum for native VDR LBD on its own (Figure 3.6E). Therefore, the buffer component

of 1,25(OH)D_3, ethanol, does not interfere with the tertiary structure of VDR LBD, nor the fluorescence signal. While 1,25(OH)D_3 does absorb light at 280 nm, it does not appear to fluoresce when excited at 295 nm (Figure 3.6E). This means that it should not interfere with the fluorescence signal, and any changes in the fluorescence spectrum observed will only be due to a change in the structure of VDR LBD in the presence of 1,25(OH)D_3. The fluorescence spectrum of VDR LBD in the presence of 1,25(OH)D_3 has a lower normalised fluorescence intensity when excited at 295 nm, although there is no shift in the wavelength of the fluorescence compared to the spectrum of apo-VDR LBD (Figure 3.6E). Therefore, 1,25(OH)D_3 does not cause a change in the tertiary structure of VDR LBD. The quenching of the fluorescence signal for VDR LBD in the presence of 1,25(OH)D_3 could be a result of two variables. Figure 3.6F shows the crystal structure, 1DB1 (Rochel et al., 2000), of VDR LBD in the presence of 1,25(OH)D_3, with tryptophan interacting with the ligand. This could cause quenching of the fluorescence signal. The other variable could be due to the inner filter effect of the ligand due to 1,25(OH)D_3 absorbing light at 280 nm. However, this cannot be confirmed without performing an experiment testing the intrinsic tryptophan fluorescence of VDR LBD in the presence of increasing concentrations of 1,25(OH)D_3.

VDR LBD can form homodimers through disulfide bonds with itself. To confirm that the solution of overexpressed and purified VDR LBD had one uniform oligomeric state, an SDS-PAGE was performed with and without reducing agent (β-marcaptoethanol). It was observed that the solution contained both monomer and homodimer with one band being observed in the presence of β-marcaptoethanol, and two bands observed in the absence (Figure 3.6G). In the non-reducing lane, a band is observed at the expected size for VDR LBD monomer, 32231.09 Da, with another band above it, around 64 kDa, double the size of the VDR LBD band, indicating that VDR LBD is present in both monomer and homodimer form in the absence of reducing agent. In the reducing lane, only 1 band is observed at around 32 kDa and is pure VDR LBD monomer. It was therefore important for subsequent experiments for VDR LBD to be stored and used in buffer containing 5 mM reducing agent (DTT or TCEP).

Using SEC, it was confirmed that when VDR LBD was in the presence of 5 mM DTT, it existed only in the monomeric state (Figure 3.6H). Based on the SEC standards in Figure 3.7, the data for which was kindly provided by Riyaad, the molecular weight of the protein in the eluted fraction collected in peak 4 was calculated to be 36307 Da. The monomeric size of VDR LBD is 32231.09 Da, therefore it can be confirmed that VDR LBD was eluted in the monomeric state. The SDS-PAGE gel in Figure 3.6I confirms pure VDR LBD in elution fractions 3, 4, and 5, with only 1 band present at 32 kDa. The quaternary structural characterisation studies were done before IEC due to low levels of protein, therefore the slight band below the thick VDR LBD band had not been removed yet. No dimer peak is present in the reducing conditions. Peak 1 in Figure 3.6H is the void volume and contains contaminants, as can be

seen by the band at around 50 kDa in lane 1 in SDS-PAGE (Figure 3.6I). The small hump 2 in the chromatogram does not contain any protein, with no band present in lane 2 in the SDS-PAGE.

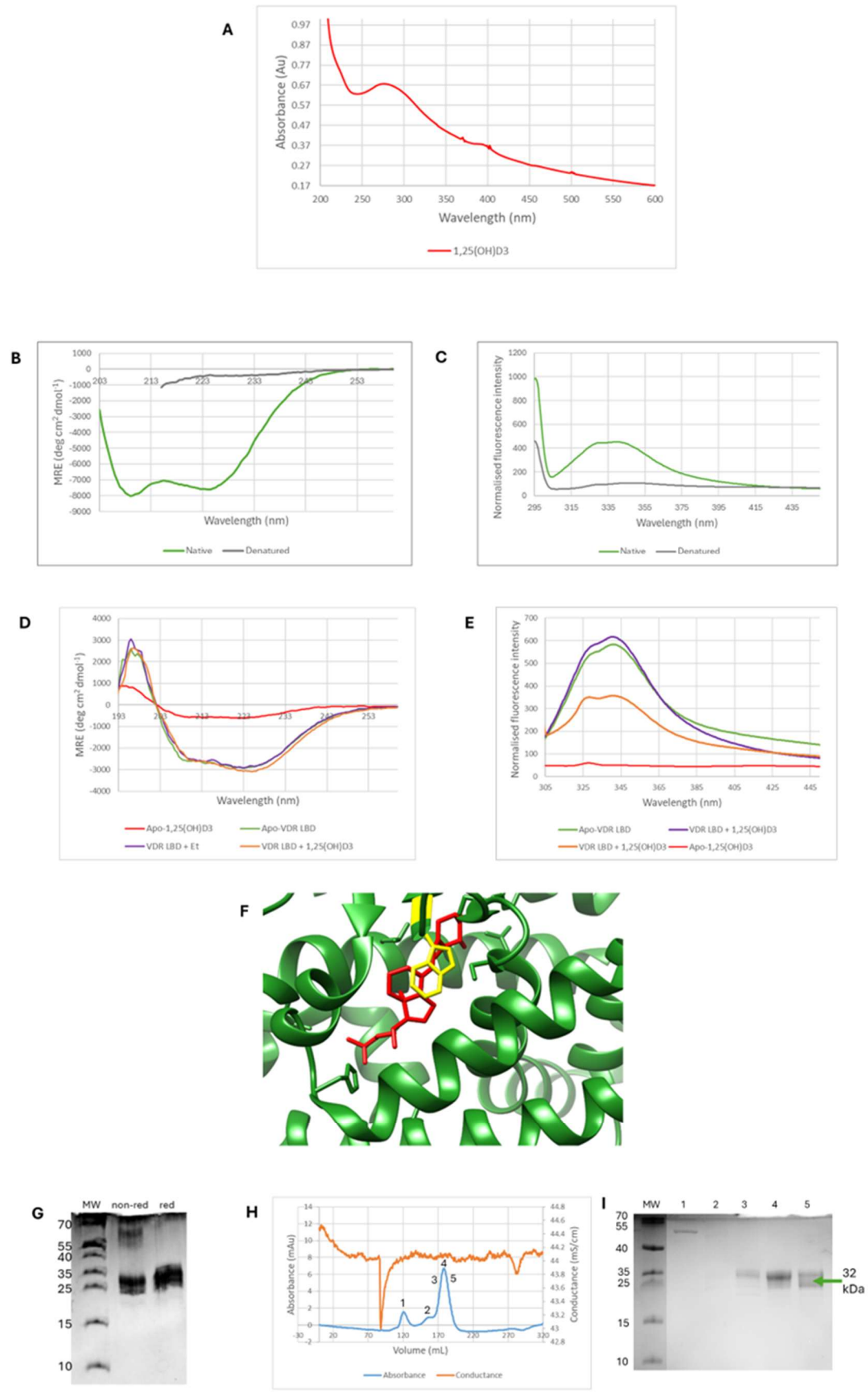

Figure 3.6. Structural characterisation for VDR LBD. Native VDR LBD is shown in green, denatured VDR LBD is shown in grey. Apo-1,25(OH)D_3 is shown in red, VDR LBD with 1,25(OH)D_3 is shown in orange, VDR LBD with 0.5%

ethanol is shown in purple. A: Far-UV CD for native and denatured VDR LBD. B: Intrinsic tryptophan fluorescence spectra with excitation at 295 nm. C: Absorbance spectrum of 1,25(OH)D₃. D: The effects of 1,25(OH)D₃ and its buffer components on the secondary structure of VDR LBD. E: Fluorescence spectra showing the effects of 1,25(OH)D₃ and its buffer components on the tertiary structure of VDR LBD at 295 nm. F: Crystal structure of VDR LBD bound to 1,25(OH)D (1DB1). G: SDS-PAGE gel to determine if VDR LBD forms homodimers through disulfide bonds (left to right: molecular weight marker, MW; VDR in the absence of β-mercaptoethanol, non-red; VDR LBD in the presence of β-mercaptoethanol, red). H: SEC chromatogram of VDR LBD in the presence of 5 mM DTT (Blue: Absorbance; Orange: Conductance; Peak 1 = void volume, Peak 2 = no protein; Peak 3, 4, 5 = VDR LBD monomer). I: SDS-PAGE of the samples collected from SEC (left to right: molecular weight marker, MW; 1 = void volume; 2 = no protein; 3, 4, 5 = VDR LBD monomer).

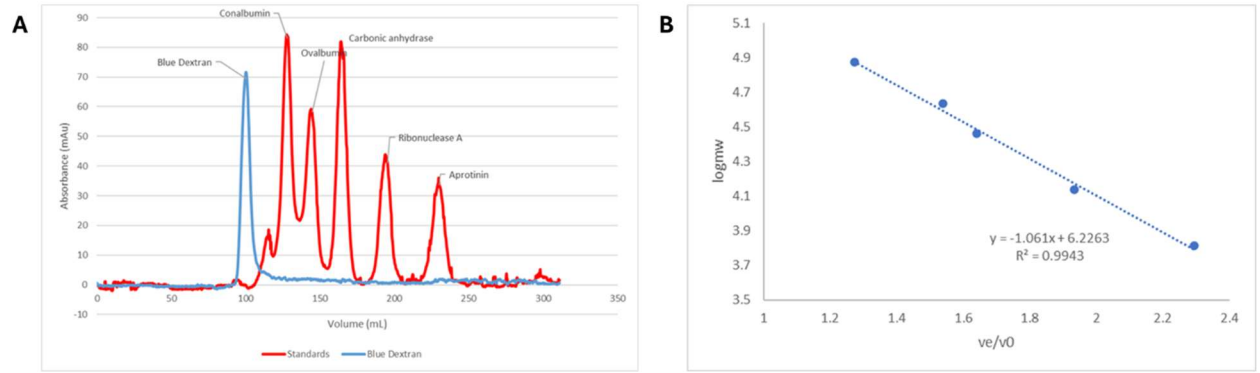

Figure 3.7 Protein standards for size exclusion chromatography. A: Absorbance spectrum of protein standards for SEC HiLoad™ 16/60 Superdex™ 75 prep grade column (GE healthcare, USA). B: Linear regression of $\log_{Mw}$ of proteins standards versus v_e/v_0. The graph has an equation of y = -1.061x + 6.2263, and an R^2 of 0.9943.

Since the structure of VDR LBD was found to be folded, a functional study was now performed to confirm if it was in its functional folded state. The ligand binding domain of VDR has been used throughout this study, therefore the ligand binding ability of VDR LBD was determined using a thermal shift assay.

VDR is known to bind 1,25(OH)D_3 with high affinity, K_d 0.1 nM (Haussler and Norman, 1969). The thermal shift assay indicates that VDR LBD in the presence of 1,25(OH)D_3 degrades at a higher melting point than VDR LBD on its own (Figure 3.8). There is a shift observed from a T_M of 52°C for VDR LBD on its own, to 54°C for VDR LBD with 2x 1,25(OH)D_3 (Figure 3.8). A shift to the right when 1,25(OH)D_3 is present indicates an increased stability of VDR LBD in the protein-ligand complex compared to the protein on its own, therefore confirming that VDR does bind 1,25(OH)D_3 and is functional (Luan et al., 2014; Scott, 2017; Kushwah et al., 2024).

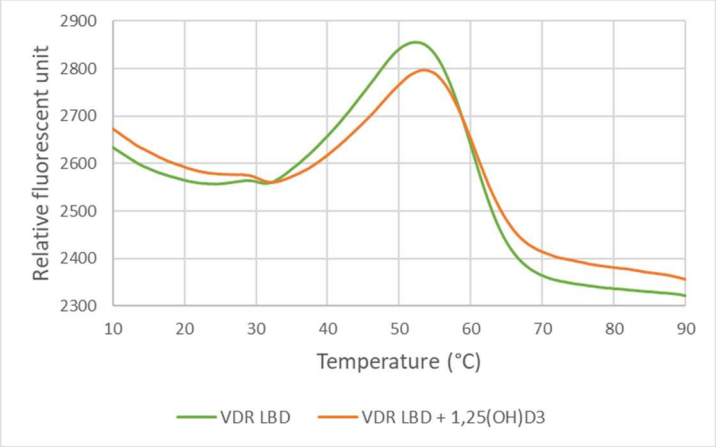

Figure 3.8. Relative fluorescent intensity versus temperature for the thermal shift between VDR and VDR + 1,25(OH)D_3. The green graph represents 25 µM of VDR, and the orange graph is 25 µM of VDR with 50 µM of 1,25(OH)D_3. The highest point of the green graph is at 52°C while that of the orange graph is 54°C.

3.3.2 FOXP3 FHD structural and functional characterisation

Now, the secondary, tertiary and quaternary structures for FOXP3 FHD were characterised using far-UV CD, intrinsic tryptophan fluorescence, and SEC, respectively. To confirm that the protein structural integrity was intact, its structure in the native and unfolded state was determined. CD and fluorescence showed that the purified protein is folded as the spectrum is different from that of the denatured protein. SEC shows the protein is pure and the correct size for a dimer with no monomer peak present.

The shape of the far-UV CD spectrum of the native protein in Figure 3.9A is representative of the characteristic alpha helical curve indicated in Figure 2.3, with troughs at 208 and 222 nm, confirming the dominant alpha helical secondary structure as expected of the FOXP3 FHD structure. The far-UV CD spectrum of the denatured protein in Figure 3.9A has no characteristic shape which indicates that the denatured protein has lost its secondary structure, thereby confirming that the secondary structure of the native FOXP3 FHD has its integrity after overexpression and purification.

The fluorescence spectrum of the native protein in Figure 3.9B has a characteristic peak at around 330 nm, while that of the denatured protein has a peak at around 350 nm. The fluorescence spectrum of the denatured protein therefore exhibits a red shift as compared to the fluorescence spectrum of the native protein. This is indicative of protein unfolding in the denatured protein as tryptophan is in a more polar environment characteristic of the polar components in the buffer. This further confirms the correct tertiary folded structure of the native FOXP3 FHD that was overexpressed and purified. The peak for the denatured protein has a higher intensity than the peak for the native protein, which also shows that when the protein is correctly folded tryptophan is near to a quencher that could be a cysteine, and when unfolded, has a higher fluorescence intensity. Overall, it can be concluded that the overexpressed and purified FOXP3 FHD has its structural integrity intact.

The far-UV CD spectra of apo-FOXP3 FHD, FOXP3 FHD in the presence of 0.5% ethanol, and FOXP3 FHD in the presence of 1,25(OH)D_3 directly superimpose onto one another (Figure 3.9C). The spectrum of apo-1,25(OH)D_3 shows that 1,25(OH)D_3 has no characteristic secondary structure. Therefore, neither 1,25(OH)D_3, nor the buffer component of the ligand, ethanol, impacts the secondary structure of FOXP3 FHD.

The tertiary structure of FOXP3 FHD as determined by intrinsic tryptophan fluorescence does not change in the presence of 0.5% ethanol, the spectra of FOXP3 FHD with 0.5% ethanol and apo-FOXP3 FHD directly superimpose onto each other (Figure 3.9D). The shape of the fluorescence spectrum does not change in the presence of 1,25(OH)D_3 either; however, the intensity of the spectrum is decreased (Figure 3.9D). This decrease in normalised fluorescence intensity in the presence of the ligand is suspected to be due to the inner filter effect; however, this can only be confirmed through performing an additional experiment, as mentioned in section 3.3.1 above.

Using SEC, the fraction 2 eluted was calculated to have a molecular weight of 27542 Da using the equation of the straight line for the protein standards in Figure 3.7B. FOXP3 FHD dimer has a molecular weight of 25877.86 Da. Therefore, FOXP3 FHD has in fact been expressed and purified in its dimeric form as observed by the peak 2 in Figure 3.9E, and the single band at 13 kDa in the SDS-PAGE gel in lane 2 of Figure 3.9F. No monomer is present in the sample. There is no protein present in the SDS-PAGE for peak 3 (Figure 3.9E and D, lane 3), therefore peak 3 is the absorbance by the buffer components in which FOXP3 FHD was stored. Therefore, it can be concluded that there is only one oligomeric state present in the solution of purified FOXP3 FHD, which is dimer.

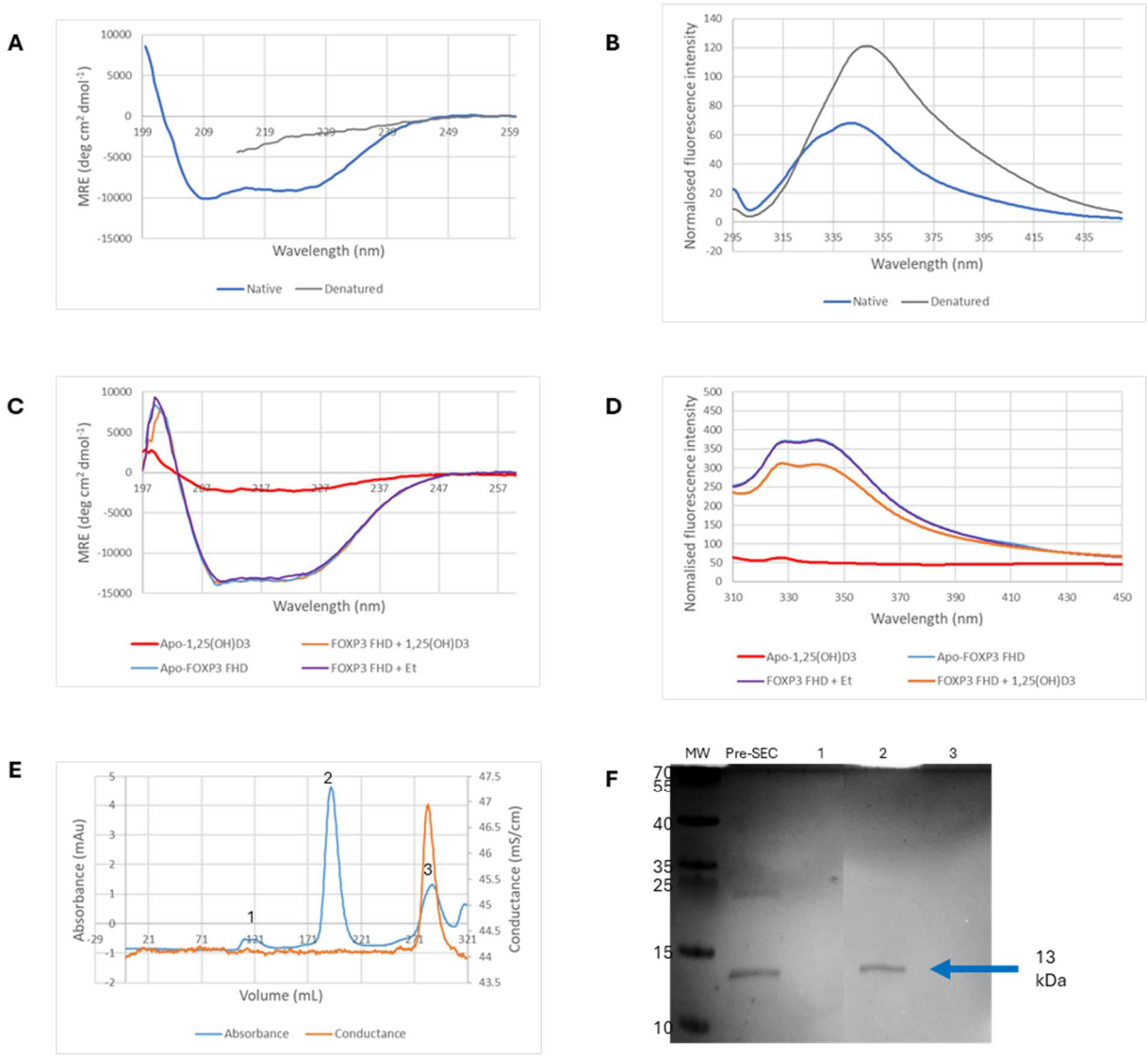

Figure 3.9. Structural characterisation results for FOXP3 FHD. Native FOXP3 FHD is shown in blue, Denatured FOXP3 FHD with is shown in grey. A: Secondary structure determination using Far-UV CD for purified native and denatured FOXP3 FHD. B: Intrinsic tryptophan fluorescence for tertiary structure characterisation at 295 nm. C: The effects of 1,25(OH)D_3 and its buffer components on the secondary structure of FOXP3 FHD. D: Fluorescence spectra showing the effects of 1,25(OH)D_3 and its buffer components on the tertiary structure of FOXP3 FHD at 295 nm. E: SEC graph for quaternary structure determination of FOXP3 FHD (Blue: Absorbance; Orange: Conductance; Peak 1 = void volume, Peak 2 = FOXP3 dimer). F: SDS-PAGE gel of the fractions collected from SEC (left to right: molecular weight marker, MW; pre-SEC sample, Pre-SEC; 1 = void volume; 2 = FOXP3 FHD dimer, and 3 = no protein).

Now that FOXP3 FHD was confirmed to be folded, a functional assay was done to determine that it was folded in its functional structure. FOXP3 is a transcription factor, with its primary function being DNA-binding. Therefore, a DNA-binding assay was performed in the form of an EMSA to prove that the purified protein is functional.

The FOXP3 FHD that was overexpressed and purified in *E. coli* cells is confirmed to be functional, according to Figure 3.10, where binding to consensus FHD DNA is observed. A clear shift of the bands in the EMSA gel is observed. For DNA to protein ratios 1:1, 1:3 and 1:5, two bands are observed, one

lower down on the gel, indicating DNA on its own, and one higher up on the gel, indicating a DNA-protein complex. For DNA to protein ratios 1:8 – 1:20, smearing of the bands are observed on the EMSA gel. Smearing indicates weak binding between protein and DNA, which is uncommon at higher concentrations of protein. It could be due to more protein competing to bind to the DNA, causing bound protein to release from the DNA.

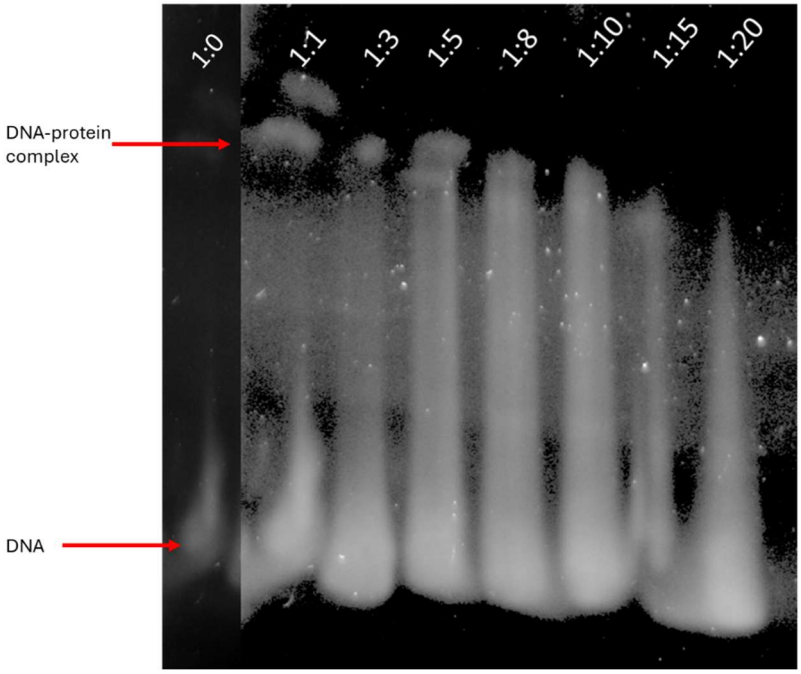

Figure 3.10. EMSA gel of FOXP3 FHD with FHD consensus DNA. FOXP3 FHD with FHD consensus DNA was run on an 8% EMSA gel made with 5X TAE buffer and binding buffer of pH 7.8. DNA was incubated with increasing protein concentrations. FOXP3 FHD is bound to consensus FHD DNA as seen for 1:1, 1:3 and 1:5, with weak binding observed at 1:8, 1:10, 1:15 and 1:20.

3.4 Protein-protein and protein-protein-ligand interactions

After successful overexpression and characterisation of both VDR LBD and FOXP3 FHD, fluorescence anisotropy was performed. Neither the presence of 1,25(OH)D_3, nor that of the buffer component that 1,25(OH)D_3 is solubilised in (ethanol), interferes with the structures of VDR LBD and FOXP3 FHD. This is important as fluorescence anisotropy was to be done next in the presence of 1,25(OH)D_3. It was necessary to confirm that any changes observed in the fluorescence anisotropy spectra in the presence and absence of 1,25(OH)D_3 were in fact due to a change in the interaction between the two proteins when 1,25(OH)D_3 was present, and not due to a change in either of the protein's structures interacting with the ligand. VDR LBD in reducing agent is in monomer form, and FOXP3 FHD is in its functional homodimer form. Both proteins were expressed and purified in the functional form as determined by thermal shift assay, where VDR LBD interacted with its ligand – 1,25(OH)D_3 – and EMSA, where FOXP3 FHD bound to its consensus DNA sequence. Finally, the two overexpressed and purified

proteins could be used to experimentally confirm if the interaction between VDR LBD and FOXP3 FHD that was predicted, *in silico*, in section 3.1 was indeed correct.

In the presence of 1,25(OH)D_3, the fluorescence anisotropy results confirmed that solutions of VDR LBD with increasing FOXP3 FHD concentration caused the relative fluorescence anisotropy to increase, indicating more larger complexes were forming in the solution, and eventually evening out when VDR LBD was saturated with FOXP3 FHD. Indeed, FOXP3 FHD does interact with VDR LBD in the presence of 1,25(OH)D_3 (Figure 3.11). This interaction between VDR LBD and FOXP3 FHD in the presence of 1,25(OH)D_3 has a medium affinity with a K_d of 0.2272 µM with a standard deviation of 0.079, and a B_{max} of 0.0732 with a standard deviation of 0.00921. The graph was fitted with an R^2 of 0.8132. K_d is the molecular dissociation constant of the interaction between the two proteins and gives an indication about the affinity of FOXP3 FHD to VDR LBD. It is the concentration of FOXP3 FHD required to reach half the B_{max}. B_{max} is the relative fluorescence anisotropy at which the graph plateaus and therefore when VDR LBD is saturated with FOXP3 FHD. Despite a clear interaction being shown between the two proteins in the presence of 1,25(OH)D_3, when in the absence of 1,25(OH)D_3, no interaction is observed between VDR LBD and FOXP FHD (Figure 3.11). The graph is flat and no K_d or B_{max} is reached between the proteins. This is contrary to the computational prediction.

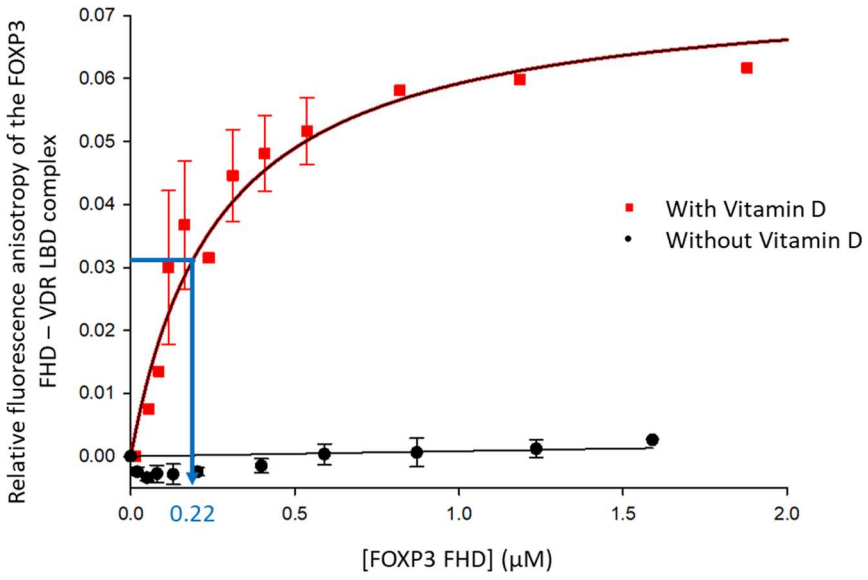

Figure 3.11. Fluorescence anisotropy showing the interaction between VDR LBD and FOXP3 FHD in the presence and absence of 1,25(OH)D_3. The x-axis shows increasing FOXP3 FHD concentrations added to 0.5 µM VDR LBD labelled with Alexa fluor 555 C2-Maleimide (30% labelling efficiency). Both proteins were in the presence of 5 mM TCEP and either 5 µM 1,25(OH)D_3 (red), or no 1,25(OH)D_3 (black). FOXP3 FHD and VDR LBD in the presence of 1,25(OH)D_3 interact with each other with a K_d of 0.2272 µM, standard deviation: 0.079, and a B_{max} of 0.0732, standard deviation: 0.00921, and an R^2 of 0.8132. The K_d is shown by the blue arrows. FOXP3 FHD and VDR LBD without 1,25(OH)D_3 (black) do not interact, as indicated by the flat graph.

Chapter 4: Discussion and conclusion

Given that there is no experimental evidence of an association between FOXP3 and VDR at a protein level in humans, despite their joint roles in the regulation of immune function, this study aimed to determine whether VDR and FOXP3 interact directly at a protein-protein level, and whether 1,25(OH)D_3 would have an impact on this interaction. This study identified, for the first time, an interaction between VDR LBD and FOXP3 FHD. Using two molecular docking programs, HDock (Yan et al., 2020) and LZerd (Christoffer et al., 2021), the VDR LBD interaction with FOXP3 FHD was predicted to occur whether or not 1,25(OH)D_3 was present. Specifically, VDR LBD was predicted to interact with helix 3, the DNA binding helix of the FHD of FOXP3. However, FOXP3 FHD was predicted to occur in different binding pockets of VDR LBD when ligand was present and absent. This is suspected to be due to a structural shift in VDR LBD when 1,25(OH)D_3 binds. A more negative HDock score indicates that the interaction is more likely to occur spontaneously. A confidence score of more than 0.7 in HDock indicates a high likelihood of the interaction occurring (Yan et al., 2020). The docking score for the FOXP3 FHD, VDR LBD interaction was negative, with a high confidence scores, and the scores are comparable to a known protein-protein interaction between FOXP3 FHD and NFAT (Bandukwala et al., 2011), with an HDock docking score of -279.04 and a confidence score of 0.9296 (Yan et al., 2020). Therefore, the interaction between FOXP3 FHD and VDR LBD is predicted to occur spontaneously, and this is predicted with a high confidence. The LZerd scores are all high negative values. The scores are less negative than LZerd docking between the known protein-protein interaction between FOXP3 FHD and NFAT (Bandukwala et al., 2011), with a GOAP score of -80122.82, a DFIRE score of -61789.76, and an ITScore of -32009.31. The interaction between FOXP3 FHD and VDR LBD is therefore predicted to be probable. Using fluorescence anisotropy, however, VDR LBD and FOXP3 FHD were found to interact with each other only in the presence of 1,25(OH)D_3 *in vitro*, having a medium affinity with a K_d of 0.2272 µM. The clear discrepancy between the *in silico* and the *in vitro* results supports the necessity for cross-verification of computational results with experimental work. In agreement, Desta et al. (2020) reported that molecular docking is not yet a reliable indicator of protein-protein interactions without experimental validation. To compliment molecular docking and increase the reliability of the computational results for this study, molecular dynamics symulation could be performed. This computational study simulates the internal environment of a cell and therefore gives a more accurate indication of potential interactions within a 3-dimensional environment (Hansson et al., 2002).

The observation that the two proteins only interact in the presence of 1,25(OH)D_3 *in vitro* is in line with literature, where the VDR-RXR heterodimer formation, as well as other heterodimers that VDR forms, are stabilised by 1,25(OH)D_3 (Cheskis and Freedman, 1994; Liu et al., 2000; Quack and Carlberg,

2000). According to the findings of Cheskis and Freedman, 1994, the presence of 1,25(OH)D_3 stabilises the monomer over the homodimer, therefore favouring the formation of the VDR-RXR heterodimer complex. Little heterodimerisation was shown in the absence of 1,25(OH)D_3 between VDR and RXR (Liu et al., 2000). However, in the presence of 1,25(OH)D_3, a 20- and 17-fold increase of heterodimerisation was observed in *in vitro* translated VDR and VDR in the cell, respectively (Liu et al., 2000). This indicates that VDR-RXR heterodimerisation is ligand-dependant and is preferred over VDR homodimerisation. Liu et al., 2000, further showed that VDR only forms heterodimers with its coactivators, steroid receptor coactivator 1, and glucocorticoid receptor-interacting protein 1, in the presence of 1,25(OH)D_3, with the interactions being completely ligand-dependent. It is important to note that Liu et al., (2000) only tested the LBD of VDR, and the full-length VDR might exhibit different results. Within our Unit, Lakhi and Fanucchi, 2024, had similar findings using another nuclear receptor, oestrogen receptor and a member of the FOXP family, FOXP2. Oestrogen binding to oestrogen receptor was found to encourage oestrogen receptor-FOXP2 interaction (Lakhi and Fanucchi, 2024).

It is suspected that heterodimerisation of VDR LBD with FOXP3 FHD in the presence of 1,25(OH)D_3, but not in the absence, could be due to potential conformational changes that VDR LBD or FOXP3 FHD undergo when interacting with 1,25(OH)D_3. Based on the findings of this study, no change is observed in the global secondary structure of VDR LBD or FOXP3 FHD in the presence of 1,25(OH)D_3, while a slight change is observed in the tertiary structure. Looking at the fluorescence spectra of VDR LBD (Figure 3.6E) and FOXP3 FHD (Figure 5.9D) with 1,25(OH)D_3, a slight change is observed in the local environment of tryptophan. The lower fluorescence intensity is suspected to be due to the inner filter effect, from 1,25(OH)D_3 having an absorbance of 280 nm (Lakowicz, 1985). However, the wavelength of the peak does not change. There is no global secondary structural change in VDR LBD (Figure 3.6F) or FOXP3 FHD (Figure 3.9C) observed from the far-UV CD results with 1,25(OH)D_3 present. Conformational changes cannot be observed in the molecular docking results because rigid body docking was performed so no structural changes occurred when 1,25(OH)D_3 was removed from the VDR LBD structure. Therefore docking with and without 1,25(OH)D_3 predicted an interaction between VDR LBD and FOXP3 FHD. Rochel et al., 2000, crystallised the monomeric form of VDR LBD in the presence of 1,25(OH)D_3. They indicated that there are multiple changes that occur in the LDB of VDR during 1,25(OH)D_3 interaction, including helix (H) 12, which interacts directly with the methyl group of the ligand through Van der Waals contacts. The interaction is stabilised by hydrophobic and polar contacts, the former involving residues of H12, H3, H5, and H11, and the latter involving the Lys-264 in H4 and Glu-420 salt bridge, and the Ser-235 in H3 hydrogen bonded with Thr-415. H12 directly interacts with the ligand, changing its positioning. The residues in the H11-H12 loop form hydrogen bonds with the end of H2, which then form hydrogen bonds with H3 (Rochel et al., 2000). Interactions

form between the hydroxyl moiety of 1,25(OH)D_3 and Ser-237 and Arg-274 of H3 and H5, respectively, and the alcohol group of 1,25(OH)D_3 hydrogen bonds with Ser-278 of H5 and Tyr-143, with a water channel being formed through Arg-274 hydrogen bonding with water molecules (Rochel et al., 2000).

The observed interaction between VDR LBD and FOXP3 FHD have the potential to impact each protein's function. Both proteins are involved in regulation of the immune system, therefore their interaction in a protein-protein manner is a key finding in elucidating the roles of each of these proteins in immune regulation and autoimmunity. FOXP3 functions by forming a domain-swapped dimer with itself allowing it to bring two distal parts of DNA together to regulate gene expression (Bandukwala et al., 2011). FOXP3 FHD binds to DNA with helix 3 of the domain swapped dimer (Bandukwala et al., 2011). From the docking results using HDock and LZerd, VDR LBD interacts with helix 3 of one chain of FOXP3 FHD. Therefore, helix 3 of one of the chains of the FHD is no longer available to bind with DNA and bring two regions together, as is FOXP3's normal function. The interaction of VDR LBD with FOXP3 FHD will either inhibit the binding of FOXP3 FHD to two regions of DNA, or, speculatively, VDR LBD could act as the other domain, and bind another region of DNA that would perhaps be inaccessible to FHD domain-swapped dimer on its own. With one of FOXP3 FHD's helix 3 binding to VDR, this could allow the FOXP3-VDR-1,25(OH)D_3 complex to bind to completely different and new, yet unidentified strands of DNA, bringing them together to regulate gene expression of very specific genes within Tregs, and therefore in immune regulation. The complex could recognise a new combination of DNA sequences and form interactions mediated by the FOXP3 FHD and VDR LBD heterodimer. Another speculation is that the binding of VDR LBD to helix 3 of one of the domains of FOXP3 FHD in its domain-swapped dimer form, could prevent FHD from binding certain sequences and therefore inhibit both proteins' ability to regulate gene expression. This could be useful in that, as observed, the two proteins are involved in activating Tregs, and therefore indirectly inactivating the immune system reaction to infection (Song et al., 2012; Yang et al., 2013). By interacting with each other, and potentially inhibiting their transcription factor activities, they could turn off immune regulation. If Tregs are activated to turn off an immune reaction, and then not inactivated afterwards, there will be no immune response to following infections. Therefore, it could be speculated that VDR and FOXP3 interaction is to inhibit their function, switching off Tregs and resuming normal immune response in an individual. Further studies could be done to observe these speculations, such as fluorescence anisotropy in the presence of FHD consensus DNA, to see if FOXP3 FHD can still bind its DNA in the presence of VDR LBD and 1,25(OH)D_3, as well as a super shift EMSA to confirm the fluorescence anisotropy results. A transcriptome analysis of Treg cells can be used to identify different gene sequences to which the complex of FOXP3 FHD, VDR LBD and 1,25(OH)D_3 could

potentially bind. Once genes have been identified, molecular dynamics simulations could be done to narrow down the number of genes to do experimental analysis with.

This research has taken a reductionist approach. It was important to start with a reductionist approach because of the large networks involved in the pathophysiology of autoimmune disorders. To extract the two proteins and work with them individually out of the large systems allows for an understanding of one interaction at a time. This is important to understand the role of each individual component within a network. The overexpression and purification of VDR LBD was optimised in this study to perform experiments with the protein.

As necessary as it is to take a reductionist approach at first, there are limitations to this method of study. The interaction between the two proteins in their natural environment and in conjunction with the rest of the pathways that they are involved cannot be observed using a reductionist approach. These factors will inevitably have an impact on the interaction between the two proteins. Reductionist research gives insights into interactions that are potentially physiologically unrelated (Peng et al., 2017). To combat these limitations, future studies can be done. Starting with the same techniques that were used in this study, but with full-length VDR and FOXP3, a deeper insight into how the proteins interact with each other can be gained. Observing the interactions between the two proteins in their native mammalian cellular environment, such as in Treg cells using immunoprecipitation can be performed. This would allow an investigation into the effect of other cellular components on the interaction. Once the interaction would have been observed in a cellular environment, it can be determined how this interaction affects the function and expression of each of the proteins. This could be done using luciferase assay and RNA extraction with quantitative reverse transcription polymerase chain reaction and transcription analysis. The use of luciferase will give an indication as to how the expression of each of the proteins would be affected by the interaction. Luciferase is an enzyme that triggers bioluminescence (Carter and Shieh 2015). It would therefore be included on the plasmid containing the DNA coding for the protein of interest (FOXP3 FHD or VDR LBD). An increase in bioluminescence would indicate an increase in expression of the protein of interest. Quantitative reverse transcription polymerase chain reaction will allow us to make many DNA copies of the extracted RNA of the proteins of interest (Taylor et al., 2010). Analysis can then be performed, thereby determining if the interaction of FOXP3 FHD and VDR LBD changes either of their protein expressions.

4.1 Conclusion

In conclusion, VDR LBD has been shown for the first time to interact with FOX FHD both *in silico* and *in vitro*. The identification of this interaction, while requiring further elucidation, is suggested to impact immune regulation and autoimmune disorders. VDR LBD and FOXP3 FHD interact with each

other with an equilibration constant of K_d = 0.2272 µM, with 1,25(OH)D_3 being a key player in this interaction. From the molecular docking studies, VDR LBD is shown to interact with helix 3 – the DNA binding helix – of FOXP3 FHD. The interaction between VDR LBD and the DNA binding helix of FOXP3 FHD is speculated to have an impact on the DNA binding ability of FOXP3. FOXP3 can bind two distal regions of DNA and bring them closer together for regulation of gene expression. It does this through forming a domain-swapped dimer with itself. If one of its DNA binding helices is occupied with VDR LBD, two options are speculated: either FOXP3 will no longer be able to bind two regions of DNA and regulate gene expression in its regular manner, or the FOXP3-VDR heterodimer complex would potentially bind different, yet undiscovered gene sequences, and regulate the expression of different genes specifically for Treg function and immune regulation. Either of these options are speculated to upregulate or downregulate immune regulation. Altogether this increases the understanding of immune regulation and the roles that FOXP3, VDR and 1,25(OH)D_3 play in immune regulation, as well as emphasising the importance of 1,25(OH)D_3 in the pathophysiology of autoimmune disorders.

References

Abramson, J., Adler, J., Dunger, J., Evans, R., Green, T., Pritzel, A., et al., 2024. Accurate structure prediction of biomolecular interactions with AlphaFold 3. Nature 630, 493–500. https://doi.org/10.1038/s41586-024-07487-w

Altschul, S.F., Gish, W., Miller, W., Myers, E.W., Lipman, D.J., 1990. Basic local alignment search tool. J. Mol. Biol. 215, 403–410. https://doi.org/10.1016/S0022-2836(05)80360-2

Alvarez, B., Martínez-A., C., Burgering, B.M.T., Carrera, A.C., 2001. Forkhead transcription factors contribute to execution of the mitotic programme in mammals. Nature 413, 744–747. https://doi.org/10.1038/35099574

Amrein, K., Scherkl, M., Hoffmann, M., Neuwersch-Sommeregger, S., Köstenberger, M., Tmava Berisha, A., et al., 2020. Vitamin D deficiency 2.0: an update on the current status worldwide. Eur. J. Clin. Nutr. 74, 1498–1513. https://doi.org/10.1038/s41430-020-0558-y

Andersen, M.H., Schrama, D., thor Straten, P., Becker, J.C., 2006. Cytotoxic T Cells. J. Invest. Dermatol. 126, 32–41. https://doi.org/10.1038/sj.jid.5700001

Andrews, C.M., 1998. The Haematopoietic System, in: Target Organ Pathology. CRC Press.

Arnson, Y., Amital, H., Agmon-Levin, N., Alon, D., Sánchez-Castañón, M., López-Hoyos, M., et al., 2011. Serum 25-OH vitamin D concentrations are linked with various clinical aspects in patients with systemic sclerosis: a retrospective cohort study and review of the literature. Autoimmun. Rev. 10, 490–494. https://doi.org/10.1016/J.AUTREV.2011.02.002

Sinha, A., Lopez, M., McDevitt, H., 1990. Autoimmune Diseases: The Failure of Self Tolerance Science 248, 1380-1388. https://doi.org/10.1126/science.1972595

Azuma, M., 2010. Role of the Glucocorticoid-Induced TNFR-Related Protein (GITR)-GITR Ligand Pathway in Innate and Adaptive Immunity. Crit. Rev. Immunol. 30. https://doi.org/10.1615/CritRevImmunol.v30.i6.40

Balistreri, C.R., Garagnani, P., Madonna, R., Vaiserman, A., Melino, G., 2019. Developmental programming of adult haematopoiesis system. Ageing Res. Rev. 54, 100918. https://doi.org/10.1016/j.arr.2019.100918

Bandukwala, H.S., Wu, Y., Feuerer, M., Chen, Y., Barboza, B., Ghosh, S., et al., 2011. Structure of a Domain-Swapped FOXP3 Dimer on DNA and Its Function in Regulatory T Cells. Immunity 34, 479–491. https://doi.org/10.1016/j.immuni.2011.02.017

Banham, A.H., Beasley, N., Campo, E., Fernandez, P.L., Fidler, C., Gatter, K., et al., 2001. The FOXP1 Winged Helix Transcription Factor Is a Novel Candidate Tumor Suppressor Gene on Chromosome 3p1. Cancer Res. 61, 8820–8829.

Barth, H.G., Boyes, B.E., Jackson, C., 1994. Size Exclusion Chromatography. Anal Chem 66, 595–620.

Barzaghi, F., Passerini, L., Bacchetta, R., 2012. Immune dysregulation, polyendocrinopathy, enteropathy, x-linked syndrome: a paradigm of immunodeficiency with autoimmunity. Front. Immunol. 3. https://doi.org/10.3389/FIMMU.2012.00211

Bennett, C.L., Christie, J., Ramsdell, F., Brunkow, M.E., Ferguson, P.J., Whitesell, L., et al., 2001. The immune dysregulation, polyendocrinopathy, enteropathy, X-linked syndrome (IPEX) is caused by mutations of FOXP3. Nat. Genet. 27, 20–21. https://doi.org/10.1038/83713

Bettelli, E., Carrier, Y., Gao, W., Korn, T., Strom, T.B., Oukka, M., et al., 2006. Reciprocal developmental pathways for the generation of pathogenic effector TH17 and regulatory T cells. Nat. 2006 4417090 441, 235–238. https://doi.org/10.1038/nature04753

Beutler, B., 2004. Innate immunity: an overview. Mol. Immunol., Innate Immunity 40, 845–859. https://doi.org/10.1016/j.molimm.2003.10.005

Block, H., Maertens, B., Spriestersbach, A., Brinker, N., Kubicek, J., Fabis, R., et al., 2009. Immobilized-metal affinity chromatography (IMAC): a review. Methods Enzymol. 463, 439–473. https://doi.org/10.1016/S0076-6879(09)63027-5

Blumenfeld, F., Gardner, J., 1985. Gel Filtration - An innovative Separation Technique. Filtrates and Residues 62.

Bonilla, F.A., Oettgen, H.C., 2010. Adaptive immunity. J. Allergy Clin. Immunol., 2010 Primer on Allergic and Immunologic Diseases 125, S33–S40. https://doi.org/10.1016/j.jaci.2009.09.017

Brunkow, M.E., Jeffery, E.W., Hjerrild, K.A., Paeper, B., Clark, L.B., Yasayko, S.-A., et al., 2001. Disruption of a new forkhead/winged-helix protein, scurfin, results in the fatal lymphoproliferative disorder of the scurfy mouse. Nat. Genet. 27, 68–73. https://doi.org/10.1038/83784

Cantorna, M.T., Mahon, B.D., 2005. Personal non-commercial use only, The Journal of Rheumatology.

Carter, M., Shieh, J., 2015. Chapter 15 - Biochemical Assays and Intracellular Signaling. Academic Press, 311-343. https://doi.org/10.1016/B978-0-12-800511-8.00015-0

Chae, W.-J., Henegariu, O., Lee, S.-K., Bothwell, A.L.M., 2006. The mutant leucine-zipper domain impairs both dimerization and suppressive function of Foxp3 in T cells. Proc. Natl. Acad. Sci. 103, 9631–9636. https://doi.org/10.1073/pnas.0600225103

Chen, J.D., Evans, R.M., 1995. A transcriptional co-repressor that interacts with nuclear hormone receptors. Nature 377, 454–457. https://doi.org/10.1038/377454A0

Chen, Y., Chen, C., Zhang, Z., Liu, C.C., Johnson, M.E., Espinoza, C.A., et al., 2015. DNA binding by FOXP3 domain-swapped dimer suggests mechanisms of long-range chromosomal interactions. Nucleic Acids Res. 43, 1268–1282. https://doi.org/10.1093/nar/gku1373

Cheskis, B., Freedman, L.P., 1994. Ligand Modulates the Conversion of DNA-Bound Vitamin D3 Receptor (VDR) Homodimers into VDR-Retinoid X Receptor Heterodimers. Mol. Cell. Biol. https://doi.org/10.1128/mcb.14.5.3329-3338.1994

Christoffer, C., Bharadwaj, V., Luu, R., Kihara, D., 2021. LZerD Protein-Protein Docking Webserver Enhanced With de novo Structure Prediction. Front. Mol. Biosci. 8. https://doi.org/10.3389/fmolb.2021.724947

Claessens, F., Gewirth, D.T., 2004. DNA recognition by nuclear receptors. Essays Biochem. 40, 59–72. https://doi.org/10.1042/bse0400059

Clark, K.L., Halay, E.D., Lai, E., Burley, S.K., 1993. Co-crystal structure of the HNF-3/fork head DNA-recognition motif resembles histone H5. Nature 364, 412–420. https://doi.org/10.1038/364412A0

Coulocheri, S.A., Pigis, D.G., Papavassiliou, K.A., Papavassiliou, A.G., 2007. Hydrogen bonds in protein-DNA complexes: where geometry meets plasticity. Biochimie 89, 1291–1303. https://doi.org/10.1016/J.BIOCHI.2007.07.020

Cowell, I.G., 1994. Repression versus activation in the control of gene transcription. Trends Biochem. Sci. 19, 38–42. https://doi.org/10.1016/0968-0004(94)90172-4

Dąbek, J., Kułach, A., Gąsior, Z., 2010. Nuclear factor kappa-light-chain-enhancer of activated B cells (NF-κB): a new potential therapeutic target in atherosclerosis? Pharmacol. Rep. PR 62, 778–783. https://doi.org/10.1016/s1734-1140(10)70338-8

Dankers, W., Colin, E.M., van Hamburg, J.P., Lubberts, E., 2017. Vitamin D in Autoimmunity: Molecular Mechanisms and Therapeutic Potential. Front. Immunol. 7. https://doi.org/10.3389/fimmu.2016.00697

Delves, P., Roitt, I., 2000. The Immune System. N Engl J Med 343, 37-49. DOI: 10.1056/NEJM200007063430107

de Oliveira, L.R.C., Mimura, L.A.N., Fraga-Silva, T.F. de C., Ishikawa, L.L.W., Fernandes, A.A.H., Zorzella-Pezavento, S.F.G., Sartori, A., 2020. Calcitriol Prevents Neuroinflammation and Reduces Blood-Brain Barrier Disruption and Local Macrophage/Microglia Activation. Front. Pharmacol. 11. https://doi.org/10.3389/FPHAR.2020.00161

Desta, I.T., Porter, K.A., Xia, B., Kozakov, D., Vajda, S., 2020. Performance and Its Limits in Rigid Body Protein-Protein Docking. Structure 28, 1071-1081.e3. https://doi.org/10.1016/j.str.2020.06.006

Dinarello, C.A., 2000. Proinflammatory Cytokines. Chest 118, 503–508. https://doi.org/10.1378/chest.118.2.503

Dubendorfft, J.W., Studier, F.W., 1991. Controlling Basal Expression in an Inducible T7 Expression System by Blocking the Target T7 Promoter with Zac Repressor, J. Mol. Biol.

Echeverria, P.C., Picard Didier, D., 2010. Molecular chaperones, essential partners of steroid hormone receptors for activity and mobility. Biochim. Biophys. Acta 1803, 641–649. https://doi.org/10.1016/J.BBAMCR.2009.11.012

Eter, P., Elves, J.D., Oitt, V.M.R., 2000. THE IMMUNE SYSTEM First of Two Parts.

Evans, R.M., 1988. The Steroid and Thyroid Hormone Receptor Superfamily. Science 240, 889–895. https://doi.org/10.1126/science.3283939

F. Holick, M., 2011. Vitamin D: evolutionary, physiological and health perspectives. Curr. Drug Targets 12, 4–18. https://doi.org/10.2174/138945011793591635

Ferland, R.J., Cherry, T.J., Preware, P.O., Morrisey, E.E., Walsh, C.A., 2003. Characterization of Foxp2 and Foxp1 mRNA and protein in the developing and mature brain. J. Comp. Neurol. 460, 266–279. https://doi.org/10.1002/cne.10654

Fluorescence Polarization Detection | BMG LABTECH [WWW Document], n.d. URL https://www.bmglabtech.com/en/fluorescence-polarization/ (accessed 12.10.24).

Fontenot, J.D., Gavin, M.A., Rudensky, A.Y., 2003. Foxp3 programs the development and function of CD4+CD25+ regulatory T cells. Nat. Immunol. 4, 986–992. https://doi.org/10.1038/NI904

Friedman, J.R., Kaestner, K.H., 2006. The Foxa family of transcription factors in development and metabolism. Cell. Mol. Life Sci. CMLS 63, 2317–2328. https://doi.org/10.1007/s00018-006-6095-6

Fruchart, JC., Santos, R.D., Aguilar-Salinas, C. Aikawa, M., Al Rasadi, K., Amarenco, P., et al. 2019. The selective peroxisome proliferator-activated receptor alpha modulator (SPPARMα) paradigm: conceptual framework and therapeutic potential. Cardiovasc Diabetol 18, 71. https://doi.org/10.1186/s12933-019-0864-7

Germain, P., Staels, B., Dacquet, C., Spedding, M., Laudet, V., 2006. Overview of Nomenclature of Nuclear Receptors. Pharmacol. Rev. 58, 685–704. https://doi.org/10.1124/pr.58.4.2

Ghisaidoobe, A.B.T., Chung, S.J., 2014. Intrinsic tryptophan fluorescence in the detection and analysis of proteins: a focus on Förster resonance energy transfer techniques. Int. J. Mol. Sci. 15, 22518–22538. https://doi.org/10.3390/IJMS151222518

Glass, C.K., Rosenfeld, M.G., 2000. The coregulator exchange in transcriptional functions of nuclear receptors. Genes Dev. 14, 121–141. https://doi.org/10.1101/GAD.14.2.121

Godfrey, V.L., Wilkinson, J.E., Russell, L.B., 1991. X-linked lymphoreticular disease in the scurfy (sf) mutant mouse. Am. J. Pathol. 138, 1379.

Hajas, A., Sandor, J., Csathy, L., Csipo, I., Barath, S., Paragh, G., et al., 2011. Vitamin D insufficiency in a large MCTD population. Autoimmun. Rev. 10, 317–324. https://doi.org/10.1016/J.AUTREV.2010.11.006

Hansson, T., Oostenbrink, C., van Gunsteren, W., 2002. Molecular dynamics simulations. Current Opinion in Structural Biology. 12.2, 190-196. https://doi.org/10.1016/S0959-440X(02)00308-1

Hardy, R.R., Hayakawa, K., 2001. B Cell Development Pathways. Annu. Rev. Immunol. 19, 595–621. https://doi.org/10.1146/annurev.immunol.19.1.595

Haussler, M.R., Norman, A.W., 1969. Chromosomal receptor for a vitamin d metabolite. Proc. Natl. Acad. Sci. 62, 155–162. https://doi.org/10.1073/pnas.62.1.155

Hazlett, L., Wu, M., 2011. Defensins in innate immunity. Cell Tissue Res. 343, 175–188. https://doi.org/10.1007/s00441-010-1022-4

Hellman, L.M., Fried, M.G., 2007. Electrophoretic mobility shift assay (EMSA) for detecting protein-nucleic acid interactions. Nat. Protoc. 2, 1849–1861. https://doi.org/10.1038/nprot.2007.249

Henderson, M.J., Holbert, M.A., Simeonov, A., Kallal, L.A., 2020. High-Throughput Cellular Thermal Shift Assays in Research and Drug Discovery. SLAS Discov. Adv. Life Sci. R D 25, 137–147. https://doi.org/10.1177/2472555219877183

Hillion, J., Le Coniat, M., Jonveaux, P., Berger, R., Bernard, O.A., 1997. AF6q21, a Novel Partner of the MLL Gene in t(6; 11)(q21; q23), Defines a Forkhead Transcriptional Factor Subfamily. Blood 90, 3714–3719. https://doi.org/10.1182/BLOOD.V90.9.3714

Honju and Habu 1985 (Immune diversity), n.d.

Hori, S., Nomura, T., Sakaguchi, S., 2003. Control of regulatory T cell development by the transcription factor Foxp3. Science 299, 981–985. https://doi.org/10.1126/SCIENCE.1079490

Hörlein, A.J., Näär, A.M., Heinzel, T., Torchia, J., Gloss, B., Kurokawa, R., et al., 1995. Ligand-independent repression by the thyroid hormone receptor mediated by a nuclear receptor co-repressor. Nature 377, 397–404. https://doi.org/10.1038/377397a0

Hsieh, J.-C., Nakajima, S., Galligan, M.A., Jurutka, P.W., Haussler, C.A., Kerr Whitfield, G., Haussler, M.R., 1995. Receptor Mediated Genomic Action of the 1,25(OH)2D3 Hormone: Expression of the Human Vitamin D Receptor in E. coli, J. Steroid Biochem. Molec. Biol.

Hu, H., Wang, B., Borde, M., Nardone, J., Maika, S., Allred, L., et al., 2006. Foxp1 is an essential transcriptional regulator of B cell development. Nat. Immunol. 7, 819–826. https://doi.org/10.1038/ni1358

Huynh, K., Partch, C.L., 2015. Analysis of protein stability and ligand interactions by thermal shift assay. Curr. Protoc. Protein Sci. 79, 28.9.1-28.9.14. https://doi.org/10.1002/0471140864.PS2809S79

Inukai, S., Kock, K.H., Bulyk, M.L., 2017. Transcription factor–DNA binding: beyond binding site motifs. Curr. Opin. Genet. Dev., Genome architecture and expression 43, 110–119. https://doi.org/10.1016/j.gde.2017.02.007

Issa, L.L., Leong, G.M., Eisman, J.A., 1998. Molecular mechanism of vitamin D receptor action. Inflamm. Res. 47, 451–475. https://doi.org/10.1007/s000110050360

James, G.T., 1978. Inactivation of the protease inhibitor phenylmethylsulfonyl fluoride in buffers. Anal. Biochem. 86, 574–579. https://doi.org/10.1016/0003-2697(78)90784-4

Jolma, A., Yan, J., Whitington, T., Toivonen, J., Nitta, K.R., Rastas, P., et al., 2013. DNA-Binding Specificities of Human Transcription Factors. Cell 152, 327–339. https://doi.org/10.1016/j.cell.2012.12.009

Kaestner, K.H., Knöchel, W., Martínez, D.E., 2000. Unified nomenclature for the winged helix/forkhead transcription factors. Genes Dev. 14, 142–146. https://doi.org/10.1101/GAD.14.2.142

Kang, S.W., Kim, S.H., Lee, N., Lee, W.-W., Hwang, K.-A., Shin, M.S., et al., 2012. 1,25-Dihyroxyvitamin D3 Promotes FOXP3 Expression via Binding to Vitamin D Response Elements in Its Conserved Noncoding Sequence Region. J. Immunol. 188, 5276–5282. https://doi.org/10.4049/jimmunol.1101211

Kawe, M., Horn, U., Plückthun, A., 2009. Facile promoter deletion in Escherichia coli in response to leaky expression of very robust and benign proteins from common expression vectors. Microb. Cell Factories 8, 8. https://doi.org/10.1186/1475-2859-8-8

Kelly, S., Price, N., 2000. The use of circular dichroism in the investigation of protein structure and function. Curr. Protein Pept. Sci. 1, 349–384. https://doi.org/10.2174/1389203003381315

Khattri, R., Cox, T., Yasayko, S.A., Ramsdell, F., 2003. An essential role for Scurfin in CD4+CD25+ T regulatory cells. Nat. Immunol. 4, 993–998. https://doi.org/10.1038/NI909

Kim, C.H., 2010. FOXP3 and Its Role in the Immune System, in: Maiese, K. (Ed.), Forkhead Transcription Factors: Vital Elements in Biology and Medicine. Springer, New York, NY, pp. 17–29. https://doi.org/10.1007/978-1-4419-1599-3_2

Kitchner, E., Seung, M., Chavez, J., Ceresa, L., Kimball, J., Gryczynski, I., Gryczynski, Z., 2022. Fluorescence measurements: importance of G-factor correction, magic angle, and observation wavelengths. Methods Appl. Fluoresc. 10, 043001. https://doi.org/10.1088/2050-6120/ac92c5

Knutson, J.R., Davenport, L., Brand, L., 1986. Anisotropy decay associated fluorescence spectra and analysis of rotational heterogeneity. 1. Theory and applications. Biochemistry 25, 1805–1810. https://doi.org/10.1021/BI00355A053

Koyama, T., Rodrigues, M.A., Athanasiadis, A., Shingleton, A.W., Mirth, C.K., 2014. Nutritional control of body size through FoxO-Ultraspiracle mediated ecdysone biosynthesis. eLife 3. https://doi.org/10.7554/ELIFE.03091

Kumar, B.V., Connors, T.J., Farber, D.L., 2018. Human T Cell Development, Localization, and Function throughout Life. Immunity 48, 202–213. https://doi.org/10.1016/j.immuni.2018.01.007

Kumar, S., Ravi, V.K., Swaminathan, R., 2008. How do surfactants and DTT affect the size, dynamics, activity and growth of soluble lysozyme aggregates? Biochem. J. 415, 275–288. https://doi.org/10.1042/BJ20071499

Kushwah, V.C., Chauhan, R., Dhaked, R.K., 2024. Fluorescence Thermal Shift Assay based High Through-put Screening in Small Molecule Drug Discovery: A Brief Overview. J. Mod. Biol. Drug Discov.

Laemmli, U.K., 1970. Cleavage of Structural Proteins during the Assembly of the Head of Bacteriophage T4. Nat. 1970 2275259 227, 680–685. https://doi.org/10.1038/227680a0

Lakhi, A., Fanucchi, S., 2024. Identification and characterisation of a novel interaction between oestrogen receptor alpha and FOXP2. Biochimie 221, 65–74. https://doi.org/10.1016/j.biochi.2024.01.014

Lakowicz, J.R., 1985. Chapter 1 Fluorescence Spectroscopy; Principles and Application to Biological Macromolecules, in: Neuberger, A., van Deenen, L.L.M. (Eds.), New Comprehensive Biochemistry, Modern Physical Methods in Biochemistry. Elsevier, pp. 1–26. https://doi.org/10.1016/S0167-7306(08)60570-0

Latchman, D.S., 1997. Transcription factors: An overview. Int. J. Biochem. Cell Biol. 29, 1305–1312. https://doi.org/10.1016/S1357-2725(97)00085-X

Lawrence, T., Gilroy, D.W., 2007. Chronic inflammation: a failure of resolution? Int. J. Exp. Pathol. 88, 85–94. https://doi.org/10.1111/j.1365-2613.2006.00507.x

Lee W, Lee GR., 2018. Transcriptional regulation and development of regulatory T cells. Exp Mol Med. 9;50(3):e456. doi: 10.1038/emm.2017.313.

Lefebvre, C., Lim, W.K., Basso, K., Favera, R.D., Califano, A., 2007. A Context-Specific Network of Protein-DNA and Protein-Protein Interactions Reveals New Regulatory Motifs in Human B Cells, in: Ideker, T., Bafna, V. (Eds.), Systems Biology and Computational Proteomics. Springer, Berlin, Heidelberg, pp. 42–56. https://doi.org/10.1007/978-3-540-73060-6_4

Lehmann, O.J., Sowden, J.C., Carlsson, P., Jordan, T., Bhattacharya, S.S., 2003. Fox's in development and disease. Trends Genet. 19, 339–344. https://doi.org/10.1016/S0168-9525(03)00111-2

Liu, Y.-Y., Nguyen, C., Peleg, S., 2000. Regulation of Ligand-Induced Heterodimerization and Coactivator Interaction by the Activation Function-2 Domain of the Vitamin D Receptor. Mol. Endocrinol. 14, 1776–1787. https://doi.org/10.1210/mend.14.11.0560

Long, Q.-Z., Du, Y.-F., Ding, X.-Y., Li, X., Song, W.-B., Yang, Y., et al., 2012. Replication and Fine Mapping for Association of the C2orf43, FOXP4, GPRC6A and RFX6 Genes with Prostate Cancer in the Chinese Population. PLOS ONE 7, e37866. https://doi.org/10.1371/journal.pone.0037866

Lu, D., Lan, B., Din, Z., Chen, H., Chen, G., 2017. A vitamin D receptor agonist converts CD4+ T cells to Foxp3+ regulatory T cells in patients with ulcerative colitis. Oncotarget 8, 53552–53562. https://doi.org/10.18632/ONCOTARGET.18614

Luan, C.-H., Light, S.H., Dunne, S.F., Anderson, W.F., 2014. Ligand Screening Using Fluorescence Thermal Shift Analysis (FTS), in: Anderson, W.F. (Ed.), Structural Genomics and Drug Discovery: Methods and Protocols. Springer, New York, NY, pp. 263–289. https://doi.org/10.1007/978-1-4939-0354-2_20

Luckheeram, R.V., Zhou, R., Verma, A.D., Xia, B., 2012. CD4+T Cells: Differentiation and Functions. J. Immunol. Res. 2012, 925135. https://doi.org/10.1155/2012/925135

MacKey-Cushman, S.L., Gao, J., Holmes, D.A., Nunoya, J.I., Wang, R., Unutmaz, D., Su, L., 2011. FoxP3 interacts with linker histone H1.5 to modulate gene expression and program Treg cell activity. Genes Immun. 12, 559–567. https://doi.org/10.1038/GENE.2011.31

Mandel, M., Higa, A., 1970. Calcium-dependent bacteriophage DNA infection. J. Mol. Biol. 53, 159–162. https://doi.org/10.1016/0022-2836(70)90051-3

Mangelsdorf, D.J., Thummel, C., Beato, M., Herrlich, P., Schütz, G., Umesono, K., et al., 1995. The nuclear receptor superfamily: the second decade. Cell 83, 835–839. https://doi.org/10.1016/0092-8674(95)90199-X

Margolis, R.N., Christakos, S., 2010. The nuclear receptor superfamily of steroid hormones and vitamin D gene regulation. Ann. N. Y. Acad. Sci. 1192, 208–214. https://doi.org/10.1111/j.1749-6632.2009.05227.x

Mazaira, G.I., Zgajnar, N.R., Lotufo, C.M., Daneri-Becerra, C., Sivils, J.C., Soto, O.B., et al., 2018. The Nuclear Receptor Field: A Historical Overview and Future Challenges. Nucl. Recept. Res. 5, 101320. https://doi.org/10.11131/2018/101320

Mijnheer, G., Lutter, L., Mokry, M., van der Wal, M., Scholman, R., Fleskens, V., et al., 2021. Conserved human effector Treg cell transcriptomic and epigenetic signature in arthritic joint inflammation. Nat. Commun. 12. https://doi.org/10.1038/s41467-021-22975-7

Nagel, T., 2007. Reductionism and Antireductionism, in: Novartis Foundation Symposium 213 - The Limits of Reductionism in Biology. John Wiley & Sons, Ltd, pp. 3–14. https://doi.org/10.1002/9780470515488.ch2

Okamoto, R., Koeffler, H.P., 2011. Hematological Malignancy. Vitam. Two-Vol. Set 2–2, 1731–1750. https://doi.org/10.1016/B978-0-12-381978-9.10088-5

Olins, D.E., Olins, A.L., 2003. Chromatin history: our view from the bridge. Nat. Rev. Mol. Cell Biol. 4, 809–814. https://doi.org/10.1038/NRM1225

Oñate, S.A., Tsai, S.Y., Tsai, M.-J., O'Malley, B.W., 1995. Sequence and Characterization of a Coactivator for the Steroid Hormone Receptor Superfamily. Science 270, 1354–1357. https://doi.org/10.1126/science.270.5240.1354

Parkin, J., Cohen, B., 2001. An overview of the immune system. Lancet 357, 1777–1789. https://doi.org/10.1016/S0140-6736(00)04904-7

Peng, X., Wang, J., Peng, W., Wu, F.-X., Pan, Y., 2017. Protein–protein interactions: detection, reliability assessment and applications. Brief. Bioinform. 18, 798–819. https://doi.org/10.1093/bib/bbw066

Perumal, C.M., Thulo, M., Buthelezi, S., Naicker, P., Stoychev, S., Lakhi, A., Fanucchi, S., 2024. Unraveling the interplay between the leucine zipper and forkhead domains of FOXP2: Implications for DNA binding, stability and dynamics. Proteins Struct. Funct. Bioinforma. 92, 1177–1189. https://doi.org/10.1002/prot.26699

Perumal, K., Dirr, H.W., Fanucchi, S., 2015. A Single Amino Acid in the Hinge Loop Region of the FOXP Forkhead Domain is Significant for Dimerisation. Protein J. 34, 111–121. https://doi.org/10.1007/S10930-015-9603-4

Pettersen, E.F., Goddard, T.D., Huang, C.C., Couch, G.S., Greenblatt, D.M., Meng, E.C., Ferrin, T.E., 2004. UCSF Chimera--a visualization system for exploratory research and analysis. J. Comput. Chem. 25, 1605–1612. https://doi.org/10.1002/jcc.20084

Pike, J.W., Meyer, M.B., Lee, S.M., Onal, M., Benkusky, N.A., 2017. The vitamin D receptor: contemporary genomic approaches reveal new basic and translational insights. J. Clin. Invest. 127, 1146–1154. https://doi.org/10.1172/JCI88887

Plevin, M.J., Mills, M.M., Ikura, M., 2005. The LxxLL motif: a multifunctional binding sequence in transcriptional regulation. Trends Biochem. Sci. 30, 66–69. https://doi.org/10.1016/j.tibs.2004.12.001

Quack, M., Carlberg, C., 2000. The Impact of Functional Vitamin D3 Receptor Conformations on DNA-Dependent Vitamin D3 Signaling. Mol. Pharmacol. 57, 375–384.

Rochel, N., Wurtz, J.M., Mitschler, A., Klaholz, B., Moras, D., 2000. The crystal structure of the nuclear receptor for vitamin D bound to its natural ligand. Mol. Cell 5, 173–179. https://doi.org/10.1016/S1097-2765(00)80413-X

Rogers, DM., Jasim, SB., Dyer, NT., Auvray, F., Réfrégiers, M., Hirst, JD., 2019. Electronic Circular Dichroism Spectroscopy of Proteins. Chem, 5, 2751 - 2774

Rosano, G.L., Ceccarelli, E.A., 2014. Recombinant protein expression in Escherichia coli: advances and challenges. Front. Microbiol. 5. https://doi.org/10.3389/FMICB.2014.00172

Roy, S., Kundu, T.K., 2021. Chemical principles of DNA sequence recognition and gene regulation. Chem. Biol. Genome 171–223. https://doi.org/10.1016/B978-0-12-817644-3.00005-2

Sakaguchi, S., 2004. Naturally Arising CD4+ Regulatory T Cells for Immunologic Self-Tolerance and Negative Control of Immune Responses. Annu. Rev. Immunol. 22, 531–562. https://doi.org/10.1146/annurev.immunol.21.120601.141122

Sam-Yellowe, T.Y., 2021. Antigens, in: Sam-Yellowe, T.Y. (Ed.), Immunology: Overview and Laboratory Manual. Springer International Publishing, Cham, pp. 65–72. https://doi.org/10.1007/978-3-030-64686-8_9

Sarkar, S., 1992. Models of reduction and categories of reductionism. Synthese 91, 167–194. https://doi.org/10.1007/BF00413566

Schägger, H., 2006. Tricine–SDS-PAGE. Nat. Protoc. 1, 16–22. https://doi.org/10.1038/nprot.2006.4

Schwartz, R.H., 1989. Acquisition of immunologic self-tolerance. Cell 57, 1073–1081. https://doi.org/10.1016/0092-8674(89)90044-5

Scott, A.D., 2017. Fluorescent Thermal Shift Assays for Identifying Small Molecule Ligands.

Shu, W., Lu, M.M., Zhang, Y., Tucker, P.W., Zhou, D., Morrisey, E.E., 2007. Foxp2 and Foxp1 cooperatively regulate lung and esophagus development. Development 134, 1991–2000. https://doi.org/10.1242/dev.02846

Song, X., Li, B., Xiao, Y., Chen, C., Wang, Q., Liu, Y., et al., 2012. Structural and Biological Features of FOXP3 Dimerization Relevant to Regulatory T Cell Function. Cell Rep. 1, 665–675. https://doi.org/10.1016/j.celrep.2012.04.012

Steiner, R.F., 2002. Fluorescence Anisotropy: Theory and Applications. Top. Fluoresc. Spectrosc. 1–52. https://doi.org/10.1007/0-306-47058-6_1

Stossel, T.P., 1974. Phagocytosis. N. Engl. J. Med. 290, 717–723. https://doi.org/10.1056/NEJM197403282901306

Stroud, J.C., Wu, Y., Bates, D.L., Han, A., Nowick, K., Paabo, S., et al., 2006. Structure of the forkhead domain of FOXP2 bound to DNA. Struct. Lond. Engl. 1993 14, 159–166. https://doi.org/10.1016/J.STR.2005.10.005

Sulkowski, E., 1985. Purification of proteins by IMAC. Trends Biotechnol. 3, 1–7. https://doi.org/10.1016/0167-7799(85)90068-X

Szklarczyk, D., Franceschini, A., Wyder, S., Forslund, K., Heller, D., Huerta-Cepas, J., et al., 2015. STRING v10: protein–protein interaction networks, integrated over the tree of life. Nucleic Acids Res. 43, D447–D452. https://doi.org/10.1093/nar/gku1003

Tata, J.R., 2002. Signalling through nuclear receptors. Nat. Rev. Mol. Cell Biol. 3, 702–710. https://doi.org/10.1038/nrm914

Taylor, S., Wakem, M., Dijkman, G., Alsarraj, M., Nguyen, M., 2010. A practical approach to RT-qPCR-Publishing data that conform to MIQE guidelines. Methods. 50, S1-S5. https://doi.org/10.1016/j.ymeth.2010.01.005

Teufel, A., Wong, E.A., Mukhopadhyay, M., Malik, N., Westphal, H., 2003. *FoxP4*, a novel forkhead transcription factor. Biochim. Biophys. Acta BBA - Gene Struct. Expr. 1627, 147–152. https://doi.org/10.1016/S0167-4781(03)00074-5

The UniProt Consortium, 2024. UniProt: the Universal Protein Knowledgebase in 2025. Nucleic Acids Res. gkae1010. https://doi.org/10.1093/nar/gkae1010

Tompkins, M.B., Howard, K.E., 2010. Lymphoid System, in: Atlas of Feline Anatomy For Veterinarians. Teton NewMedia.

Tosi, M.F., 2005. Innate immune responses to infection. J. Allergy Clin. Immunol. 116, 241–249. https://doi.org/10.1016/j.jaci.2005.05.036

Turvey, S.E., Broide, D.H., 2010. Innate immunity. J. Allergy Clin. Immunol., 2010 Primer on Allergic and Immunologic Diseases 125, S24–S32. https://doi.org/10.1016/j.jaci.2009.07.016

Vakser, I.A., 2014. Protein-protein docking: from interaction to interactome. Biophys. J. 107, 1785–1793. https://doi.org/10.1016/J.BPJ.2014.08.033

van Loosdregt, J., Coffer, P., 2014. Post-translational modification networks regulating FOXP3 function. Trends in Immunology, 35, 368 - 378

Vector database. Addgene. Available at: https://www.addgene.org/vector-database/2625/ (Accessed: 15 February 2025).

Veldman, C.M., Cantorna, M.T., DeLuca, H.F., 2000. Expression of 1,25-dihydroxyvitamin D3 receptor in the immune system. Arch. Biochem. Biophys. 374, 334–338. https://doi.org/10.1006/abbi.1999.1605

Walker, M.R., Carson, B.D., Nepom, G.T., Ziegler, S.F., Buckner, J.H., 2005. De novo generation of antigen-specific CD4+CD25+ regulatory T cells from human CD4+CD25– cells. Proc. Natl. Acad. Sci. 102, 4103–4108. https://doi.org/10.1073/pnas.0407691102

Wan, X., Marsafari, M., Xu, P., 2019. Engineering metabolite-responsive transcriptional factors to sense small molecules in eukaryotes: Current state and perspectives. Microb. Cell Factories 18. https://doi.org/10.1186/s12934-019-1111-3

Wei, D., Tao, R., Zhang, Y., White, M.F., Dong, X.C., 2011. Feedback regulation of hepatic gluconeogenesis through modulation of SHP/Nr0b2 gene expression by Sirt1 and FoxO1. Am. J. Physiol. Endocrinol. Metab. 300. https://doi.org/10.1152/AJPENDO.00524.2010

Westermarck, J., Ivaska, J., Corthals, G.L., 2013. Identification of protein interactions involved in cellular signaling. Mol. Cell. Proteomics MCP 12, 1752–1763. https://doi.org/10.1074/MCP.R113.027771

Wilson, C.B., 1991. The ontogeny of T lymphocyte maturation and function. J. Pediatr. 118, S4–S9. https://doi.org/10.1016/S0022-3476(05)82182-1

Wu, Q., Chambliss, K., Umetani, M., Mineo, C., Shaul, P.W., 2011. Non-nuclear estrogen receptor signaling in the endothelium. J. Biol. Chem. 286, 14737–14743. https://doi.org/10.1074/JBC.R110.191791

Yan, Y., Tao, H., He, J., Huang, S.-Y., 2020a. The HDOCK server for integrated protein–protein docking. Nat. Protoc. 15, 1829–1852. https://doi.org/10.1038/s41596-020-0312-x

Yan, Y., Tao, H., He, J., Huang, S.-Y., 2020b. The HDOCK server for integrated protein–protein docking. Nat. Protoc. 15, 1829–1852. https://doi.org/10.1038/s41596-020-0312-x

Yan, Y., Zhang, D., Zhou, P., Li, B., Huang, S.-Y., 2017. HDOCK: a web server for protein–protein and protein–DNA/RNA docking based on a hybrid strategy. Nucleic Acids Res. 45, W365–W373. https://doi.org/10.1093/nar/gkx407

Yang, C.Y., Leung, P.S.C., Adamopoulos, I.E., Gershwin, M.E., 2013. The implication of vitamin D and autoimmunity: A comprehensive review. Clin. Rev. Allergy Immunol. 45, 217–226. https://doi.org/10.1007/s12016-013-8361-3

Yang, S., Cho, S.S., Levy, Y., Cheung, M.S., Levine, H., Wolynes, P.G., Onuchic, J.N., 2004. Domain swapping is a consequence of minimal frustration. Proc. Natl. Acad. Sci. U. S. A. 101, 13786–13791. https://doi.org/10.1073/PNAS.0403724101

Yuan, W., Pan, W., Kong, J., Zheng, W., Szeto, F.L., Wong, K.E., Cohen, R., et al., 2007. 1,25-Dihydroxyvitamin D3 suppresses renin gene transcription by blocking the activity of the cyclic AMP response element in the renin gene promoter. J. Biol. Chem. 282, 29821–29830. https://doi.org/10.1074/jbc.M705495200